Atmospheric Pollution Research 12 (2021) 101142

Contents lists available at ScienceDirect

Atmospheric Pollution Research

journal homepage: www.elsevier.com/locate/apr

Assessing the magnitude of $PM_{2.5}$ polycyclic aromatic hydrocarbon emissions from residential solid fuel combustion and associated health hazards in South Asia

Madhuri Verma [a,**], Shamsh Pervez [a,*], Judith C. Chow [b,c,***], Dipanjali Majumdar [d], John G. Watson [b,c], Yasmeen Fatima Pervez [e], Manas Kanti Deb [a], Kamlesh Shrivas [a], Vikas Kumar Jain [f], Noor A. Khan [g], Papiya Mandal [g], Rajan K. Chakrabarty [h,****]

[a] School of Studies in Chemistry, Pt. Ravishankar Shukla University, Raipur, 492 010, Chhattisgarh, India
[b] Division of Atmospheric Sciences, Desert Research Institute, Reno, NV, 89512, USA
[c] Institute of Earth and Environment, Chinese Academy of Science, Xian, China
[d] CSIR-National Environmental Engineering Research Institute, Kolkata Zonal Centre, Kolkata, 700107, West Bengal, India
[e] Department of Chemistry, Government Eklavya College, Dondi-Lohara, Balod, CG, India
[f] Department of Chemistry, Government Engineering College, Raipur, CG, 492 015, India
[g] NEERI, Delhi Zonal Centre, A-93/94, Phase 1, Naraina Industrial Area, New Delhi, 110028, India
[h] Department of Energy, Environmental and Chemical Engineering, Washington University in St. Louis, St. Louis, MO, 63130, USA

ARTICLE INFO

Keywords:
Emission factors
Particulate PAHs (*p*-PAHs)
Carcinogenic toxicity
Biofuels
Coal balls
Household heating activities
Solid fuel

ABSTRACT

In South Asia, combustion of solid fuel for residential heating and cooking is a major emission source of particulate-phase polycyclic aromatic hydrocarbons (*p*-PAHs), a potent carcinogen for human health. The emission factors (EFs) and source diagnostic ratios of PAHs currently used in regional inventory models have been estimated from controlled laboratory tests, which do not accurately reflect real-world combustion scenarios observed in rural Indian households. Consequently, the health effects associated with *p*-PAH levels in indoor and ambient air could be severely underestimated and undervalued. We performed a nationwide study across ten different states in the Indian subcontinent to evaluate the EFs and source diagnostic ratios of sixteen U.S. Environmental Protection Agency (EPA) identified high priority *p*-PAHs emitted from residential solid biomass combustion. Our estimated average annual EFs were 2.4–18.3 fold higher than those reported from previous laboratory-based investigations. Carcinogenic toxicity analysis shows that combustion of dung cake and coal ball, both widely used residential solid fuels, posed the most risk (80% and 59% respectively) in comparison to other PAHs owing to predominant emission of benzo[a]pyrene. Our findings underscore the importance of improved laboratory testing and field validations as crucial steps toward more accurate emission inventories and better assessment of public health impacts.

1. Introduction

A large portion of the population in developing countries depends on unprocessed solid fuels (coal balls, fuel wood, dung cake, and crop residues), with unvented stoves, for household cooking and heating. Emissions of fine particulate matter ($<PM_{2.5}$), trace gases, and polycyclic aromatic hydrocarbons (PAHs) contribute to local and region pollution and adverse health effects (Bond et al., 2004; ; Zhang and Tao, 2009).

PAHs are a class of organic compounds that originate from both petrogenic (e.g. vehicle exhausts, incinerators and power generation plants) and pyrogenic (incomplete combustion of fossil fuel and

Peer review under responsibility of Turkish National Committee for Air Pollution Research and Control.
* Corresponding authors.
** Corresponding author.
*** Corresponding authors. Division of Atmospheric Sciences, Desert Research Institute, Reno, NV, 89512, USA.
**** Corresponding author.
E-mail addresses: shamshpervez@gmail.com (S. Pervez), judy.chow@dri.edu (J.C. Chow), chakrabarty@wustl.edu (R.K. Chakrabarty).

https://doi.org/10.1016/j.apr.2021.101142
Received 14 April 2021; Received in revised form 13 July 2021; Accepted 13 July 2021
Available online 15 July 2021

Table 1
State wise average Emission Factor and standard deviation of 16 PAH (mg.kg^{-1}) separated by five fuel types; coal balls (CB), fuel wood (FW), dung cakes (DC), crop residues (CR), mixed fuels: dung cakes + fuel wood (MF) during real-world household cooking practices in eleven (11) locations across the ten different States of India.

Fuel type	Sampling locations	PAHs (mg.kg^{-1})																
		Naph	Ace	Anth	Flu	Phe	B[a]A	Flt	Pyr	Chry	B[a]P	D[ah]A	B[b]F	B[k]F	B[ghi]P	I(cd)P	I(cd)F	Σ*p*-PAHs
CB	SLH(CG)	39.0 ± 16.1	7.1 ± 5.0	8.1 ± 5.2	5.9 ± 5.6	10.3 ± 5.7	12.1 ± 11.2	15.3 ± 10.2	4.5 ± 2.9	7.2 ± 3.9	26.02 ± 15.22	10.7 ± 4.7	32.4 ± 25.7	12.0 ± 5.8	9.7 ± 6.8	9.5 ± 6.4	8.4 ± 6.2	218.3 ± 100.4
	JRI(JH)	23.4 ± 6.4	5.9 ± 3.3	12.1 ± 7.1	6.6 ± 2.1	23.3 ± 14.3	20.0 ± 7.2	16.5 ± 9.9	8.6 ± 5.2	11.6 ± 7.4	47.72 ± 23.36	16.6 ± 13.2	49.4 ± 19.9	26.9 ± 10.9	12.4 ± 6.6	22.4 ± 7.7	8.7 ± 4.2	312.1 ± 105.6
	Avg.	28.9 ± 14.0	5.2 ± 3.9	8.1 ± 6.1	5.2 ± 3.9	12.8 ± 12.3	11.9 ± 9.7	13.6 ± 9.3	5.2 ± 4.5	8.1 ± 5.9	31.8 ± 21.6	11.5 ± 9.7	35.1 ± 23.1	16.5 ± 11.3	9.4 ± 6.4	12.9 ± 9.5	6.9 ± 4.9	231.5 ± 114.7
FW	PNBE(BR)	22.1 ± 9.5	9.3 ± 6.2	23.2 ± 6.9	**ND**	14.0 ± 5.4	**ND**	22.9 ± 8.1	11.0 ± 8.4	**ND**	**ND**	5.6 ± 4.2	**ND**	**ND**	4.2 ± 1.6	2.6 ± 1.2	2.9 ± 1.5	134.2 ± 28.1
	JP(RJ)	18.7 ± 7.7	11.4 ± 7.3	18.5 ± 15.9	**ND**	21.4 ± 17.6	**ND**	48.9 ± 38.5	15.6 ± 9.3	**ND**	**ND**	7.5 ± 3.9	**ND**	**ND**	11.0 ± 4.8	7.5 ± 5.3	5.2 ± 2.7	171.7 ± 88.7
	CNB(UP)	36.9 ± 35.9	14.8 ± 5.3	23.1 ± 19.1	**ND**	16.3 ± 15.3	**ND**	19.5 ± 8.0	18.9 ± 9.2	**ND**	**ND**	12.9 ± 10.5	**ND**	**ND**	19.9 ± 15.4	7.9 ± 4.3	4.8 ± 1.2	198.4 ± 113.2
	HYB(TG)	25.7 ± 16.4	9.77 ± 7.5	17.1 ± 10.3	**ND**	10.4 ± 7.0	**ND**	35.8 ± 14.8	13.4 ± 9.3	**ND**	**ND**	5.8 ± 5.1	**ND**	**ND**	15.5 ± 11.2	9.9 ± 7.8	4.6 ± 4.1	159.1 ± 79.7
	FZP(PB)	20.4 ± 13.2	7.4 ± 5.4	9.6 ± 6.8	**ND**	20.9 ± 15.2	**ND**	19.2 ± 14.6	10.3 ± 8.5	**ND**	**ND**	8.9 ± 4.1	**ND**	**ND**	12.018.5	6.4 ± 4.3	5.7 ± 2.8	129.1 ± 73.1
	RE(HR)	41.4 ± 23.9	4.1 ± 5.9	6.6 ± 5.5	**ND**	12.2 ± 6.1	**ND**	14.6 ± 9.9	10.2 ± 8.1	**ND**	**ND**	5.0 ± 3.9	**ND**	**ND**	10.4 ± 7.2	4.2 ± 3.4	4.1 ± 3.3	146.0 ± 90.6
	BBS(OR)	50.8 ± 22.3	10.9 ± 7.6	20.8 ± 15.2	**ND**	24.7 ± 19.5	**ND**	20.9 ± 15.8	7.3 ± 3.9	**ND**	**ND**	7.1 ± 2.6	**ND**	**ND**	18.1 ± 6.8	5.5 ± 1.0	6.1 ± 3.9	211.5 ± 106.5
	R(CG)	26.4 ± 10.4	8.6 ± 4.4	11.4 ± 6.4	**ND**	16.8 ± 10.8	**ND**	23.3 ± 8.7	4.1 ± 1.6	**ND**	**ND**	6.2 ± 4.6	**ND**	**ND**	9.9 ± 3.8	4.7 ± 0.8	2.2 ± 1.4	133.1 ± 36.9
	Avg.	24.5 ± 20.4	6.9 ± 6.3	12.1 ± 12.1	**ND**	13.1 ± 12.5	**ND**	19.2 ± 18.8	8.6 ± 8.1	**ND**	**ND**	5.8 ± 5.3	**ND**	**ND**	10.2 ± 8.9	4.8 ± 4.3	3.5 ± 2.8	108.7 ± 99.5
DC	PNBE(BR)	13.3 ± 9.7	**ND**	14.7 ± 8.3	**ND**	1.6 ± 1.3	**ND**	5.2 ± 5.1	1.6 ± 1.5	**ND**	52.2 ± 16.1	7.4 ± 3.7	62.6 ± 42.4	3.4 ± 1.6	9.8 ± 3.4	15.2 ± 7.9	10.0 ± 7.5	184.9 ± 70.3
	JP(RJ)	30.3 ± 19.1	**ND**	18.7 ± 7.9	**ND**	2.2 ± 0.8	**ND**	9.7 ± 8.9	0.9 ± 0.5	**ND**	98.9 ± 50.7	11.9 ± 7.7	64.4 ± 33.6	3.9 ± 1.7	12.7 ± 6.6	30.9 ± 25.6	6.2 ± 2.6	284.1 ± 125.7
	CNB(UP)	18.9 ± 15.3	**ND**	13.0 ± 7.7	**ND**	1.8 ± 0.9	**ND**	5.7 ± 1.6	1.3 ± 1.1	**ND**	66.3 ± 41.7	13.5 ± 2.1	32.7 ± 21.1	2.1 ± 1.2	6.4 ± 2.7	15.6 ± 2.1	5.6 ± 3.3	180.6 ± 81.7
	HYB(TG)	16.4 ± 9.7	**ND**	14.1 ± 11.9	**ND**	1.9 ± 0.9	**ND**	6.6 ± 3.9	1.6 ± 1.1	**ND**	81.9 ± 57.5	15.7 ± 9.5	54.9 ± 32.6	2.3 ± 0.3	13.2 ± 8.4	25.0 ± 10.8	15.3 ± 7.3	225.0 ± 107.7
	FZP(PB)	15.7 ± 8.4	**ND**	25.2 ± 23.3	**ND**	0.5 ± 0.2	**ND**	5.6 ± 2.9	1.2 ± 0.5	**ND**	72.2 ± 38.2	5.5 ± 3.9	22.7 ± 21.0	0.7 ± 0.3	16.9 ± 5.8	19.5 ± 17.4	6.1 ± 5.4	181.9 ± 83.8
	RE(HR)	29.9 ± 22.1	**ND**	26.9 ± 12.3	**ND**	2.0 ± 1.5	**ND**	10.5 ± 7.3	1.2 ± 0.8	**ND**	111.8 ± 38.2	20.9 ± 12.2	34.3 ± 15.5	1.1 ± 0.6	23.0 ± 20.9	18.4 ± 5.3	11.8 ± 5.4	291.6 ± 121.9
	BBS(OR)	18.8 ± 16.1	**ND**	22.5 ± 12.5	**ND**	1.5 ± 0.7	**ND**	11.6 ± 9.3	1.3 ± 0.5	**ND**	45.9 ± 27.6	4.9 ± 3.6	21.9 ± 8.3	0.9 ± 0.4	15.1 ± 7.9	16.9 ± 7.7	13.0 ± 8.6	163.1 ± 88.9
	R(CG)	14.8 ± 13.6	**ND**	11.9 ± 7.2	**ND**	0.7 ± 0.5	**ND**	11.8 ± 6.8	1.9 ± 1.4	**ND**	23.8 ± 9.3	13.4 ± 3.7	30.5 ± 17.1	1.2 ± 0.8	14.4 ± 7.1	19.2 ± 14.8	3.3 ± 0.8	139.1 ± 64.3
	Avg.	15.1 ± 14.6	**ND**	14.8 ± 12.3	**ND**	1.2 ± 1.0	**ND**	6.3 ± 6.2	1.1 ± 0.9	**ND**	**53.5 ± 43.2**	9.2 ± 7.9	31.9 ± 28.4	1.5 ± 1.5	11.7 ± 9.6	16.5 ± 12.9	6.8 ± 6.4	169.6 ± 144.9
CR (rice straw)	VSKP(AP)[a]	50.2 ± 38.1	9.7 ± 3.3	6.6 ± 3.3	**ND**	8.1 ± 4.7	6.1 ± 2.3	17.9 ± 6.8	5.8 ± 1.5	41.1 ± 13.8	**ND**	4.1 ± 2.1	25.2 ± 6.8	**ND**	2.6 ± 1.2	2.3 ± 1.0	4.1 ± 2.1	227.7 ± 113.4
(rice straw)	WR(MH)[a]	31.2 ± 20.1	2.7 ± 1.4	2.3 ± 1.5	**ND**	3.5 ± 1.7	3.9 ± 3.9	9.5 ± 5.8	3.1 ± 2.0	29.8 ± 8.1	**ND**	1.9 ± 1.6	12.3 ± 3.6	**ND**	1.4 ± 0.3	0.8 ± 0.2	2.4 ± 1.0	132.7 ± 65.9
(turr.stik)	BYT(CG)**	37.9 ± 16.5	7.2 ± 3.1	2.8 ± 1.3	**ND**	7.2 ± 1.6	5.5 ± 1.9	16.1 ± 8.5	4.7 ± 2.8	44.8 ± 20.5	**ND**	2.4 ± 1.1	18.7 ± 7.9	**ND**	2.4 ± 0.7	1.2 ± 0.4	2.8 ± 2.2	187.7 ± 75.9

(*continued on next page*)

Table 1 (*continued*)

Fuel type	Sampling locations	PAHs (mg.kg^{-1})														
		Naph	Ace	Anth	Flu	Phe	B[a]A	Flt	Pyr	Chry	B[a]P	D[ah]A	B[b]F	B[k]F	B[ghi]P	I(cd)P	I(cd)F	Σp-PAHs
	Avg.	33.7 ± 25.5	5.3 ± 3.9	3.1 ± 2.9	**ND**	5.4 ± 3.4	4.4 ± 2.8	12.7 ± 7.5	3.9 ± 2.3	36.2 ± 15.1	**ND**	2.4 ± 1.8	17.2 ± 7.9	**ND**	1.9 ± 0.9	1.2 ± 0.9	2.5 ± 1.8	129.9 ± 76.7
MF	PNBE(BR)	25.4 ± 15.2	5.5 ± 2.7	11.8 ± 11.0	**ND**	21.0 ± 5.5	**ND**	10.7 ± 2.6	4.3 ± 3.9	9.4 ± 8.2	12.6 ± 7.5	25.5 ± 14.8	7.7 ± 3.8	4.8 ± 1.6	34.8 ± 19.9	10.7 ± 9.9	7.7 ± 5.5	170.9 ± 98.2
	JP(RJ)	37.7 ± 20.9	12.9 ± 6.1	18.2 ± 6.1	**ND**	24.1 ± 6.6	**ND**	9.7 ± 3.2	3.6 ± 2.5	11.6 ± 11.0	18.9 ± 7.6	27.6 ± 11.5	6.5 ± 2.7	9.9 ± 4.0	28.1 ± 14.1	13.7 ± 4.6	11.9 ± 4.3	210.2 ± 62.1
	GNB(UP)	38.9 ± 20.9	11.6 ± 4.2	33.0 ± 12.9	**ND**	26.3 ± 17.9	**ND**	19.0 ± 4.5	6.9 ± 2.9	11.9 ± 3.7	19.9 ± 10.5	31.4 ± 7.7	14.1 ± 6.5	7.3 ± 4.6	34.5 ± 12.4	25.8 ± 21.7	15.9 ± 3.2	270.1 ± 89.6
	HYB(TG)	27.7 ± 9.4	22.9 ± 15.4	33.6 ± 21.2	**ND**	12.2 ± 4.2	**ND**	11.7 ± 6.3	3.9 ± 1.7	13.2 ± 10.0	22.4 ± 10.8	21.8 ± 4.3	8.2 ± 1.7	3.7 ± 1.9	42.8 ± 26.2	13.2 ± 8.1	17.4 ± 11.4	242.4 ± 95.5
	FZP(PB)	46.2 ± 30.6	28.4 ± 16.1	21.4 ± 14.2	**ND**	6.1 ± 2.6	**ND**	16.5 ± 11.1	5.3 ± 4.3	10.8 ± 7.7	12.9 ± 6.9	13.8 ± 6.3	7.2 ± 4.8	1.8 ± 0.4	29.6 ± 12.9	18.1 ± 14.6	11.6 ± 7.9	223.5 ± 116.0
	RE(HR)	35.4 ± 22.5	39.8 ± 9.2	32.1 ± 4.9	**ND**	14.6 ± 5.9	**ND**	8.9 ± 1.1	5.7 ± 1.3	9.7 ± 5.4	14.1 ± 1.9	32.9 ± 5.2	8.7 ± 2.2	2.3 ± 0.7	30.9 ± 14.4	16.9 ± 11.5	14.2 ± 6.5	251.7 ± 35.9
	BBS(OR)	49.9 ± 28.9	25.6 ± 9.0	23.1 ± 12.3	**ND**	10.2 ± 2.3	**ND**	10.3 ± 8.2	5.0 ± 1.7	9.5 ± 3.2	26.9 ± 12.5	23.9 ± 7.8	9.0 ± 5.6	2.4 ± 0.6	47.58 ± 14.91	11.7 ± 7.6	12.7 ± 8.2	257.6 ± 100.1
	R(CG)	37.7 ± 21.0	9.72 ± 6.2	18.7 ± 12.7	**ND**	9.4 ± 5.6	**ND**	8.0 ± 3.9	4.8 ± 2.3	8.1 ± 4.9	21.24 ± 10.08	18.3 ± 8.9	6.8 ± 3.9	2.9 ± 0.9	23.9 ± 13.3	10.9 ± 8.0	10.1 ± 8.3	181.9 ± 98.1
	Avg.	31.8 ± 20.9	14.60 ± 13.9	19.6 ± 13.7	**ND**	12.9 ± 9.9	**ND**	10.4 ± 6.4	4.3 ± 2.6	8.7 ± 6.6	16.5 ± 9.3	22.1 ± 9.9	7.5 ± 4.4	3.5 ± 3.4	29.7 ± 16.4	11.9 ± 11.5	10.7 ± 7.1	204.2 ± 145.5

[a] ND –not detected.

biomass) sources (Ramdahl and Beecher, 1982; Agency for Toxic Substances and Disease Registry, ATSDR, 1995; Takasuga et al., 2007; Boström et al., 2002; Keyte et al., 2013; Shafy and Mansour, 2016). Assessment of ambient PAHs contributions from unprocessed solid fuels with traditional emission inventories presents a challenge due to variations in reported PAH emissions, spanning over several orders of magnitude (e.g., 1–370 μg of PAHs per kilogram of wood) (Ramdahl and Beecher, 1982). The hydrophobicity nature of PAHs shows great affinity to environmental matrices like soil, water, and air (Senthilkumar et al., 2008). In the atmosphere, low molecular weight (2–4 aromatic ring) PAHs are partitioned in the gases/vapour phase, whereas high molecular weight (5–6 aromatic ring) PAHs present in particulate phase. The International Agency for Research on Cancer (IARC, 2006) reported that high molecular weight PAHs (e.g. benzo(a)pyrene) show potential carcinogenic effects on human health, resulting DNA damage by the formation of adducts in organs (e.g. liver, kidney, lungs) (Vineis and Husgafvel-Pursiainen, 2005; Xue and Warshawsky, 2005). Past studies on indoor and outdoor PAHs have focused on health implications and quantitative analysis of 16 high priority PAHs by the United States Environmental Protection Agency (USEPA) (Yan et al., 2005; Kakareka et al., 2005; Tiwari et al., 2015; USEPA, 2014).

Atmospheric particulate-bound PAHs in India, mainly emitted from solid fuel combustion, have become a matter of concern in recent years (Chakraborty et al., 2014; Ray et al., 2017). EFs of $PM_{2.5}$, temperature-resolved thermal fractions of carbonaceous matter (organic and elemental carbon, OC and EC) along with ionic and elemental species, known as source markers of selected solid fuels at 10 different states in India can be found in Pervez et al. (2018). The present work is the second part of the study on real-world $PM_{2.5}$ emission characterization of household solid fuel combustion in India, emphasizing the thermal and molecular (PAHs) properties of carbonaceous material at 11 locations in 10 different states of India.

The objectives are to: 1) estimate real-world $PM_{2.5}$ particulate PAHs (*p*-PAHs) EFs from solid fuels combustion and 2) evaluate the toxicity levels of different solid fuels. The EFs of sixteen high-priority PAHs in emitted $PM_{2.5}$ were determined. Diagnostic ratios, toxicity levels and annual emission estimates for the five fuel types were calculated.

2. Methodology

2.1. Field campaign

Household cooking emissions were sampled with minivol $PM_{2.5}$ samplers (Airmetrics, Oregon, USA) at 11 sites across 10 states as shown in Supplemental Fig. S1. Five types of solid fuels were selected to represent common cooking practices of India: coal balls (CB), fuel wood (FW), dung cake (DC), crop residues (CR), mixed fuels (MF, a mixture of coal powder with paddy husk soil (10:2:1 ratios), used in Jharkhand and Chhattisgarh states). Details of the study design, site selection, sampling frequency and duration, transportation and preservation of $PM_{2.5}$ samples, and associated QA/QC have been documented in Pervez et al. (2018). Sampling was conducted twice a day during morning and evening cooking time using five different types of traditional cook stoves for the period of March–June 2017.

2.2. Extraction method

Particulate PAHs were collected on pre-fired (900 °C for 3 h) 47-mm quartz microfiber filters (Whatman QMA) (Chow et al., 1993). One-fourth of the filter was cut into strips and ultrasonically extracted with 50 mL of high-performance liquid chromatography (HPLC) grade dichloromethane (DCM) for 30 min. The extraction procedure was repeated twice to ensure maximum extraction efficiency (Bi et al., 2003; Singh et al., 2013). The extract was evaporated ~5 mL using a rotary evaporator at 30–40 °C prior to a clean-up process. The extract was then loaded on top of the column (10 cm × 1.0 cm id) slurry packed with 5 g

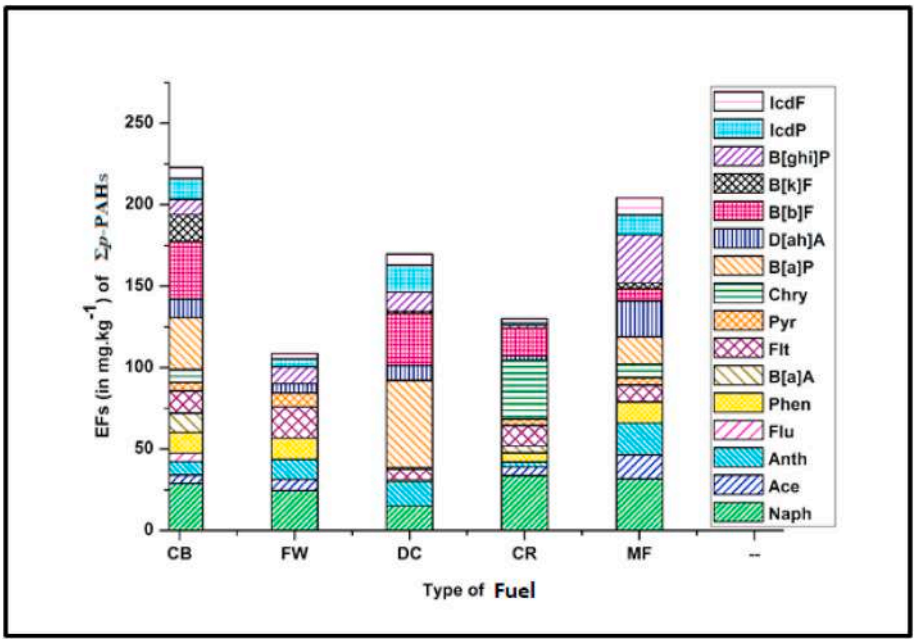

Fig. 1. Averaged Emission Factor (mg.kg^{-1}) of 16 PAHs for burning of coal balls (CB), fuel wood (FW), dung cakes (DC), crop residues (CR), mixed fuels: dung cakes + fuel wood (MF) during real-world household cooking practices in eleven locations across the ten different States of India.

silica gel mesh. The column was eluted with DCM and concentrated to 1 mL under an ultrapure nitrogen gas flow and stored in vials at low temperature (−4 °C) (Singh et al., 2013; Dewangan et al., 2014). The samples were filtered with 0.45 μm polyvinylidene fluoride (PVDF) syringe (Millipore) prior to injection for analysis . Field blank samples were extracted following the same procedure. Recovery of PAHs was determined by spiking blank filter paper with a known concentration standard.

2.3. Gas chromatography –mass spectrometry/mass spectrometry analysis

Particulate PAHs are analysed using an automated GC-MS/MS (GC-Trace 1300; MS- TSQ DUO) equipped with a 30 m long silica capillary column(Thermo Scientific Trace GOLD GC Column, Model TG-5MS) (0.25 mm ID, 5% phenylmethylpolysiloxane stationary phase, 0.25 μm film thickness). Samples were injected (0.1 μl) in split mode (1:10), with the injection port at 290 °C and an initial oven temperature of 150 °C for 2 min. The oven temperature was ramped to 250 °C at 50 °C/min, followed by 10 °C/min ramp rate to 300 °C and held at 300 °C for 7 min. Helium was used as the carrier gas at a 1.0 mL/min flow rate. The total ion chromatograms were analysed qualitatively with the aid of the U.S. National Institute of Science and Technology (NIST) 2.0 mass spectral library after background subtraction. Chromatographic peaks with mass spectral match of 80% or greater were retained, while peaks showing significant abundance but <80% spectral match were noted by their retention times. For quantitative analysis (U.S.EPA 610, 1984), a mixture of 16 PAH standards (1000 μg/L by Supelco, Sigma-Aldrich) was used to identify the relationships between various fuels and air/-fuel ratios (Devangen et al. 2014). Sixteen PAHs were identified and quantified including 2 rings: naphthalene (Naph), 3 rings: acenaphthene (Ace), fluorene (Flu), phenanthrene (Phe), anthracene (Anth), 4rings: fluoranthene (Flt), pyrene (Pyr), benz[a]anthracene (BaA), chrysene (Chry), 5 rings: benzo[b]fluoranthene (BbF), benzo[k]fluoranthene (BkF), benzo[a]pyrene (BaP), dibenz[a,h]anthracene (DahA), 6 rings: benzo[g,h,i]perylene (BghiP), indeno[1,2,3-cd]pyrene (IcdP) and indeno[1,2,3-cd] fluoranthene (IcdF).

2.4. Quality assurance/quality control (QA/QC)

Known concentrations of the standard (EPA 625–16 PAHs mix) were added to 10% of the total samples to determine the recovery ratio. The average recoveries range is 70–80% for total PAHs. Both field and solvent blanks were also analysed to ensure adequate QA/QC. An insignificant amount (<5%) of *p*-PAHs was found in the field/solvent blanks. The method detection limit (MDL) has been established as three times the standard deviation of concentration of the target species for seven repeat injections of the lowest concentration of the calibration curve.

2.5. Emission factor (EF) and annual emission budget

The method used to calculate PAHs EFs is reported elsewhere (Andreae, and Merlet, 2001; Dhammapala, et al., 2007) and described in Pervez et al. (2018). It is based on the conversion of carbon (C) in the form of carbon dioxide (CO_2) and carbon monoxide (CO), from fuel combustion. The fuel-based EFs can be estimated from in-plume measurements (Moosmuller et al., 2009).

3. Results and discussion

3.1. Emission factors of PAHs

Table 1 summarises state-wise averaged EFs by fuel types for the 16 PAHs. There are some variabilities in fuel quality depending on the regions; type of sampling, stoves, and cooking environment leads to a range of EFs. Among the four most volatilized PAHs (i.e., Naph, Ace, Anth, and Flu) emissions were detected for all five fuel types with the exception of Ace from dung cake (DC) and Flu, from coal balls (CB). Fig. 1 shows that average emissions varied by 1.7 fold among five fuel types. The highest Σ*p*-PAHs was found for coal balls of 244.9 ± 106 mg kg^{-1}, ranging 102–490 mg kg^{-1}, followed by MF 223.4 ± 89 mg kg^{-1}, range 81–448 mg kg^{-1}; DC of 196.1 ± 91.3 mg kg^{-1} (range: 70–384 mg kg^{-1}), CR 137.1 ± 56 mg kg^{-1} (range: 71–305 mg kg^{-1}), and fuel wood (FW) 127.7 ± 62.9 mg kg^{-1} (range: 59–348 mg kg^{-1}). Higher *p*-PAH EFs for CB might be due to the higher content of unprocessed carbon fraction (Keene, et al., 2006) and the smouldering combustion condition favouring the condensation of PAHs in particulate phase (Jenkins et al.,

Table 2
Comparison of EFs of ∑ *P*-PAHs of 16 USEPA Criteria PAHs, measured for burning of coal balls (CB), fuel wood (FW), dung cakes (DC), crop residues (CR), mixed fuels: dung cakes + fuel woods (MF) with those reported from previous studies. Only reported the EFs of 16 USEPA criteria PAHs for similar types of fuel combustion are included.

Fuel Type	*p*-PAHs (mg/kg)	study type	References
CB (India)	**239.6 ± 114.7**	**Household combustion –real world**	**present study**
Coal combustion (China)	0.85–214	Residential combustion	Shen et al. (2013)
Coal briquettes and Charcoal	25–100	Domestic combustion	Oanh et al.(1999)
FW	**141.2 ± 84.7**	**Household combustion –real world**	**Present study**
	45.28	test chamber study	Singh et al. (2013)
	43.9 ± 4.3	test chamber study	Gadi et al. (2012)
	24–114	open burning	Keshtkar and Ashbaugh (2007)
Birch Firewood	0.2–16		Hedberg et al. (2002)
	2.3	chamber based study	Venkataraman et al. (2002)
Fireplace/ softwood	79.8		McDonald et al., 2000
Fuelwood (Pine)	6.9		Rogge et al. (1998)
FW	6.4–8.9		Smith, 2000
FW	28	test chamber study	Ramdahl and Beecher (1982)
DC	**181.4 ± 102.9**	**Household combustion –real time**	**present study**
	56.46	test chamber study	Singh et al. (2013)
	59.7 ± 4.4	test chamber study	Gadi et al. (2012)
CR	**163.8 ± 91.1**	**Household combustion –real world**	**present study**
	35.84	test chamber study	Singh et al. (2013)
	35.9 ± 1.9	test chamber study	Gadi et al. (2012)
sugarcane	8.18 ± 3.26	chamber study	Hall et al. (2012)
Wheat straw	62 ± 35	test chamber study	Shen et al. (2013)
	140	test chamber study	Keshtkar and Ashbaugh (2007)
	18.6	open burning	Keshtkar and Ashbaugh (2007)
	240–571	test chamber study	Kakareka and Kukharchyk (2003)
MF	**205.6 ± 90.1**	**Household combustion –real world**	present study

1996). Maximum *p*-PAHs EFs for each fuel type were found at different location, ranging 266–312 mg kg^{-1} these includes: CB at JRI JH. (312.1 ± 105.6 mg kg^{-1}); for FW at CNB (UP) (174.6 ± 73.1 mg kg^{-1}); for DC at RE (HR) (183.9 ± 53.9 mg kg^{-1}); for CR at VSKP (AP) 83.9 ± 53.9 mg kg^{-1}); and for MF at RE (HR) (266.2 ± 22.4 mg kg^{-1}).

Statistically significant variability with p values < 0.05 at 95% confidence interval was found for all individual PAHs across the fuel types and sampling locations based on two-way ANNOVA (SPSS Ver. 16). Among all fuels Σ*p*-PAHs EFs, FW showed the highest variability (59.9–174.6 mg kg^{-1}) across all the locations.

The coefficient of spatial variations (CV) for Σ*p*-PAH EFs across the 11 locations, (by dividing the standard deviation to the corresponding grand mean of locations averaged EFs) varied from 40 to 49% among the five fuel types: 49.3% (FW), 46.5% (DC), 43.2% (CB), 41.1% (CR) and 39.8% (MF) (Röösli et al., 2001).

Table 2 compares the Σ*p*-PAH EFs with previous studies, Σ*p*-PAHs EF for coal balls (CB) (239.6 ± 114.7 mg kg^{-1}) was higher than those reported for residential coal combustion (0.85–214 mg kg^{-1}) by Shen et al. (2013) in China, and more than two-fold higher than the coal briquettes and charcoal cook stove combustion (25–100 mg kg^{-1}) by Oanh et al. (1999) in Southeast Asia. When compared with test chamber studies, the average Σ*p*-PAH EFs for dung cake (DC) (181.4 ± 102.9 mg kg^{-1}) was 3.2–3.4 fold higher than 59.7 ± 4.4 mg kg^{-1} in Gadi et al. (2012), and 56.46 mg kg^{-1} in Singh et al. (2013). Similarly, Σ*p*-PAH EF for fuel wood (FW) (141.15 ± 84.72 mg kg^{-1}) were 1.6–66.5 fold higher than test chamber studies 45.28 mg kg^{-1} by Singh et al. (2013); 43.9 ± 4.3 mg kg^{-1} by Gadi et al. (2012); 28.0 mg kg^{-1} by Ramdahl and Beecher (1982) and 2.3 mg kg^{-1} by Venkataraman et al. (2002); and However fuel wood combustion by residential cook stove in India are lower than these of residential furnace (2890 mg kg^{-1}) (Kakareka et al., 2005) and hard wood-burning activity (Khalfi et al., 2000). In case of crop residue (CR), EFs (163.8 ± 91.1 mg kg^{-1}) was similar in magnitude to the test chamber study of 140 mg kg^{-1} by Keshtkar and Ashbaugh (2007), but much higher than 62 ± 35 mg kg^{-1} by Shen et al. (2013); 35.9 ± 1.9 mg kg^{-1} by Gadi et al. (2012), 35.84 mg kg^{-1} by Singh et al. (2013) and open burning; 18.6 mg kg^{-1} by Keshtkar and Ashbaugh (2007); 8.18 ± 3.26 mg kg^{-1} (Hall et al., 2012), EFs for coal balls (CB) showed predominance of high molecular weight PAHs (H*p*-PAHs) ranging 8–35 mg kg^{-1} with the two highest PAH EFs found for benzo[b]fluoranthene (B[b]F) of 35.1 ± 23.1 mg kg^{-1} and benzo[a]pyrene (B[a]P) of 31.8 ± 21.6 mg kg^{-1} commonly found in coal combustion other elevated PAH EFs exceeding 10 mg kg^{-1} includes B[k]F (16.5 ± 11.3 mg kg^{-1}); Flt (13.6 ± 9.3 mg kg^{-1}); IcdP(12.9 ± 9.5 mg kg^{-1}); B[a]A (11.9 ± 9.7 mg kg^{-1})and D[ah]A (11.5 ± 9.7 mg kg^{-1}). Elevated B[ghi]P (9.4 ± 6.4 mg kg^{-1}) and, Chry (8.1 ± 5.9 mg kg^{-1}) was also found Average EFs of B[a]P for dung cake (DC) 53.5 ± 43.2 mg kg^{-1} was 5.2 fold higher than the test chamber studies (Singh et al., 2013). For fuel wood (FW) higher EFs were found for Naph (24.46 ± 20.38 mg kg^{-1}); Flt (19.2 ± 18.8 mg kg^{-1}); with elevated Phe (13.1 ± 12.5 mg kg^{-1}) and B[ghi]P (10.2 ± 8.9 mg kg^{-1})., whereas elevated EFs for Naph (33.7 ± 25.5 mg kg^{-1}), B[b]F (17.2 ± 7.9 mg kg^{-1}), Flt (12.7 ± 7.5 mg kg^{-1}) were found in crop residue (CR). Mixed fuel (MF) were dominated by Naph (31.8 ± 20.9 mg kg^{-1}), B[ghi]P (29.7 ± 16.4 mg kg^{-1}), D[ah]A (22.1 ± 9.9 mg kg^{-1}) and Anth (19.6 ± 13.7 mg kg^{-1}) different. These variations might be due to the presence of high moisture content, design of cook stoves and burning phase of fuels (Jenkins et al., 1996).

Mass fraction of 2–6 rings PAH to Σ*p*-PAH is given in Fig. 2. Abundance of EFs low (2–3 rings) and high (4–6 rings) PAHs varied by fuel types with a predominance of the 4–6 ring PAHs for all but fuel wood and crop residue. Σ*Hp*-PAHs (4–6 ring) emissions were highest in coal balls (CB) (171.34 ± 96.17 mg kg^{-1}) whereas Σ*Lp*-PAHs (2–3 ring) were predominant in CR (77.9 ± 53.9 mg kg^{-1}) as shown Table S1. Higher emissions of H*p*-PAHs were found from the combustion of coal balls (CB), which might be due to the physical adsorption of PAHs in the particulate phase only (Zou, et al., 2003). Fig. 3 shows the highest H*p*-PAHs to total PAHs was 72.7% dung cake followed by 67.2% for coal balls and 63.2% for mixed fuel (MF). Combustion efficiency has been reported to significantly impact emission rates of particulate organics (Gupta et al., 1998; Tissari et al., 2019). Pervez et al. (2018), attributed higher emissions of H*p*-PAHs for coal balls, dung cake and mixed fuel with modified combustion efficiency of 0.88–0.99.

3.2. Diagnostic ratio

PAHs source diagnostic ratios and binary diagnostic ratios have been used as a tool to categorize and assess the emission sources. These ratios are useful in understanding PAH origins of different environmental media: air (gas + particle phase), water, sediment, soil, as well as bio-monitored organisms such as leaves or coniferous needles, and mussels (Tobiszewski, and Namiesnik, 2012). These ratios distinguish PAHs originating from petroleum products, petroleum combustion, and solid fuel (bio- and fossil fuels) combustions. PAH diagnostic ratios also showed intra-source variability as well as inter-source similarity (Galarneau, 2008). EF ratios of eight groups that are commonly found for

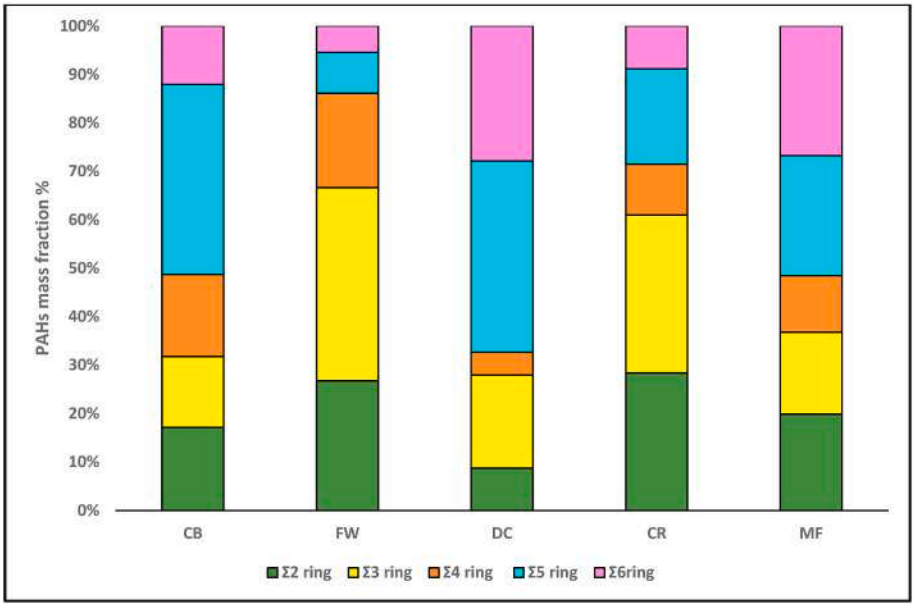

Fig. 2. Average percentage of 2–6 ring PAHs' mass fractions to Σ*Tp*-PAHs, as a function of different fuels during real-world household cooking practices in eleven locations across the ten different States of India. 2 rings: naphthalene (Naph), 3 rings: acenaphthene (Ace)+ fluorene (Flu) + phenanthrene (Phe) + anthracene (Anth), 4 rings: fluoranthene (Flt) + pyrene (Pyr) + benz[a]anthracene (BaA) + chrysene (Chry), 5 rings: benzo[b]fluoranthene (BbF) + benzo[k]fluoranthene (BkF) + benzo[a]pyrene (BaP), dibenz[a,h]anthracene (DahA), 6 rings: benzo [g,h,i]perylene (BghiP) + indeno[1,2,3-cd]pyrene (IcdP) + indeno[1,2,3-cd] fluoranthene (IcdF).

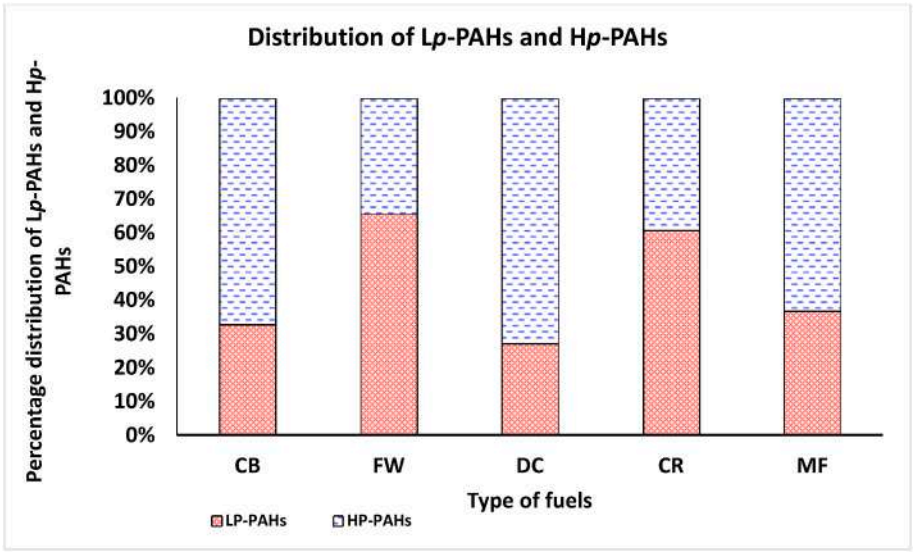

Fig. 3. Averaged Percentage distribution of L*p*-PAHs and H*p*-PAHs in T-PAH EFs for burning of different fuels during real-world household cooking practices in eleven locations across the ten different States of India. L*p*- PAHs (including 2–3 rings PAHs): naphthalene (Naph), acenaphthene (Ace), fluorene (Flu), phenanthrene (Phe), anthracene (Anth), H*p*-PAHs (including 4–6 rings PAHs): fluoranthene (Flt), pyrene (Pyr), benz[a]anthracene (BaA), chrysene(Chry), benzo[b]fluoranthene(BbF),benzo[k]fluoranthene (BkF), benzo[a]pyrene (BaP), dibenz[a,h]anthracene (DahA), benzo[g,h,i]perylene (BghiP), indeno[1,2,3-cd]pyrene (IcdP) and indeno[1,2,3-cd] fluoranthene (IcdF).

fossil fuel and biomass combustion emissions includes: Anth/(Anth + Phe), Flt/Pyr, Flt/(Flt + Pyr), B[a]P/IcdP, B[a]P/B[ghi]P, I(cd)P/B[ghi]P, I(cd)P/(I(cd)P + B[ghi]P) and B[a]A/(B[a]A + Chry) emissions (Rajput et al., 2011; De La Torre-Roche et al., 2009; Bari et al., 2010; Hays et al., 2005; Jenkins et al., 1996) all compare with past studies for five fuel types in Table 3.

3.2.1. Simple source diagnostic ratio

The ratios of Flt/Pyr, Bap/IcdP, Bap/BghiP, and IcdP/BghiP were used to identify the fossil and biomass fuel burning sources. This study reported 10 fold difference in Flt/Pyr ratios 1.09–9.66 ranging from 1.09 to 3.54 for MF; 1.22–6.19 for FW; 2.78–3.69 for CB; 3.35–9.66 for DC; and 3.12–3.66 for CR. Similarly Bap/BghiP, ratios were ranged between 0.88 and 9.88 with 2.17–3.18 for CB; 2.35–6.19 for DC; 0.88–2.46 (MF), 0.43–9.88 (3.13–4.14 (CB); 1.73–9.88 (DC); 0.43–0.99 (MF)]. Ratios IcdP/BghiP are less variable from 0.32 to 2.68 with 1.00–1.95 (CB); 0.32–0.71 (FW); 1.31–2.68 (DC); 0.52–0.64 (CR); 0.35–1.58 (MF) respectively. Diagnostic ratios of post and present studies are given in Table 3.

3.2.2. Binary diagnostic ratios

The EFs ratios of Anth/(Anth + Phe) of <0.1 and >0.1 are used to infere petrogenic and pyrogenic sources respectively (Pies et al., 2008). This study yield high Anth/(Anth + Phe) EFs ratios of 0.36–0.80 with lower ratios for crop residue 0.36 ± 0.09 and coal balls: 0.36 ± 0.17; 0.43 ± 0.21 for fuel wood; and highest 0.89 ± 0.10 for dung cake;; 0.56 ± 0.18 for mixed fuel suggesting less efficient combustion in the presence of insufficient oxygen. Ratios of Flt/(Flt + Pyr), have been used to indicate for many sources: <0.5 for gasoline engine (Fang et al., 2004); >0.5 for diesel engine) (Rogge et al., 1993; Mandalakis et al., 2004), >0.50 coal combustion (Yunker, et al., 2002), >0.60 wood combustion) (Dvorska, et al., 2011)), and in the range of 0.45–0.53 rice straw burning (Jenkins et al., 1996), and 0.49–0.55 biomass burning (Wiriya, et al., 2016). As expected, ratios of Flt/(Flt + Pyr) in all five fuel types exceeded 0.5 consistent with those found in chamber studies (Hays et al., 2005; Jenkins et al., 1996). However, these ratios are lower for the open burning studies; 0.4–0.5 for fossil fuel combustions, 0.43 ± 0.04 for wood burning and 0.49 ± 0.03 for crop residue burning (Rajput et al., 2011).

Table 3
Averaged values of source diagnostic ratios (mean ± standard deviation) of *p*-PAHs for emissions resulting from burning of coal balls (CB), fuel wood (FW), dung cakes (DC), crop residues (CR), mixed fuels: dung cakes + fuel woods (MF) during household cooking practices in eleven locations across the 10 different states of India and comparison with those reported for other industrial and domestic combustions.

sources	Study type	Anth/(Anth + Phe)	Flt/Pyr	Flt/(Flt + Pyr)	B[a]P/I(cd)P	B[a]P/BghiP	I(cd)P/B[ghi]P	I(cd)P/(I(cd)P + B[ghi]P)	B[a]A/(B[a]A + Chry)	Reference
Coal balls	Real-world household combustion	0.36 ± 0.17	2.63 ± 1.90	0.68 ± 0.17	2.47 ± 1.08	3.40 ± 1.34	1.37 ± 0.60	0.57 ± 0.09	0.56 ± 0.18	Present study
Fossil- & bio-fuels		0.14 ± 0.04	0.90 ± 0.09	0.47 ± 0.03	0.70 ± 0.54	0.74 ± 0.54	1.07 ± 0.23	0.51 ± 0.06	–	Rajput et al. (2011)
Coal combustion		–	–		–	–	–	–	0.2–0.35	Akyüz and Cabuk (2010)
Fossil fuel combustion		–	–	0.4–0.5	–	–	–	–	–	De La Torre-Roche et al. (2009)
Coal combustion		–	–	1.0–1.4	–	–	–	–	–	Lee et al. (1995)
Fuel wood	real world household combustion	0.43 ± 0.21	2.22 ± 1.89	0.65 ± 0.15	–	–	0.48 ± 0.32	0.31 ± 0.11	–	present study
Wood-fuel	Chamber based	0.18 ± 0.03	0.75 ± 0.12	0.43 ± 0.04	–	–	–	–	–	Bari et al. (2010)
Grass, wood combustion		–	–	>0.5	–	–	–	–	–	De La Torre-Roche et al. (2009)
Wood burning		–	–		–	–	–	–	0.79	Dickhut et al. (2000)
Dung cake	real world household combustion	0.89 ± 0.10	5.80 ± 4.56	0.83 ± 0.10	3.25 ± 2.88	4.56 ± 4.44	1.40 ± 1.27	0.55 ± 0.15		Present study
Crop residues	real world household combustion	0.36 ± 0.09	3.22 ± 0.95	0.76 ± 0.05	–	–	0.64 ± 0.30	0.38 ± 0.09	0.11 ± 0.05	Present study
Paddy-residue	Test chamber study	0.17 ± 0.01	0.97 ± 0.21	0.49 ± 0.05	1.63 ± 0.45	2.20 ± 0.20	1.43 ± 0.51	0.58 ± 0.09	–	Hays et al., (2005); Jenkins et al., (1996)
Wheat-residue	Test chamber study	0.21 ± 0.01	1.05 ± 0.08	0.51 ± 0.02	1.22 ± 0.66	1.43 ± 0.37	1.28 ± 0.39	0.55 ± 0.08	–	Hays et al., (2005); Jenkins et al., (1996)
Wheat-residue	Open biomass burning	0.10 ± 0.05	0.97 ± 0.13	0.49 ± 0.03	0.34 ± 0.09	0.27 ± 0.15	0.80 ± 0.27	0.43 ± 0.08	–	Rajput et al. (2011)
Paddy-residue	Open biomass burning	0.15 ± 0.03	0.84 ± 0.04	0.46 ± 0.01	0.64 ± 0.16	0.64 ± 0.21	0.98 ± 0.13	0.49 ± 0.03		Rajput et al. (2011)
MF	real world household combustion	0.56 ± 0.18	2.44 ± 1.55	0.69 ± 0.11	1.37 ± 0.95	0.56 ± 0.27	0.40 ± 0.56	0.27 ± 0.14	–	Present study
Vehicle emission		–	–	–	–	–	–	–	>0.35	Akyüz and Cabuk (2010)
		–	–	–	–	–	–	–	0.53	Dickhut et al. (2000)

Ratios of B[a]A/(B[a]A + Chry) in the range of 0.2–0.35 infer coal combustion (Akyüz and Cabuk, 2010) and higher (0.79) for wood burning (Dickhut et al., 2000). Ratios of B[a]A/Chry found in coal balls (0.56 ± 0.18) and crop residue (0.11 ± 0.05) were ~2-fold higher than those reported Akyüz and Cabuk (2010) for a chamber-based study. These values are helpful in differentiating the emissions of fossil fuels and solid biomass combustion applied in this study. .

Moreover, I(cd)P/(I(cd)P + B[ghi]P) ratio was also used to distinguish the fossil fuel from biomass combustion emissions. This study yield ratio >0.5 for coal balls and dung cake and <0.5 for the other three fuels.

It should be noted that these source diagnostic ratios, determined by the respective PAH's concentrations in the emissions plume does not necessarily represent the same *p*-PAH sources in air. These ratios change with vapour/particle partitioning of PAH compounds in the atmosphere via dispersion and aging (Zhang, et al., 2005). The Measured diagnostic ratios of Anth/Phe, BaA/Chry, BbF/BkF, and Flt/Pyr in this study showed significant variation compared to those reported for outdoor air (Fang et al., 2004; Bourotte et al., 2005; Ravindra et al., 2008). This indicates that these diagnostic ratios should be used with caution for source identification.

3.3. Toxicity assessment

The PAHs are toxic upon chronic human exposure through inhalation of combustion fumes that lead to health hazards. The toxicity of the solid fuels are assessed based on the individual PAH emission, potential inhalation exposure integrated life time cancer risk (ILCR), and non-cancer hazard potential. Similar methodology has been used in previous studies to assess human health impact from air toxics (Mukherjee et al., 2012, 2014; Srivastava and Som, 2007).

3.3.1. Exposure assessment

The potential inhalation exposure (E_i in mg/kg/day for an individual PAH species 'i) for a person engaged in cooking using solid fuel can be calculated as follows

$$E = C_i \times IR_a \times ED/BW_a \quad (1)$$

Where C_i is the average concentration of the PAH specie 'i' in combustion plume in mg/m^3; IR_a is the inhalation rate for an adult (0.83 m^3/h); ED is the exposure duration (2 h/day) and BW_a is average body weight for Indian adult (60 kg) (ICMR, 2010).

3.3.2. ILCR and non-cancer Hazard assessment

The integrated life time cancer risk or ILCR for PAHs species esti-

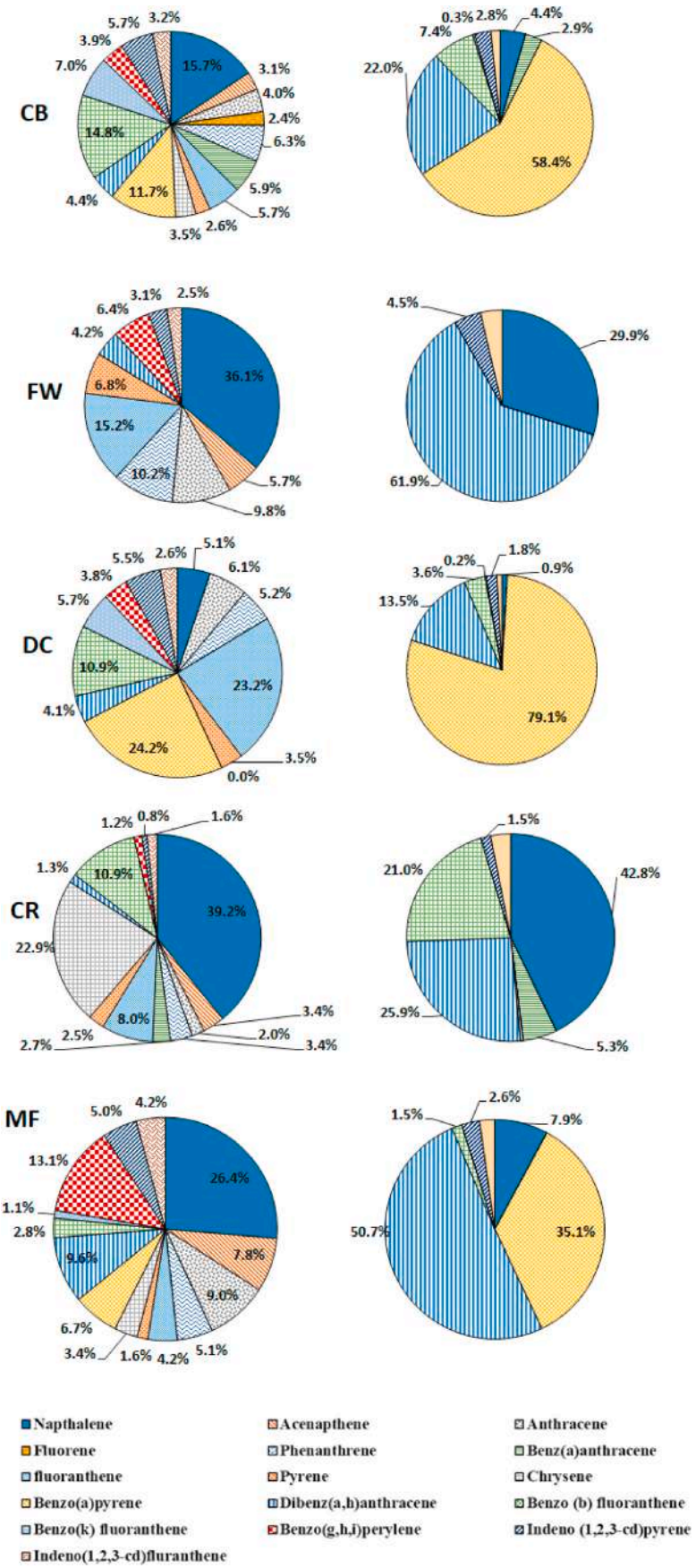

Fig. 4. Percent contribution of individual PAH to: (a) total *p*-PAH emissions (b) total carcinogenic risk due to combustion of solid fuel.

Table 4
Ranking the fuel as per the toxicity.

Solid fuel	Rank	*p*-PAH Emission compared to FW	toxicity compared to FW	most toxic *p*-PAH species
Fuel wood	1	1	1	Dibenzo(a,h) anthracene
Crop resedue	2	3	2	Naphthalene
Dung Cake	3	1	5	Benzo (a)pyrene
Mixed fuel	4	19	52	Dibenzo(a,h) anthracene
Coal ball	5	25	76	Benzo (a)pyrene

Toxicity scale:1 - least toxic; 5 - most toxic.

Table 5
Annual emission estimates of *p*-PAHs from household solid fuel burning emission in India.

PAHs	Fuel type			
(M.yr^{-1})	Coal balls	Fuel wood	Dung cake	Crop residues
Naph	1.5 ± 0.9	2251.2 ± 1954.4	341.2 ± 333.4	552.1 ± 401.1
Ace	3.1 ± 2.2	712.3 ± 640.1		93.1 ± 69.1
Anth	5.2 ± 2.5	1125.0 ± 1100.6	340.5 ± 276.2	51.0 ± 48.1
Flu	2.7 ± 2.3	–		
Phen	6.9 ± 6.5	1216.2 ± 1161.31	30.3 ± 21.5	90.2 ± 64.1
B[a]A	6.8 ± 5.1	–		65.3 ± 49.0
Flt	7.3 ± 4.8	1782.11 ± 1653.0	137.8 ± 135.0	215.3 ± 132.2
Chry	3.3 ± 3.1	802.1 ± 801.0	19.0 ± 15.2	67.3 ± 40.4
Pyr	5.2 ± 3.1	–		627.4 ± 264.7
B[a]P	18.0 ± 12.3	–	1214.7 ± 975.1	
D[ah]A	6.1 ± 5.0	491.1 ± 483.5	218.7 ± 181.0	40.4 ± 31.3
B[b]F	18.5 ± 4.7	–	717.7 ± 640.0	291.1 ± 144.5
B[k]F	8.9 ± 5.7	–	32.7 ± 28.36	1061.1 ± 502.5
B[ghi]P	4.6 ± 4.2	860.1 ± 815.7	265.7 ± 223.1	32.1 ± 20.9
IcdP	6.9 ± 3.3	516.4 ± 491.2	369.7 ± 291.0	20.3 ± 9.2
IcdF	3.9 ± 3.8	300.3 ± 292.7	154.7 ± 145.1	41.1 ± 25.2
[a]Σ*p*-PAHs	0.1 ± 0.01	10.0 ± 5.8	3.8 ± 2.1	3.2 ± 0.2

[a] whereas indicate the value of Σ*p*-PAHs in Gg.yr^{-1}; Mega gram per year abbreviated as M.yr^{-1}.

mated as

$$ILCR_i = C_i \times UR_i \quad (2)$$

where UR_i is the inhalation unit risk of the PAH species 'i'.

The non-cancer health hazard from exposure to HAPs has been estimated as hazard quotient, (HQ),

$$HQ = C_i / RfC_i \quad (3)$$

where RfC_i is the chronic inhalation reference concentration for PAHs species 'i', below which adverse health effects are not likely to occur (RAIS, 2020).

The cumulative non-cancer health hazard from exposure to all estimated PAHs is expressed as the hazard index (HI):

$$HI = \sum_i HQ \quad (4)$$

The chronic inhalation reference concentration and unit risk values for individual compounds have been adapted from the US EPA, The Risk Assessment Information System (RAIS, 2020). The supporting data has been given in Tables S2–S4.

The non-cancer hazard index has been found <1.0 for all cooking fuels, indicating no harmful exposure from solid fuel fumes. However, 7 of the 16 measured PAHs (i.e., B[a]A, Chry, B[a]P, D[ah]A, B[b]F, B[k]F, IcdP) are known as probable/possible carcinogens (Nisbet and LaGoy, 1992; Jia et al., 2011; Ramírez et al., 2011; IARC, 2019). Fig. 4 compares the relative percentage concentrations of individual 16 PAHs to total-PAHs and compares of 8 PAHs to carcinogenic toxicity, for five fuel types. B[a]P was the major contributor to PAHs carcinogenic toxicity risks for dung cake (79%), coal balls (58%), and mixed fuel (35%), Fig. 4 (b), In contrast, it contributed 24%, 12%, and 7% of the total of *p*-PAHs Fig. 4(a), for the respective fuels. Dibenz(a,h)anthracene was the second largest contributor to PAH carcinogenic risks with 62% for fuel wood and 51% for mixed fuel; corresponding to 4% and 10% PAHs emission from respective fuels. Carcinogenic contribution for naphthalene (Naph) was also high and accounted for 44% in crop residues and 31% in fuel wood, corresponding to 39% and 36% of the total PAHs, from respective fuels. Table 4 shows emissions and toxicity rankings compared to the fuel wood (FW). The cancer risk from *p*-PAH in fuel wood (1.4×10^{-6}) marginally higher than the acceptable risk of one in a million. The cancer risks for coal balls and mixed fuels were higher than other fuels.

3.4. Annual PAHs emission estimates

The biomass fuel consumption data for Indian states were obtained based on a survey of Indian government agencies (TERI. 2015) as reported by Pervez et al. (2018). Annual emissions were calculated using the method by Dhammpala et al. (2007). Without contribution for mixed fuel combustion, total PAHs emissions from household solid fuel-burning were 17.1 ± 8.1 Gg yr^{-1}, accounting for 0.82% of the total $PM_{2.5}$ emissions (2.00 Tg yr^{-1}) from household solid fuel-burning activity in India. Table 5 showed 10 ± 5.8 Gg yr^{-1} for fuel wood, 3.8 ± 2.1 Gg yr^{-1} (DC), 3.2 ± 0.1 Gg yr^{-1} for crop residue, 0.1 ± 0.1 Gg yr^{-1} for coal balls.

4. Conclusion

The evaluation of emission factors, based on the real-world sampling of domestic cooking emissions for 10 Indian states, shows the highest PAH emissions in coal balls and lowest in fuel wood. All of the five most commonly used solid fuels have shown 4–6 fold higher emissions than those of measured in open burning or laboratory test chamber studies. Large variations were found in cooking characteristics, air supplies, and moisture content in the flaming and smouldering phases of combustion. Naphthalene, fluorene, anthracene, phenanthrene, fluoranthene, dibenzo[ah] anthracene, and benzo [ghi] perylene, were estimated at significant levels in emission plumes. Emission factors of mixed fuel (MF) showed the lowest variability (39.8%) with the highest variability (49.3%), found in fuel wood (FW), attributing to the moisture content. High EF variabilities were also found for dung cake (46.5%), coal balls (43.2%) and crop residues (41.1%). Diagnostic ratios of IcdP/(IcdP + BghiP) > 0.5 were found to be associated to be with coal ball fuel emission, whereas ratios of Flt/(Flt + Pyr) > 0.5 were linked to crop residue burning. Higher carcinogenic risk toxicity order was found for coal ball > mixed fuel > dung cake > crop residue > fuel wood. High variabilities associated with PAHs EFs from household solid fuel combustion activities across the selected regions address the need to assess PAHs emissions from different types of burning activities in real-world situations and on a regional scale to evaluate nation-wide emission estimates.

Credit author statement

Madhuri Verma: Field sampling, chemical analysis, data analysis, writing-original draft preparation. **Shamsh Pervez**: PI of the project, designing the study, conceptualization, visualization and investigation, paper editing, data-validation, supervising and leading the study. **Judith C. Chow**: Assisting in designing the study and data analysis, Reviewing-Paper Editing, English and Grammar correction. **Dipanjali**

Majumdar: Assisted in chemical analysis of PAHs and editing the manuscript. **John G. Watson**: Assisting in designing sampling plan, Reviewing-Paper Editing, English and Grammar correction. **Yasmeen Fatima Pervez**: Participated in designing sampling plan and assisted in chemical analysis. **Manas Kanti Deb**: Co-Investigator of the sponsored project, participated in writing the manuscript. **Kamlesh Shrivas**: Assisted in sample extraction procedures and editing the manuscript. **Vikas Kumar Jain**: Assisted in sampling campaign and editing the manuscript. **Noor A. Khan**: Co-investigator of the sponsored project, participated in PAHs analysis and editing the manuscript. **Papiya Mandal**: Co-investigator of the sponsored project and assisted in editing the manuscript. **Rajan K. Chakrabarty**: Assisted in designing the study, Reviewing-Paper Editing, English and Grammar correction.

Declaration of competing interest

The authors declare the following financial interests/personal relationships which may be considered as potential competing interests: Shamsh Pervez reports financial support was provided by Science and engineering research board (SERB). Rajan Chakrabarty reports partial financial support of U.S. National Science Foundation.

Acknowledgement

This study was supported by the Science and Engineering Research Board (SERB) project (EMR/2015/000928) and partially supported by the Department of Science and Technology, Ministry of Science and Technology, New Delhi (DST) FIST program (SR/FST/CSI-259/2014 (c)) and UGC-SAP-DRS-II program (F-540/7/DRS-II/2016 (SAP-I)). Rajan Chakrabarty (RC) acknowledges the partial support of U.S. National Science Foundation (AGS-1455215, and AGS-1926817).

Appendix A. Supplementary data

Supplementary data to this article can be found online at https://doi.org/10.1016/j.apr.2021.101142.

References

Akyüz, M., Cabuk, H., 2010. Gas–particle partitioning and seasonal variation of polycyclic aromatic hydrocarbons in the atmosphere of Zonguldak, Turkey. Sci. Total Environ. 408 (22), 5550–5558.

Andreae, M.O., Merlet, P., 2001. Emission of trace gases and aerosols from biomass burning. Glob. Biogeochem. Cycles 15 (4), 955–966.

ATSDR, 1995. Toxicological Profile for Polycyclic Aromatic Hydrocarbons (PAHs). United States Department of Health and Human Services, Public Health Service, Atlanta, GA. http://www.atdsr.cdc.gov/toxpro.les/phs69.

Bi, X.H., Sheng, G., Peng, P., Chen, Y., Zhang, Z., Fu, J., et al., 2003. Distribution of particulate- and vapor-phase n-alkanes and polycyclic aromatic hydrocarbons in urban atmosphere of Guangzhou, China. Atmos. Environ. 37, 289–298.

Bond, T.C., Streets, D.G., Yarber, K.F., et al., 2004. A technology-based global inventory of black and organic carbon emission from combustion. J. Geophys. Res. 109, D14203. https://doi.org/10.1029/2003JD003697.

Boström, C.E., Gerde, P., Hanberg, A., Jernström, B., Johansson, C., Kyrklund, T., Rannug, A., Törnqvist, M., Victorin, K., Westerholm, R., 2002. Cancer Risk Assessment, Indicators, and Guidelines for Polycyclic Aromatic Hydrocarbons in the Ambient Air. Environ. Health Perspect. 110, 451–488.

Bourotte, C., Forti, M.C., Taniguchi, S., Caruso, M., Lotufo, P.A., 2005. A wintertime study of PAHs in fine and coarse aerosols in Sao Paulo City, Brazil. Atmos. Environ. 39, 3799–3811.

Bari, M.A., Baumbach, G., Brodbeck, J., Struschka, M., 2010. Characterisation of particulates and carcinogenic polycyclic aromatic hydrocarbons in wintertime wood-fired heating in residential areas. Atmos. Environ. https://doi.org/10.1016/j.atmosenv.2010.11.053.

Chow, J.C., Watson, J.G., Pritchett, L.C., Pierson, W.R., Fraz1er, C.A., Purcell, R.G., 1993. The dri thermal/optical reflectance carbon analysis System: description, evaluation and applications in U.S. Air quality studies. Atmos. Environ. 27A. 8, 1185–1201.

Chakraborty, D., Mondal, N.K., Datta, J.K., 2014. Indoor pollution from solid biomass fuel and rural health damage: a micro-environmental study in rural area of Burdwan, West Bengal. Int. J. Sustain. Built Environ. 3 (2), 262–271. https://doi.org/10.1016/j.ijsbe.2014.11.002.

De La Torre-Roche, R.J., Lee, W.Y., Campos-Díaz, S.I., 2009. Soil-borne polycyclic aromatic hydrocarbons in El Paso, Texas: analysis of a potential problem in the United States/Mexico border region. J. Hazard. Mater. 163, 946–958.

Dewangan, S., Pervez, S., Chakrabarty, R., Zielinska, B., 2014. Uncharted sources of particle bound polycyclic aromatic hydrocarbons from South Asia: Religious/ritual burning practices. Atmos. Pollut. Res. 5 (0), 283–291.

Dhammapala, R., Claiborn, C., Jimenez, J., Corkil, J., Gullett, B., Simpson, C., Paulsen, M., 2007. Emission factors of PAHs, methoxyphenols, levoglucosan, elemental carbon and organic carbon from simulated wheat and Kentucky bluegrass stubble burns. Atoms. Environ. 41 (12), 2660–2669.

Dickhut, R.M., Canuel, E.M., Gustafson, K.E., Liu, K., Arzayus, K.M., Walker, S.E., Edgecombe, G., Gaylor, M.O., Macdonald, E.H., 2000. Automotive sources of carcinogenic polycyclic aromatic hydrocarbons associated with particulate matter in the Chesapeake Bay Region. Environ. Sci. Technol. 34, 4635–4640.

Dvorska, A, Lammel, G, Klanova, J., 2011. Use of diagnostic ratios for studying source apportionment and reactivity of ambient polycyclic aromatic hydrocarbons over Central Europe. Atoms. Environ. 45, 420–427.

Fang, G.C., Chang, C.N., Wu, Y.S., Fu, P.P.C., Yang, I.L., Chen, M.H., 2004. Characterization, identification of ambient air and road dust polycyclic aromatic hydrocarbons in central Taiwan, Taichung. Sci. Total Environ. 327, 135–146.

Gadi, R., Singh, D.P., Mandal, T.K., Saud, T., Saxena, M., 2012. Emission estimates of particulate PAH from biomass fuels used in Delhi, India. Human Ecol. Risk Assess. 18 (4), 871–887.

Galarneau, E, 2008. Source specificity and atmospheric processing of airborne PAHs: implications for source apportionment. Atmos. Environ. 42, 8139–8149.

Gupta, S., Saksena, S., Shankar, V.R., et al., 1998. Emission factors and thermal efficiencies of cooking biofuels from five countries. Biomass Bioenergy 14, 547–559.

Hedberg, E., Kristensson, A., Ohlsson, M., Johansson, C., et al., 2002. Chemical and physical characterization of emissions from birch wood combustion in a wood stove. Atmos. Environ. 36, 4823–4837.

Hall, D., Wu, Y.C., Stormer, J., Engling, G., Capeto, K, Wang, J., Brown, S, Li, H.W, Yu, K. M., 2012. PAHs, carbonyls, VOCs and $PM_{2.5}$ emission factors for pre-harvest burning of Florida sugarcane. Atmos. Environ. 55, 164–172.

Hays, M.D., Fine, P.M., Geron, C.D., Kleeman, M.J., Gullett, B. K. al, 2005. Open burning of agricultural biomass: physical and chemical properties of particle-phase emissions. Atmos. Environ. 39, 6747–6764.

International Agency for Research on Cancer, 2006. Polycyclic Aromatic Hydrocarbons, IARC Monogaraph 92, Lyone, France. http://monographs.iarc.fr/ENG/Meetings/92-pahs.pdf.

IARC, 2019. Agents Classified by the IARC Monographs, vols. 1–124. International Agency for Research on Cancer, Lyon. Available at: https://monographs.iarc.fr/listof-classifications.

Jenkins, B.M., Jones, A.D., Turn, S.Q., et al., 1996. Emission factors for polycyclic aromatic hydrocarbons from biomass burning. Environ. Sci. Technol. 30, 2462–2469.

Jia, Y., Stone, D., Wang, W., Schrlau, J., Tao, S., Simonich, S.L.M., 2011. Estimated reduction in cancer risk due to PAH exposures if source measures during the 2008 Beijing olympics were sustained. Environ. Health Perspect. 119, 815–820. https://doi.org/10.1289/ehp.1003100.

Khalfi, A., Trouve, G., Delobel, R., et al., 2000. Correlation of CO and PAH emissions during laboratory-scale incineration of wood waste furnitures. J. Anal Applied Pyrolysis 56, 243–262.

Kakareka, S.V., Kukharchyk, T.I., 2003. PAH emission from the open burning of agricultural debris. Sci. Total Environ. 308, 257–261.

Kakareka, S.V., Kukharchyk, T.I., Khomich, V.S., 2005. Study of PAH emission from solid fuels combustion in residential furnances. Environ. Pollut. 133, 383–387.

Keene, W.C., Lobert, R.M., Crutzen, P.J., Maben, J.R., Scharffe, D.H., Landmann, T., Hely, C., Brain, C., 2006. Emissions of major gaseous and particulate species during experimental burns of southern African biomass. J. Geophys. Res. 111 https://doi.org/10.1029/2005JD006319.

Keshtkar, H., Ashbaugh, L.L., 2007. Size distribution of polycyclic aromatic hydrocarbon particulate emission factors from agricultural burning. Atmos. Environ. 41, 2729–2739.

Keyte, I.J., Roy, M., Harrison, R.M., Lammel, G., 2013. Chemical reactivity and long-range transport potential of polycyclic aromatic hydrocarbons – a review. Chem. Soc. Rev. 42, 9333–9391.

Lee, W.J., Wang, Y.F., Lin, T.C., Chen, Y.Y., Lin, W.C., Ku, C.C., Cheng, J.T., 1995. PAH characteristics in the ambient air of traffic-source. Sci. Total Environ. 159, 185–200.

McDonald, J.D., Zielinska, B., Fujita, E.M., et al., 2000. Fine particle and gaseous emission rates from residential wood combustion. Environ. Sci. Technol. 34, 2080–2091.

Majumdar, D., Ray, S., Chakraborty, S., Rao, P.S., et al., 2014. Emission, speciation, and evaluation of impacts of non-methane volatile organic compounds from open dump site. J. Air Waste Manag. Assoc. 64 (7), 834–845. https://doi.org/10.1080/10962247.2013.873747.

Mandalakis, M., Gustafsson, Ö., Reddy, C.M., Xu, Li, 2004. Radiocarbon Apportionment of Fossil versus Biofuel Combustion Sources of Polycyclic Aromatic Hydrocarbons in the Stockholm Metropolitan Area. Environ. Sci. Technol. 38 (20), 5344–5349.

Moosmuller, H., Chakrabarty, R.K., Arnott, W.P., 2009. Aerosol light absorption and its measurement: a review. J. Quant. Spectrosc. Radiat. Transf. 110 (11), 844–878.

Mukherjee, A.K., Mukhopadhaya, K., Sen, S., 2012. Variability of BTEX in residential indoor air of Kolkata metropolitan city. Indoor Built Environ. 21 (3), 374–380. https://doi.org/10.1177/1420326X11409465.

Nisbet, I.C.T., LaGoy, P.K., 1992. Toxic equivalency factors (TEFs) for polycyclic aromatic hydrocarbons (PAHs). Regul. Toxicol. Pharmacol. 16, 290–300.

Pies, C., Hoffman, B., Petrowsky, J., Yang, Y., Ternes, T.A., Hofmann, T ., 2008. Characterization and source identification of polycyclic aromatic hydrocarbons (PAHs) in river bank soils. Chemosphere 72, 1594–1601.
Oanh, N.T.K., Lars, B.R., Nghiem, T.D., 1999. Emission of polycyclic aromatic hydrocarbons and particulate matter from domestic combustion of selected fuels. Environ. Sci. Technol. 33 (16), 2703–2709.
Pervez, S., Verma, M., Tiwari, S., Chakrabarty, R.K., Watson, J.G., Chow, J.C., Paniker, A. S., Deb, M.K., Siddiqui, M.N., Pervez, Y.F., 2018. Household solid fuel burning emission characterization and activity levels in India. Sci. Total Environ. 654, 493–504.
Rajput, P., Sarin, M.M., Rengarajan, R., Singh, D., 2011. Atmospheric polycyclic aromatic hydrocarbons (PAHs) from post-harvest biomass burning emissions in the Indo-Gangetic Plain: isomer ratios and temporal trends. Atmos. Environ. 45, 6732–6740.
Ramdahl, T., Beecher, G., 1982. Combustion of wood in residential sector in small-air tight wood-stove. Anal. Chim. Acta 144, 83–91.
Rogge, W.F., Hildemann, L.N., Mazurek, M.A., et al., 1998. Sources of fine organic aerosol. 9. Pine, oak, and synthetic log combustion in residential fireplaces. Environ. Sci. Technol. 32, 13–22.
Ramírez, N., Cuadras, A., Rovira, E., Marcé, R.M., Borrull, F., 2011. Risk Assessment Related to Atmospheric Polycyclic Aromatic Hydrocarbons in Gas and Particle Phases near Industrial Sites. Environ. Health Perspect. 119, 1110–1116.
Ravindra, K., Sokhi, R., Grieken, R.V., 2008. Atmospheric polycyclic aromatic hydrocarbons: source attribution, emission factors and regulation. Atmos. Environ. 42, 2895–2921.
ICMR, 2010. Development of an Atlas of Cancer in India, A project of national Cancer Registry Programme. (n.d.). Retrieved from http://www.ncrpindia.org/Cancer_Atlas_India/map.
RAIS, 2020. (The risk assessment information System) chemical toxicity value. USEPA. https://rais.ornl.gov/tools/rais_chemical_risk_guide.html. (Accessed December 2020). Last accessed.
Ray, D., Chatterjee, A., Majumdar, D., Ghosh, S.K., Raha, S., 2017. Polycyclic aromatic hydrocarbons over a tropical urban and a high altitude Himalayan Station in India: temporal variation and source apportionment. Atmos. Res. 197, 331–341. https://doi.org/10.1016/j.atmosres.2017.07.010.
Smith, K.R., 2000. Indoor air pollution implicated in alarming health problems. In: Indoor Air Pollution-Energy and Health for the Poor. Newsletter published by World Bank, Washington, DC, USA, p. 1.
Rogge, W.F., Hildemann, L.M., Mazurek, M.A., Cass, G.R., Simoneit, B.R.T., 1993. Sources of fine organic aerosol. 5.Natural gas home appliances. Environ. Sci. Technol. 27 (13), 2736–2744.
Srivastava, A., Som, D., 2007. Hazardous air pollutants in industrial area of Mumbai - India. Chemosphere 69 (3), 458–468. https://doi.org/10.1016/j.chemosphere.2007.04.050. Epub 2007 Jun 4. PMID: 17544479.
Röösli, M., Theis, G., Künzli, N., Staehelin, J., Mathys, P., Oglesby, L., 2001. Temporal 602 and spatial variation of the chemical composition of PM10 at urban and rural sites in the 603 Basel area, Switzerland. Atoms. Environ. 35 (21), 3701–3713.
Senthilkumar, K., Sajwan, K.S., Richardson, J., Kannan, K., 2008. Contamination profiles of heavy metals, organochlorine pesticides, polycyclic aromatic hydrocarbons, and alkylphenols in sediment and oyster collected from marsh/estuarine Savannah GA USA. Mar. Pollut. Bull. 56, 136–149.
Shen, G., Xue, M., Wei, S., Chen, Y., Wang, B., Wang, R., Lv, Y., Shen, H., Li, W., Zhang, Y., Huang, Y., Wei, W., Zhao, Q., Li, B., Wu, H., Tao, S., 2013. The influence of fuel moisture, charge size, burning rate and air ventilation conditions on emissions of PM, OC, EC, parent PAHs, and their derivatives from residential wood combustion. J. Environ. Sci. 25 (9), 1808–1816.
Singh, D.P., Gadi, R., Mandal, T.K., Saud, T., Saxena, M., Sharma, S.K., 2013. Emissions estimates of PAH from biomass fuels used in rural sector of Indo-Gangetic Plains of India. Atmos. Environ. 68, 120–126 (2013).
Shafy, H.I.A., Mansour, M.S.M., 2016. A review on polycyclic aromatic hydrocarbons: source, environmental impact, effect on human health and remediation. Egypt. J. Petrol. 25, 107–123.
Takasuga, T., Umetsu, N., Makino, T., Tsubota, K., Sajwan, K.S., Senthilkumar, K., 2007. Role of temperature and hydrochloric acid on the formation of chlorinated hydrocarbons and polycyclic aromatic hydrocarbons during combustion of paraffin powder, polymers, and newspaper. Arch. Environ. Contam. Toxicol. 53, 8–21.
Tata Energy Research Institute (TERI), 2015. Household energy demand, TERI Energy and Environment Data Diary and Yearbook 2014-15. The Energy and Resources Institute (TERI), New Delhi, India.
Tissari, J., Väätäinen, S., Leskinen, J., Savolahti, M., Lamberg, H., Kortelaine, M., Karvosenoja, N., Sippula, O., 2019. Fine Particle Emissions from Sauna Stoves: Effects of Combustion Appliance and Fuel, and Implications for the Finnish Emission Inventory.
USEPA, 2014. Technical Factsheet on Polycyclic Aromatic Hydrocarbons (PAHs).
Tiwari, M, Sahu, S.K, Pandit, G.G., 2015. Inhalation risk assessment of PAH exposure due to combustion aerosols generated from household fuels. Aeros. Air Qual. Res. 15, 582–590.
Tobiszewski, M., Namiesnik, J., 2012. PAH diagnostic ratios for the identification of pollution emission sources. Environ. Pollut. 162, 110–119.
USEPA, 1984. Method 610; Polynuclear Aromatic Hydrocarbons. United States Environmental protection Agency, USA.
Venkataraman, C., Negi, G., Sardar, S.B., et al., 2002. Size distribution of polycyclic aromatic hydrocarbons in aerosol emissions from biofuel combustion. J. Aerosol Sci. 33, 503–518.
Vineis, P., Husgafvel-Pursiainen, K., 2005. Air pollution and cancer: biomarker studies in human populations. Carcinogenesis 26 (11), 1846–1855.
Wiriya, W., Chantara, S., Sillapapiromsuk, S., Lin, N.H., 2016. Emission profiles of PM_{10}-bound polycyclic aromatic hydrocarbons from biomass burning determined in chamber for assessment of air pollutants from open burning relationship to air-mass movement. Aero. Air Qual. Res. 16 (11), 2716–2727.
Xue, W, Warshawsky, D, 2005. Metabolic activation of polycyclic and heterocyclic aromatic hydrocarbons and DNA damage: A review. Toxicol. Appl. Pharmacol. 206 (1), 73–93. https://doi.org/10.1016/j.taap.2004.11.006.
Yan, B, Abrajano, TA, Bopp, RF, Chaky, DA, Benedict, L, Chillrud, SN, 2005. Molecular tracers of saturated and polycyclic aromatic hydrocarbon inputs into Central Park Lake, New York City. Environ. Sci. Technol. 39, 7012–7019.
Yunker, M.B., Macdonald, R.W., Vingarzan, R., Mitchel, R.H., Goyette, D., Sylvestre, S, 2002. PAHs in the Fraser River basin: a critical appraisal of PAH ratios as indicators of PAH source and composition. Organic Geochemistry 33, 489–515.
Zhang, Y., Tao, S., 2009. Global atmospheric emission inventory of polycyclic aromatic hydrocarbons (PAHs) for 2004. Atmos. Environ. 43 (4), 812–819.
Zhang, X.L., Tao, S., Liu, W.X., Yang, Y., Zuo, Q., Liu, Z., 2005. Source diagnostics of polycyclic aromatic hydrocarbons based on species ratios: A multimedia approach. Environ. Sci. Technol. 39, 9109–9114.
Zou, L.Y., Zhang, W., Atkinson, S., 2003. The characterization of polycyclic aromatic hydrocarbons emissions from burning of different firewood species in Australia. Environ. Pollut. 124, 283–289.
Brumsack, H., Heinrichs, H., Lange, H., 1984. West German coal power plants as sources of potentially toxic emissions. Environ. Technol. Lett. 5, 7–22.
Benner, B.A., Wise, S.A., Currie, L.A., Klouda, G.A., Klinedinst, D.B., Zweidinger, R.B., Stevens, R.K., Lewis, C.W., 1995. Distinguishing the contributions of residential wood combustion and mobile source emissions using relative concentrations of dimethylphenanthrene isomers. Environ. Technol. Lett. 29, 2382–2389.
Bruce, N., Perez-Padilla, R., Albalak, R., 2000. Indoor air pollution in developing countries: a major environmental and public health challenge. Bull. World Health Organis. 78, 1078–1092.
Bhargava, A., Khanna, R.N., Bhargava, S.K., 2004. Exposure risk to carcinogenic PAHs in indoor-air during biomass combustion whilst cooking in rural India. Atmos. Environ. 38, 4761–4767.
Chen, S.C., Liao, C.M., 2006. Health risk assessment on human exposed to environmental polycyclic aromatic hydrocarbons pollution sources. Sci. Total Environ. 366, 112–123.
Dasch, J.M., 1982. Particulate and gaseous emissions from wood burning fireplaces. Environ. Sci. Technol. 16, 639–645.
Ezzati, M., Lopez, A.D., Vander Hoorn, S., et al., 2002. Selected major risk factors and global and regional burden of disease. Lancet 360, 1347–1360.
Gibbs, G.W., 1985. Mortality of aluminium reduction plant workers, 1950 through 1977. J. Occup. Med. Toxicol. 27, 761–770.
He, X., Chen, W., Liu, Z., Chapman, R.S., 1991. An epidemiological study of lung cancer in Xuan Wei County, China: current progress. Case-control study on lung cancer and cooking fuel. Environ. Health Perspect. 94, 9–13.
IARC (International Agency for Research on Cancer), 1987. IARC Monograph of carcinogenic risk to humans, Suppl 7, Overall evaluation of carcinogenicity. An updating of IARC monograph 1 (42), 321–324.
Mastral, A.M., Callen, M.S., 2000. A review on polycyclic aromatic hydrocarbon (PAH) emission from energy generation. Environ. Sci. Technol. 34, 3051–3057.

Groundwater for Sustainable Development 14 (2021) 100628

Contents lists available at ScienceDirect

Groundwater for Sustainable Development

journal homepage: www.elsevier.com/locate/gsd

Research paper

Sources and health risk assessment of potentially toxic elements in groundwater in the mineral-rich tribal belt of Bastar, Central India

Shamsh Pervez [a,*], Princy Dugga [a], Mohammad Nahid Siddiqui [b], Shahina Bano [a], Madhuri Verma [a], Carla Candeias [c], Archi Mishra [a], Sushant Ranjan Verma [a], Aishwaryashri Tamrakar [a], Indrapal Karbhal [a], Manas Kanti Deb [a], Kamlesh Shrivas [a], Yasmeen Pervez [d], Rakesh Kumar Jha [e]

[a] School of Studies in Chemistry, Pt. Ravishankar Shukla University, Raipur, 492010, Chhattisgarh, India
[b] Department of Chemistry and IRC Membranes and Water Security, King Fahd University of Petroleum & Minerals, Dhahran, Saudi Arabia
[c] GeoBioTec, Geosciences Department, University of Aveiro, Aveiro Santiago Campus, Portugal
[d] Government Eklavya College, Dondi Lohara, Chhattisgarh, India
[e] Thermo Fischer Scientific, Powai, Mumbai, 400076, India

ARTICLE INFO

Keywords:
Groundwater
Potentially toxic element
Carcinogenic risk
Principal component analysis
Positive matrix factorization

ABSTRACT

Concentrations of trace elements (Al, B, As, Be, Cd, Ba, Co, Cu, Fe, Cr, Sb, Ni, Li, Sn, Mn, Zn, V and Se) were determined in 160 groundwater samples, collected during pre-monsoon (PRM) and post-monsoon (POM) period (2017) in the tribal belt of Bastar, central India, using inductive coupled plasma mass spectrometry (ICP-MS). The concentrations of Al, As, Fe, Mn and Ni were found exceeding the permissible limits in 49% of samples. Cd, Sn and Se elements have shown two-fold increment in POM samples than those collected during PRM. On the contrary, Al, Ba, Co, Cr and Fe have shown a declining trend from PRM to POM period. On applying Principal component analysis (PCA) and Positive matrix factorization (PMF) approaches to the dataset, observed three primary sources (natural, geogenic and agricultural) for groundwater elemental components. Among the measured potentially toxic elements (PTEs), As has shown higher carcinogenic and non-carcinogenic risk in children as well as adults This study recommends the regular monitoring of heavy metal contamination of groundwater as various geogenic and anthropogenic activities may elevate the risk of severe health hazards.

1. Introduction

Worldwide, 71% of the population access clean drinking water while 844 million people across the world still lack clean drinking water. This issue is more severe in rural areas where only one out of three people use safe drinkable water (WHO, 2019). In India, most rural and suburban regions rely on groundwater to meet water demand for drinking and domestic purposes (Clark et al., 1996; Ahada and Suthar 2018).

Among all contaminants, inorganic trace elements are of much concern as they are xenobiotic compounds and can accumulate in the water resources for a long period (Ravindra and Mor 2019). Groundwater has the potential to accumulate trace elements that reach the water table and pollute it through various natural and anthropogenic sources such as precipitation, rock-water interaction, percolation of soil-water, industrial wastewater, agricultural, domestic wastes, etc. (Boateng et al., 2016; Bouderbala and Gharbi 2017; Hossain and Patra 2020).

However, depletion in water quality is related to public health concerns, so it is essential to estimate the exposure risk to understand groundwater sources' toxicity level imposing health hazards. Trace metals in groundwater may be exposed to human beings through two key pathways, direct ingestion and dermal absorption (Duggal and Rani 2018; Brindha et al., 2020; Hu et al., 2020). Some trace metal(loid)s such as arsenic (As), lead (Pb), nickel (Ni), chromium (Cr), copper (Cu), zinc (Zn), cadmium (Cd), and cobalt (Co) are potentially toxic if found above their threshold value in drinking water (Islam et al., 2019; Hossain and Patra 2020). Lead can cause neurological diseases as it can trigger the central nervous system mostly in children which results in fatigue, anaemia, and a decrease in intelligence quotient (IQ) level (Emenike et al., 2019). Cadmium excess affects renal function and can

* Corresponding author.
E-mail address: shamshpervez@gmail.com (S. Pervez).

https://doi.org/10.1016/j.gsd.2021.100628
Received 20 March 2021; Received in revised form 13 June 2021; Accepted 14 June 2021
Available online 19 June 2021

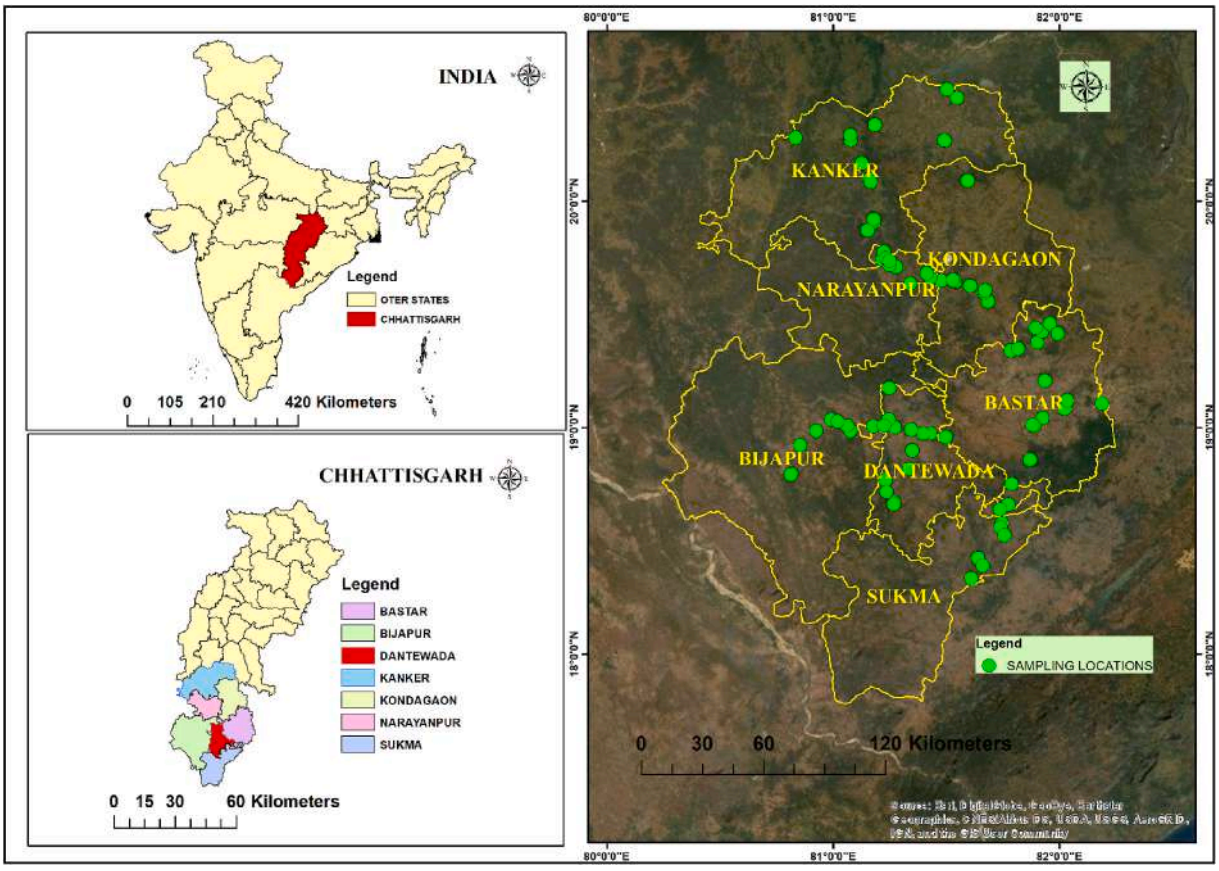

Fig. 1. Map of groundwater sampling locations across the Bastar region.

induce severe kidney diseases and even cancer. Consumption of water with high concentrations of arsenic can cause cardiovascular, neurological, and skin diseases such as hyperpigmentation, hyperkeratosis and can develop cancer (Emenike et al., 2019). Pandey et al. (2015) have reported higher As contamination in the groundwater of Kanker district (India) and carried out an epidemiological investigation reporting sub-acute As poisoning that resulted in gastrointestinal disease diarrhoea in inhabitants of the study area.

Previously very few studies on the evaluation of groundwater contamination have been reported for the study region and all of those studies were mainly focused on reporting selected major constituents and few toxic elements for a small number of location (Behera et al., 2012; Rubina and Kavita, 2013; Pandey et al., 2015). Source apportionment of trace elements, including potentially toxic species in groundwater allows to address the relative contribution from different major source routes viz. geogenic, anthropogenic (e.g., agricultural), and atmospheric (re)suspended materials, and studies that relate these results to assess health risks are scarce for the tribal belt of Bastar region. Thus, investigation of the potential source of groundwater contaminants, particularly potentially toxic trace elements and associated health risks is mandatory. Further this study aims to, 1) evaluate the spatio-temporal variations in trace element concentrations in groundwaters during pre-monsoon (PRM) and post-monsoon (POM) periods; 2) identify the significant sources of groundwater contamination using Principal Component Analysis (PCA) and chemical mass balance approach through positive matrix factorization (PMF); and 3) assess health risk caused by potentially toxic elements (PTEs).

2. Materials and methods

2.1. Study area

Sampling was performed at ninety-five locations across the seven districts of the Bastar division (80° 35′E – 82° 15′E and17° 46′ N-20° 35′N). QGIS 3.14 software was used to make a detailed map of the study area (Fig. 1).

Bastar region is considered a mineral-rich area of the Chhattisgarh state (India). Geologically, the study area is located on the Bastar Craton, with an ~215,000 km^2 extension, mainly composed of gneisses, granitoid, granulites, supracrustals, and mafic igneous rocks, being these last ones exposed in diverse locations, along with dykes characterized with a high-Mn and high-Fe quartz tholeiitic composition (Dora, 2014). The lithology of the study area is characterized by gneiss granitoids, metasediments in the Sukma region (Bengpal), Bhopalpatnam, Kondagaon and Balaghat granulites, Bailadila Iron Formation, Dongargarh and Kotri Supergroup that includes the Dongargarh- Malajkhand and equivalent granitoids, the Sauser and Sonakhan Group of rocks and the platform sediments of Purana basins, among others. Soils are mainly vertisol and alfisol, these last ones with origin in the cratonic rocks (Gupta et al., 2012). Limestones and bauxites are common in this region, with Fe and Ti enrichment (Mineral Resource Department, 2014).

The study region is mainly drained by the Indravati and Sabri rivers which are tributaries of the Godavari River. It constitutes the agro-climatic region with sandy to clayey soil structure with considerable variation in soil types such as laterite, alluvial and loamy soil (Sinha, 2011). The total irrigated area in this region is 12,085 ha while the net sown area covers 6,37,965 ha (Department of Land Resource Management, 2014). The total forest area of the Bastar region is 7112 km^2, accounting for more than 75% of its land area (Sinha, 2011). The annual temperature variation ranges between 10° C to 46° C and the annual

rainfall across the Bastar region is in mean ~1387 mm. Precipitation occurs in this region due to the southwest monsoon attributed to the Bay of Bengal during June–September. Groundwater aquifers mostly arise in phreatic and semi-confined conditions.

2.2. Sampling and chemical analysis

The representative 160 groundwater samples were collected during pre and post-monsoon season out of which 65 samples were collected in the Pre-monsoon season (50 bore wells+15 Dug wells) while in post-monsoon season 95 samples were collected (72 bore wells+23 dug wells) using the stratified random sampling method applying pooled study design. The stagnant water of the column was pumped out for at least 10 min before sampling. For heavy metal analysis, water samples were filtered using Whatman 42 filter papers and immediately acidified with concentrated HNO_3 acid (pH < 2). AR grade acids and reagents were used in the study. Each sampling bottle was rinsed with the sampled groundwater before collection. Physical parameters such as pH, electrical conductivity (EC), total dissolved solids (TDS), and temperature (T) were measured in situ using HANNA® sensors (HI 98129) (Varghese and Jaya 2014; Guo et al., 2017). Water samples were filled up to the bottle's rim and were sealed tightly to prevent exposure to air. Samples were placed in an icebox and carefully transported to the laboratory and stored in a deep freezer (-4°C) for further analysis.

2.3. Chemical analysis

Selected trace elements (Al, B, As, Be, Cd, Ba, Co, Cu, Fe, Cr, Sb, Ni, Li, Sn, Mn, Zn, V, and Se) were analyzed in groundwater samples using inductively coupled plasma mass spectrometry (ICP-MS; Thermofischer, Model iCAP RQ.ASX-560). Thermo Scientific Qtegra Intelligent Scientific Data Solution (ISDS) software was used for operating the instrument. Helium gas flow rate was set at 4.5 mL min^{-1}, while nebulizer argon flow rate was 1.14 min^{-1} and the integration time was set at 0.02 s per point for analysis. The internal standards (Sc, Tl, Ge, In, and Bi) with the known concentrations of 0.1,0.5,1,10 and 50 μg. L^{-1} were used for calibration purposes. Samples were pre-treated with 0.1 N HNO_3 acid and internal standards. Replicate measurements were carried out for all trace elements to maintain the relative standard deviation within 10%. The recovery percentage of the heavy metal/metalloids ranged between 76 and 98% indicating a good correlation between the actual and measured values.

2.4. Quality control

Quality control was obtained by applying standard laboratory measures and quality assurance strategies were applied during analysis such as replicate measurement of samples, use of analytical grade reagents and chemicals, and by adopting standard operational procedures of sample analysis. Throughout the analysis reagent blank, metal concentration, and its standard detection limits were observed.

2.5. Data compilation and statistical methods

The spatial variability of trace elements across the monitoring locations was calculated by dividing the standard deviation with the mean value of chemical species and taking its percentage and designated it as the coefficient of spatial variation (% CV). Source signatures of groundwater chemical components were determined using the PCA technique using IBM SPSS® 22 statistic software. The quantification of source contribution estimates of groundwater contaminants was carried out by executing USEPA PMF 5.0 using concentrations and associated analytical uncertainties of trace elements (US-EPA, 2014). Reported concentrations of groundwater ionic species (Dugga et al., 2020) were also included in the chemical input profiles of groundwater samples during the execution of PMF5.0 for evaluating more precise and appropriate results of source apportionment.

3. Human health risk assessment

3.1. Exposure assessment

The exposure assessment estimates the magnitude and potential concerning chemical exposure to individuals, considering the pathways through which chemicals are usually transported and the major routes by which an individual is exposed to chemicals (USEPA, 2004). To evaluate the health risk impact posed by each element, USEPA (2004) risk assessment protocol was used. Due to the distinct behavior, exposure dose and body weight, health risk assessment was calculated for the two age groups: children (0–15 years) and adults (>15 years) (USEPA, 2011). Exposure to potentially toxic elements (PTEs) present in groundwater can occur via two major exposure pathways: (a) ingestion via drinking water intake through the mouth; and (b) dermal contact (Prasanth et al., 2012; Li et al., 2016). Daily exposure and health risk assessment were evaluated for nineteen trace elements (Al, As, B, Ba, Be, Cd, Co, Cr, Cu, Fe, Li, Mn, Ni, Sb, Se, V, Zn, F^- and NO_3^-) associated with the groundwater using: (i) chemical daily intake (CDI) which account for direct ingestion via drinking water intake (Liu et al., 2020) (Eq. (1)); and (ii) dermal absorbed dose (DAD) which accounts for the dermal absorption of PTEs adhered to skin (Eq. (2))

$$CDI = \frac{C \times IR \times EF \times ED}{BW \times AT} \tag{1}$$

$$DAD = \frac{C \times SA \times Kp \times ET \times EF \times ED}{BW \times AT} \times CF \tag{2}$$

Where CDI and DAD are in $mg.kg^{-1.}\ day^{-1}$, C denotes the concentration of trace elements in $mg.L^{-1}$, IR is ingestion rate in $mg.day^{-1}$ and EF is relative exposure frequency in $days.year^{-1}$, ED is exposure duration in years, BW is average body weight in kg, AT is the average time in days, SA denotes the exposed skin area (cm^2), Kp is coefficient of dermal permeability in $Cm.h^{-1}$, ET is the exposure time ($h.day^{-1}$) and CF is the conversion factor (unitless) Factor values of each parameter used in the calculation of exposure assessment have been mentioned in Table 3.

3.2. Non-carcinogenic risk assessment

Risk assessment is described as the method of analyzing and determining the potential event that probably causes harmful health effects over a specific time duration and concludes the ability to tolerate risk based on risk analysis (EPA 1989; Mohammadi et al., 2019). In this study, non-carcinogenic risk assessment was evaluated using hazard quotient (HQ) and hazard index (HI) expressed as

$$HQ_{ing} = \frac{CDI}{RfD} \tag{3}$$

$$HQ_d = \frac{DAD}{RfD \times GIABS} \tag{4}$$

$$HI_i = HQ_{ing} + HQ_d \tag{5}$$

$$HI = \sum HI_i \tag{6}$$

Where HQ_{ing} and HQ_d are hazard quotient for oral ingestion and dermal exposure, respectively, RfD represents oral reference dose, GIABS denotes the gastrointestinal absorption factor, while the total non-carcinogenic risk was calculated as the summation of hazard quotient of oral and dermal exposure using hazard index (HI). HQ and HI values < 1.00 E+00 considered safe while values > 1.00 E+00 indicate that an individual is exposed to non-carcinogenic risk (Ravindra and Mor 2019; Yavar Ashayeri and Keshavarzi 2019).

Table 1
Descriptive statistics of trace and potentially toxic elements in the 160 groundwater samples, collected from Bastar region during Pre-Monsoon (PRM) and Post-monsoon (POM) periods.

Species	BIS Limit	WHO Limit	MDL values (ICPMS)	Pre- Monsoon				Post-Monsoon			
				Overall water samples (n = 73)	Dug Well (n = 20)		Bore Well(n = 53)	Overall water sample (n-87)	Dug Well (n = 18)		Bore Well (n = 69)	
				Geo mean ± SD (Min-Max)	Mean ± SD	%CV	Mean ± SD	%CV	Geo mean ± SD (Min-Max)	Mean ± SD	%CV	Mean ± SD	%CV
Al	30	–	0.199	**8.01 ± 21.60 (0.25–13.64)**	17.49 ± 21.09	120.58	15.64 ± 21.97	140.47	**5.82 ± 18.05 (0.79–94.06)**	6.86 ± 4.36	63.67	12.45 ± 20.02	160.80
As	10	10	0.003	**7.22 ± 3.46 (1.02–20.03)**	8.24 ± 2.20	26.69	8.20 ± 8.67	105.73	**7.29 ± 2.57 (1.24–12.33)**	8.37 ± 2.52	30.10	7.73 ± 2.59	33.50
B	300	2400	0.123	**10.56 ± 26.79 (0.25–135.64)**	23.47 ± 27.22	115.98	19.92 ± 26.83	134.68	**9.77 ± 24.38 (0.86–141.06)**	9.70 ± 7.46	76.90	19.71 ± 26.78	135.87
Ba	700	700	0.034	**73.14 ± 132.81 (11.68–615.32)**	83.99 ± 57.92	68.96	119.69 ± 151.14	126.27	**67.75 ± 108.24 (0.03–759.29)**	69.14 ± 41.01	59.31	109.64 ± 118.53	108.11
Be	–	–	0.032	**6.05 ± 14.92 (0.89–66.94)**	12.82 ± 18.39	143.45	10.57 ± 13.53	128.00	**6.24 ± 13.80 (0.35–65.96)**	11.65 ± 14.87	127.63	10.63 ± 13.62	128.13
Cd	3	3	0.023	**0.03 ± 0.28 (0.001–0.99)**	0.13 ± 0.30	230.77	0.14 ± 0.27	192.85	**0.06 ± 0.27 (0.01–1.17)**	0.13 ± 0.29	223.07	0.15 ± 0.26	173.33
Co	–	–	0.002	**1.61 ± 1.70 (0.06–6.52)**	2.67 ± 1.61	60.30	2.27 ± 3.53	155.51	**0.13 ± 0.84 (0.0005–6.97)**	0.23 ± 0.24	104.16	0.42 ± 0.44	104.76
Cr	50	50	0.003	**1.79 ± 14.00 (0.16–60.34)**	9.28 ± 15.13	163.04	8.14 ± 13.69	168.18	**1.08 ± 9.10 (0.12–40.72)**	4.75 ± 10.50	221.11	3.95 ± 4.76	120.51
Cu	50	2000	0.036	**2.15 ± 6.95 (0.14–30.43)**	5.13 ± 8.94	174.27	4.28 ± 6.12	142.99	**2.09 ± 7.25 (0.18–31.70)**	5.31 ± 1.58	29.75	4.46 ± 7.02	157.39
Fe	300	–	0.011	**388.41 ± 374.29 (164.32–2023.76)**	450.89 ± 316.73	70.25	491.25 ± 396.06	80.62	**357.37 ± 405.90 (104.27–2353.81)**	364.95 ± 232.01	63.57	471.08 ± 438.85	93.16
Li	–	–	0.069	**5.97 ± 25.65 (0.13–99.87)**	15.10 ± 28.61	189.47	14.42 ± 24.73	171.49	**6.76 ± 23.23 (0.18–97.78)**	11.51 ± 22.94	199.30	15.14 ± 23.41	154.62
Mn	100	–	0.006	**145.57 ± 170.79 (52.49–823.89)**	164.77 ± 104.99	63.72	202.09 ± 189.66	93.85	**178.07 ± 338.07 (32.71–2090.03)**	167.33 ± 52.17	31.18	270.71 ± 147.59	54.52
Ni	20	–	0.007	**2.88 ± 13.09 (0.140–53.10)**	8.94 ± 15.18	169.80	7.82 ± 15.59	199.36	**3.59 ± 7.79 (0.26–35.06)**	9.15 ± 9.15	100.00	5.99 ± 7.33	122.37
Sb	–	20	0.003	**0.06 ± 0.30 (0.004–0.99)**	0.21 ± 0.30	142.86	0.19 ± 0.31	163.16	**0.05 ± 0.19 (0.01–0.91)**	0.12 ± 0.22	183.33	0.11 ± 0.18	163.63
Se	10	40	0.063	**0.09 ± 0.44 (0.004–1.73)**	0.30 ± 0.51	170.00	0.27 ± 0.42	155.55	**0.19 ± 0.79 (0.004–3.98)**	0.57 ± 0.92	161.40	0.47 ± 2.60	553.19
Sn	–	–	0.009	**0.03 ± 0.26 (0.001–0.99)**	0.16 ± 0.32	200.00	0.13 ± 0.23	176.92	**0.06 ± 0.22 (0.002–0.99)**	0.12 ± 0.24	200.00	0.13 ± 0.21	161.53
V	–	–	0.002	**0.53 ± 10.91 (0.01–45.07)**	4.91 ± 12.20	248.47	4.52 ± 10.51	232.52	**0.85 ± 8.38 (0.03–35.04)**	3.44 ± 8.62	250.58	4.55 ± 8.36	183.73
Zn	5000	–	1.183	**178.26 ± 275.49 (12.09–1538.75)**	295.56 ± 234.76	79.43	281.35 ± 434.85	154.56	**256.85 ± 427.55 (66.81–2612.25)**	258.16 ± 151.00	58.49	397.32 ± 470.56	118.43

All concentrations in μg.L^{-1}; MDL-Minimum detection limit (μg.L^{-1}); Geo mean – Geometric mean; SD – standard deviation; CV - coefficient of spatial variation.

3.3. Carcinogenic risk assessment

The potential carcinogenic risk (CR) represents the probability of developing cancer in an individual during lifetime exposure to carcinogenic elements (El Nemr et al., 2016; Yavar Ashayeri and Keshavarzi 2019). The carcinogenic risk was evaluated for two carcinogenic elements (As and Cr) using the following equations:

$$CR_{ing} = CDI \times SF_o \quad (7)$$

$$CR_d = DAD \times \left(\frac{SFo}{GIABS}\right) \quad (8)$$

$$CR_i = CR_{ing} + CR_d \quad (9)$$

$$CR = \sum CR_i \quad (10)$$

Where CR_{ing} and CR_d represent carcinogenic risk by oral and dermal exposure, respectively, SF_o denotes oral slope factor (mg.kg^{-1}.day^{-1})$^{-1}$ while CR is the total carcinogenic risk (Li et al., 2016). The CR value < 10^{-6} shows no significant risk, 10^{-6} to10^{-4} considered tolerable, while values > 10^{-4} indicate a high carcinogenic risk.

4. Results and discussion

4.1. Groundwater chemical characterization

This study shows the concentration of eighteen trace elements in groundwater samples collected from the Bastar region during the PRM and POM periods of 2017. In addition to the tabulation of mean concentrations of the elemental species for all groundwater samples collected on the two periods, similar statistics were presented separately for dug-well and bore-well groundwater samples in Table 1. Further, these concentrations were used to evaluate the spatiotemporal variability, source apportionment, and health risk assessment to achieve a clear groundwater hydrochemistry scenario in the study area.

The abundance order based on the geometric mean (GM) value of trace elements concentration in overall groundwater samples of the study area were as follows: Fe > Zn > Mn > Ba > B > Al > As > Be > Li > Ni > Cu > Cr > Co > V > Se > Sb > Sn > Cd in PRM and Fe > Zn > Mn > Ba > B > As > Li > Be > Al > Ni > Cu > Cr > V > Se > Co > Sn > Cd > Sb in POM.

Among all the trace elements, the highest average concentration was obtained for Fe (GM: 388.40 ± 374.29 μg.L^{-1} in PRM and GM: 357.37 ±

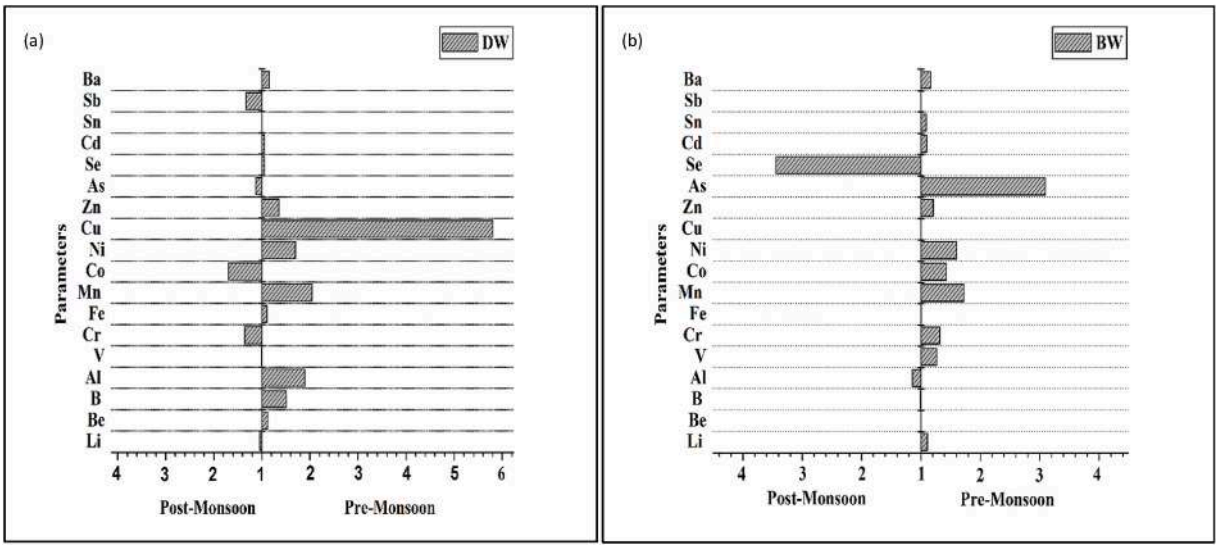

Fig. 2. Spatiotemporal variation trend shown by trace and toxic elements in (a) dug well (DW) and (b) borewell (BW) samples [(%CV) between pre and post-monsoon periods].

405.90 μg.L^{-1} in POM). The insignificant variation between PRM and POM indicates the consistency of a similar source of origin (geological crustal) during both seasonal periods (Mondal et al., 2010; Bhutiani et al., 2016; Singh and Kamal 2017). The concentration of Fe in approximately 49% of samples in PRM and POM was above the permissible limit of 300 μg.L^{-1} given by (BIS, 2012). Mn, another abundant crustal element usually found in groundwater (Singh and Kamal, 2017), revealed concentrations of GM:145.57 ± 170.79 μg.L^{-1} in PRM and GM: 178.07 ± 338.07 μg.L^{-1} in POM. Mn in 37% and 42% of the PRM and POM samples, respectively, found exceeding the permissible limit of 100 μg.L^{-1} (BIS, 2012).

Arsenic (As) has been categorized as a human carcinogen that results in skin and lung cancer (IARC, 2012). Exposure at higher levels can cause severe neurological, cardiovascular, reproductive, and respiratory disorders (Wang et al., 2007; Rahman et al., 2009). The concentration of As in groundwater was found GM: 7.22 ± 3.46 μg.L^{-1} and GM:7.29 ± 2.57 μg.L^{-1} in PRM and POM, respectively, with a higher concentration in 11% PRM and 24% POM samples compared to the permissible level of 10 μg. L^{-1} (WHO, 2011). The higher concentration of Fe and Mn oxides and As suggests that it is mobilized because of the reductive dissolution of Fe and Mn oxides with As-oxy anions in groundwater aquifer (Rahman et al., 2009).

Aluminium was found to be GM: 8.01 ± 21.60 μg.L^{-1} (PRM) and GM: 5.82 ± 18.05 μg.L^{-1} (POM) in groundwater samples with exceeding in

Table 2
Varimax orthogonal rotation factor loadings of twenty-seven parameters of groundwater on execution of PCA for PRM and POM periods.

Parameters	Components					
	Pre monsoon			Post monsoon		
	Factor 1	Factor 2	Factor 3	Factor 1	Factor 2	Factor 3
Li	**0.879**	0.078	0.095	**0.929**	0.123	0.007
Be	**0.867**	0.101	0.078	**0.904**	0.011	0.048
B	0.025	0.213	**0.924**	−0.017	0.153	**0.921**
Al	0.128	0.220	**0.903**	0.020	0.255	**0.878**
V	**0.936**	0.011	0.064	**0.915**	0.181	0.006
Cr	**0.862**	−0.069	−0.014	**0.965**	0.094	0.020
Mn	−0.101	**0.781**	0.249	0.167	**0.884**	0.025
Fe	0.068	**0.837**	0.281	0.272	**0.789**	−0.041
Se	**0.847**	−0.088	0.19	**0.873**	0.081	-.057
Co	0.204	**0.655**	0.201	0.007	**0.811**	0.043
Ni	**0.948**	0.003	0.021	**0.819**	0.039	0.029
Cu	**0.940**	0.071	0.111	**0.917**	0.159	0.125
Zn	−0.013	0.127	**0.906**	0.129	0.169	**0.839**
As	0.093	**0.771**	−0.033	0.060	**0.789**	0.054
Cd	**0.945**	0.022	0.026	**0.936**	0.128	0.011
Sn	**0.908**	0.005	0.055	**0.958**	0.040	0.052
Sb	**0.869**	−0.048	−0.054	**0.942**	0.115	0.001
Ba	−0.210	**0.816**	−0.034	0.051	**0.780**	0.112
Mg^{2+}	0.131	**0.921**	0.177	0.125	**0.897**	0.245
Na^{+}	**0.873**	0.097	0.117	**0.847**	0.005	0.064
K^{+}	**0.910**	0.040	0.083	**0.921**	0.098	0.137
Ca^{2+}	0.113	**0.902**	0.166	−0.094	**0.799**	0.271
Cl^{-}	0.161	0.191	**0.903**	0.303	−0.148	0.427
F^{-}	−0.110	**0.870**	0.127	0.007	**0.718**	−0.160
NO_3^{-}	0.061	0.195	**0.933**	0.124	0.165	**0.919**
SO_4^{2-}	**0.829**	0.199	0.216	**0.938**	0.154	0.022
HCO_3^{-}	0.553	**0.721**	−0.027	0.210	**0.862**	0.052

Table 3
Factor values of different parameters used for calculation of exposure assessment.

Parameter	Value		Reference
	Children	Adult	
IR	1Lday^{-1}	2 L day^{-1}	EPA (1989)
EF	365 days year^{-1}	365 days year^{-1}	USEPA (2004)
ED	12 years	30 years	USEPA (2004)
CF	10^{-3}	10^{-3}	Yavar Ashayeri and Keshavarzi (2019)
BW	15 kg	70 kg	USEPA (2004)
AT	ED × 365 day (non-carcinogen)		USEPA (2004)
	70 × 365 = 25,550 days (carcinogen)		(Islam et al., 2019)
SA	18000 cm^2	6600 cm^2	(USEPA, 2011)
Kp	Ba = 0.07,Be = 0.007,Cd = 0.05, Cr = 0.025,Ni = 0.04,Sb = 0.15, V = 0.026, for other elements = 1		(US-EPA, 2014) Hu et al. (2012)

11% and 6% samples in PRM and POM samples from the permissible limit of 30 μg.L^{-1} (BIS, 2012). Higher Al concentrations may disturb the physical and cellular process of the body as it replaces the Mg^{2+} and Fe^{3+} ions in the body disrupting the cellular function, secretory function, and intercellular interactions (Ravindra and Mor, 2019). Ni, a potentially toxic element, was also found exceeding the permissible limits of 20 μg.L^{-1} in 16% and 9% samples of PRM and POM, respectively (BIS, 2012). Sites with higher groundwater Ni concentrations are mostly located in agricultural fields. The use of Ni-enriched insecticides/fertilizers might be the primary reason for increased Ni concentration in groundwater samples (Gimeno-García et al., 1996; Defarge et al., 2018). Other measured elemental species (B, Ba, Be, Cd, Cr, Co, Cu, Li, Se, Sn, Sb, V, Zn) were found in trace amounts and within the respective permissible limits for drinking water.

4.2. Spatiotemporal variability of trace elements

The coefficient of spatial variation (CV), determined by dividing the standard deviation by the overall mean across the sites, is presented in Table 1 separately for DW and BW sites and for PRM and POM seasons to evaluate spatiotemporal variability. A graph was also plotted using origin 8.1 between the values obtained by dividing %CV for each trace element in POM by PRM and visa-versa with a mathematical factor >1 to evaluate spatiotemporal variability (Fig. 2). Except for Fe, As, Co, and Mn, all other elemental species concentrations have shown higher spatial variability of >100% across both DW and BW sites during PRM. It underscores the wide contribution of mineral-rich beds to hydrochemistry of the study region through mineral dissolution. On evaluating the spatial variability in temporal scale (spatiotemporal variability) across DW sites, Cu, Zn, Ni, Mn, Al and B elemental concentrations have shown multi-fold higher spatial variability in PRM compared to the POM period. On the contrary, CV% associated with Co, Sb, and Cr concentrations were higher in POM than PRM. In BW sites, concentrations of several elements (As, Zn, Ni, Co, Mn, Cr, V) have shown higher spatial variability in PRM than POM. This may be attributed to an increase in mineral concentration and a decrease in groundwater table during PRM.

4.3. Factor analysis using PCA technique

The principal component analysis (PCA) is a receptor technique for recognizing patterns, explaining the variance of significant intercorrelated variables, and could be altered to independent variables (Helena et al., 2000; Krishna et al., 2009; Belkhiri and Narany 2015). PCA method has been described in detail in S1. PCA was executed for extracting significant factors to evaluate possible source types of groundwater chemical contaminants using chemical profiles of elemental concentrations along with reported ionic concentrations.

Factors were determined with a group of heavy elements and ions in groundwater which were strongly correlated in the factor matrix after operating the varimax rotation (Table 2). Supplementary Tables S2–S3 show details of PCA including principal components(PCs), percentage of variance, and cumulative percentage of each PCs for PRM and POM period respectively. KMO and Bartlett's sphericity test was performed in data sets of both PRM and POM periods for examining the accuracy of factor analysis and found p = 0.85 (for PRM) and p = 0.84 (for POM), well beyond the prescribed values of p > 0.5 (Haji Gholizadeh et al., 2016). Similarly, χ^2-values were also within prescribed good fit parameters, underscore the appropriateness of factor analysis using PCA.

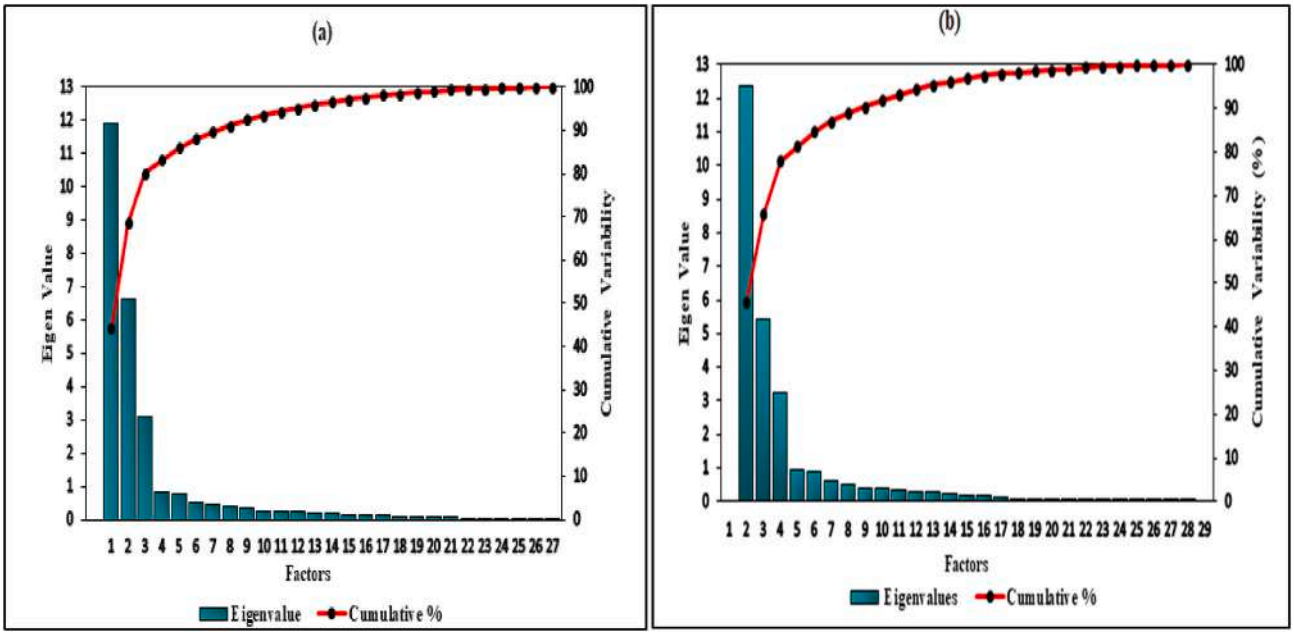

Fig. 3. Scree plot drawn for determining the number of factors in PCA receptor model indicating common source of chemical species in groundwater during (a) PRM and (b) POM periods.

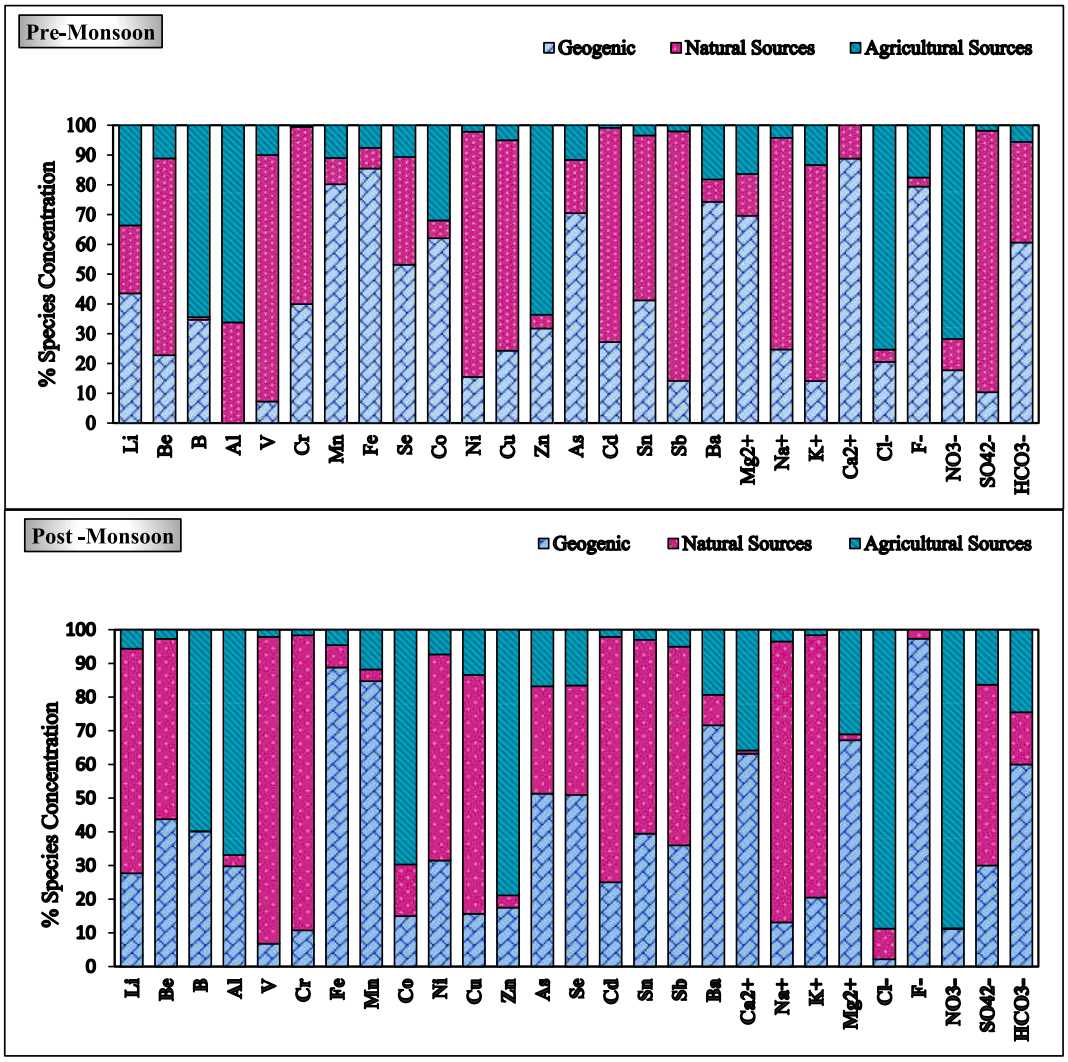

Fig. 4. The relative contribution estimates of source-factors of trace and potentially toxic elements using EPA PMF 5.0 model for pre-monsoon and post-monsoon periods.

The total variance was found 80.18% (PRM) and 77.95% (POM). Three factors were extracted by relevant variables based on Kaiser's rule as the Eigenvalue for the first three components was >1 in both sampling periods. The scree plots of PRM and POM were depicted in Fig. 3(a) and (b). The first factor exhibits 42.53% (PRM) and 43.68% (POM) of total variance with a positive factor loading of Be, Cd, Cr, Cu, K^+, Li, Na^+, Ni, Se, Sb, Sn, V, and SO_4^{2-} while negative loading on Ba, F^- and Mn. Interaction of acidic components of atmospheric wet precipitation with soil, followed by percolation to groundwater might be the indicator of the first source factor. This factor could be attributed to the natural sources which signify the percolation of elements and ions present in the soil through the rainwater or may enter the groundwater aquifer through surface water via various biochemical processes such as oxidation-reduction and ion exchange etc. (Drever 1997; Sethy et al., 2016; Loh et al., 2020).

The second factor shows 20.84% (PRM) and 19.19% (POM) of total variance with a positive factor loading of As, Ba, Ca^{2+}, Co, F^-, Fe, HCO_3^-, Mg^{2+}, and Mn while negative loading of Cr, Se, and Sb. The second factor might be originated by geogenic sources, which resulted in the dissolution of minerals like calcite [$CaCO_3$] and iron oxides (e.g. goethite [FeO(OH)] and hematite [Fe_2O_3]) (Lu et al., 2012; Kashyap et al., 2018). Crustal elements, e.g. Fe, Mn, Ca^{2+}, and Mg^{2+} found in minerals present in the study area are dissolved into groundwaters by rock-water interaction processes.

The third factor exhibits 16.82% (PRM) and 15.07% (POM) of total variance with a positive factor loading of Al, B, Cl^-, NO_3^- and Zn while negative factor loading of Cr, As, Sb, Ba, and HCO_3^-. This factor could be attributed to the agricultural sources as the fertilizer-rich water may enter the aquifer and contaminate the groundwater (Hudak 2012; Jassas and Merkel 2015).

4.4. Source apportionment using positive matrix factorization (PMF 5.0)

U.S. EPA's PMF 5.0 was executed using chemical profiles of 27 chemical species (concentrations and related uncertainties) of 160 groundwater samples for source apportionment of ions and heavy elements during PRM and POM sampling seasons, respectively. PMF 5.0 receptor model has been described in detail in S2. The Optimal number of factors (03) were determined by the iteration with the lowest Q (Robust)/Qexp value, picked up by performing 20 random runs (Paatero 1997; Norris et al., 2014). The factor fingerprints, obtained from PMF5.0, were presented using the percentage of individual species concerning all species and the species concentration related to source factors have been shown in Fig. 4. Species with >50% contribution were used to designate a particulate source-factor. The factor profile of groundwater chemical species for PRM and POM has been shown in Figs. 5 and 6 respectively.

In PRM, Factor 1 contributes 41.26% to chemical contaminants of

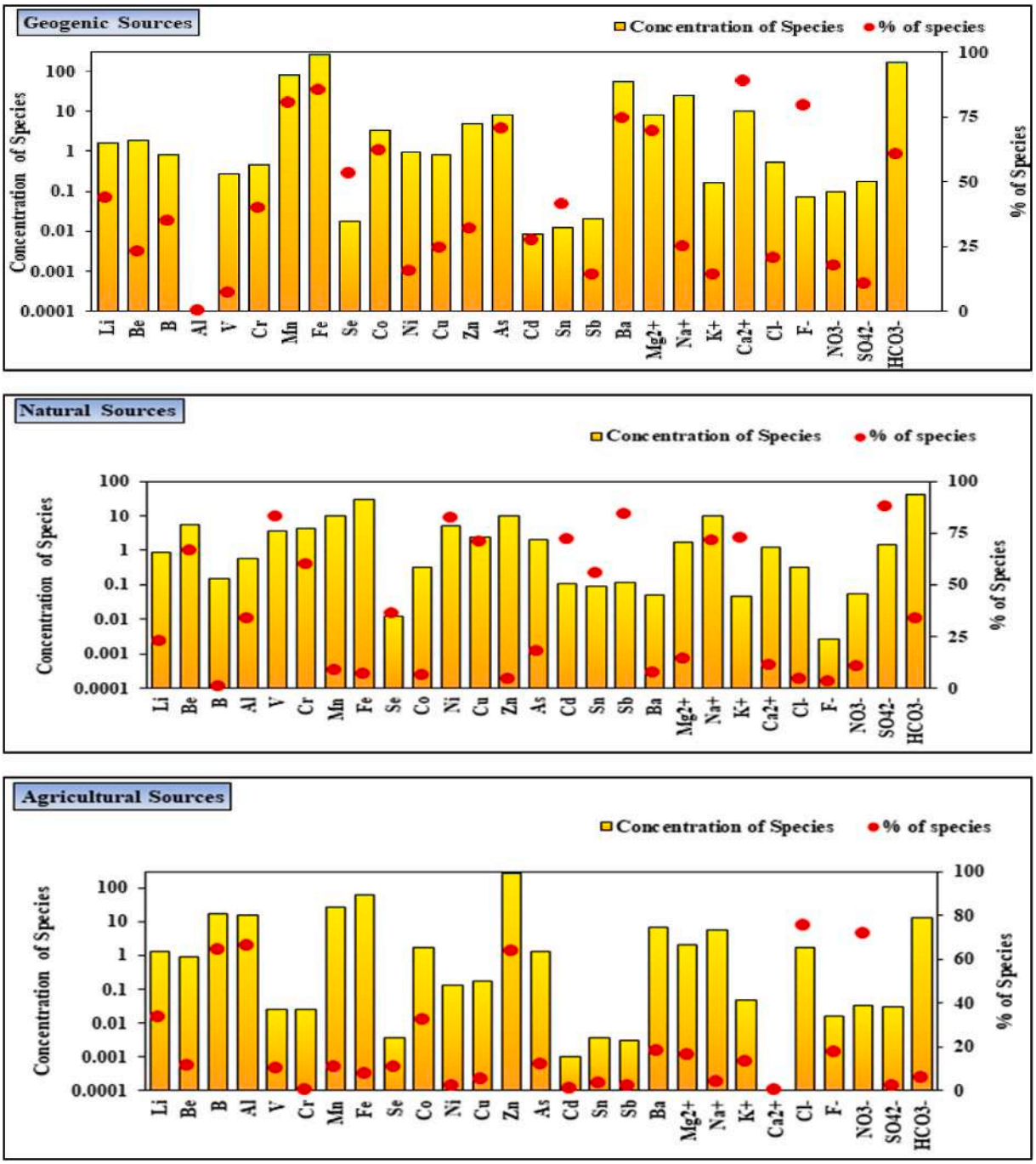

Fig. 5. Factor profile of chemical species in groundwater determined using EPA PMF5.0 receptor model for pre-monsoon period.

groundwater samples with a major contribution of Mn, Fe, Se, Co, Ba, F^{-},Ca^{2+}, As, Mg^{2+}, Ba, and HCO_3^- species derived from geogenic sources viz. rock weathering (e.g. fluorite [CaF_2], hematite and arsenopyrite [FeAsS]) into groundwaters (Lu et al., 2012; Mahato et al., 2016). Factor 2 is characterized by higher concentrations of Be, V, Cr, Ni, Cu, Cd, Sn, Sb, Na^{+}, $K^{+,}$ and SO_4^{2-} with 35.97% factor contribution, indicates the natural source. These chemical species are commonly found in soil and may enter the groundwater aquifers by percolation through rainwater or surface water (Chen et al., 2019; Loh et al., 2020).

Factor 3 represents the agricultural sources with a 20.76% factor contribution and higher factor loading of B, Al, Zn, Cl^{-} and NO_3^- (Jassas and Merkel, 2015). Comparatively higher contribution of geogenic sources in PRM might be due to lowering in groundwater table in summertime (PRM), consequently increasing the concentrations of species known for geogenic origin.

For the POM period, Factor 1 has shown 38.56% factor contribution with a higher concentration of V, Cr, Ni, Cu, Cd, Se, Sn, Sb, Na^{+}, K^{+}, and SO_4^{2-}; representing the natural sources. Factor 2 contributes 36.56% with a higher factor loading of Fe, Mn, As, Se, Ba, Ca^{2+}, Mg^{2+}, F^{-}, HCO_3^-, representing the geogenic sources. In contrast, Factor 3 has shown 25.10% factor contribution, representing the agricultural sources with a higher concentration of B, Al, Co, Zn, Cl^{-} and NO_3^-. The relatively higher contribution of natural sources in groundwater contamination in the POM period might be due to wet monsoon precipitation. The average contribution of sources in PRM and POM is shown in Fig. 7

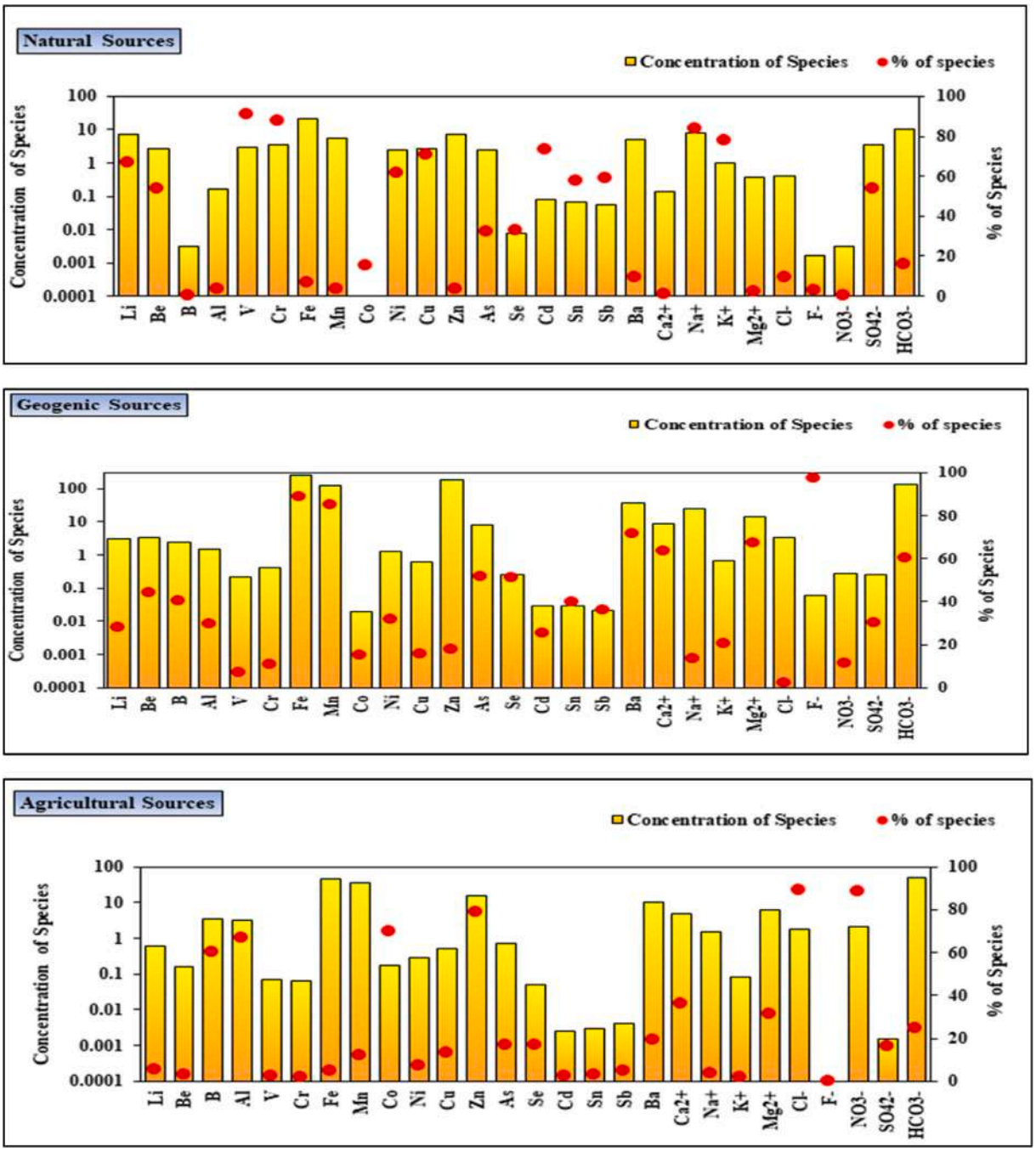

Fig. 6. Factor profile of chemical species in groundwater determined using EPA PMF5.0 receptor model for post-monsoon period.

4.5. Inter-comparison of PCA and PMF results

Source identifications and quantitative source contribution estimates of groundwater chemical contaminants were performed using the PCA and PMF 5.0 receptor modelling techniques, respectively. Both methods are different in the aspects of the software, method, and associated operations. In PCA, scree plot and KMO values were used to estimate the principal components or number of factors. Whereas in PMF 5.0, factor fingerprint represented the factor contribution of each chemical species, which was used to identify the marker species for each factor. Although both models have shown a similar source of the chemical contaminant of groundwater samples. But PCA technique is limited to predicting the possible source factors, whereas PMF5.0 results are quantitative and more precise as it is applicable in complete data including outliers and can estimate each source's composition (Comero et al., 1999).

4.6. Health risk assessment

Health risk assessment is an important aspect to understand the potential of trace elements to cause health hazards in humans via different exposure routes. Health risk has been evaluated for the heavy elements in groundwater samples through oral and dermal exposure routes in children and adults. For evaluating the annual health risk data, the mean value of PRM and POM concentrations has been considered. Outcomes of health risk analysis relevant to the carcinogenic and non-carcinogenic risks have been summarized in Table 4.

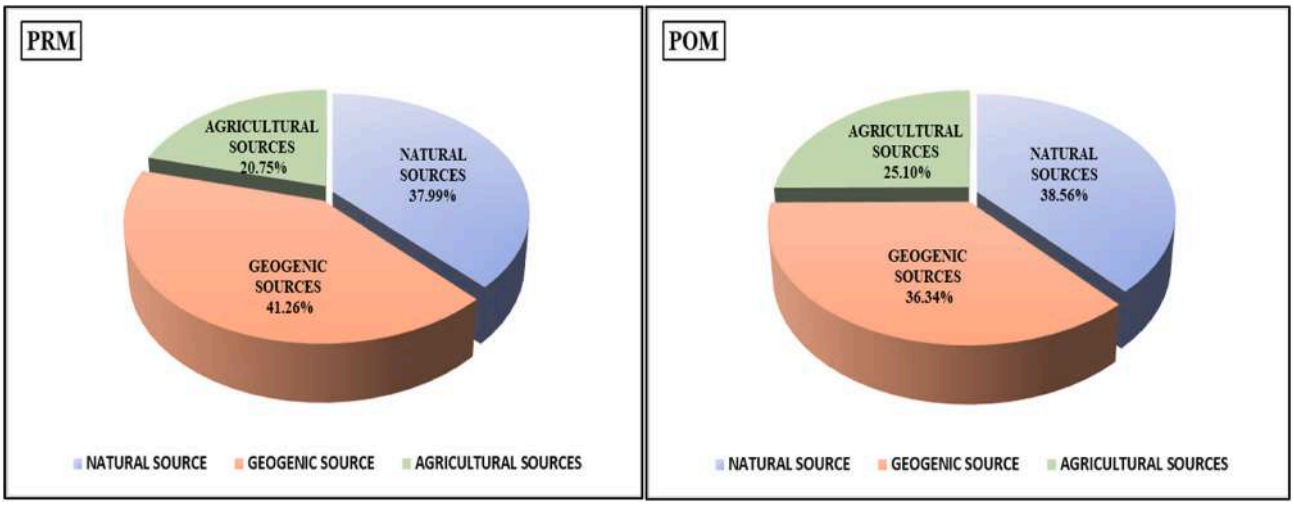

Fig. 7. Estimation of average contributions of sources in PRM and POM using EPA PMF 5.0 model.

Table 4
Average daily dose of each element from different exposure pathways: HQ, hazard quotient; HI, hazard index of groundwater; CR, Carcinogenic Risk.

Non-Carcinogenic Risk

Species	CDI (mg.kg^{-1}. day^{-1})		DAD (mg.kg^{-1}. day^{-1})		HQ_{ing}		HQ_d		HI	
	Children	Adult	Children	Adult	Children	Adult	Children	Adult	Children	Adult
Al	4.62E-04	1.98E-04	1.22E-06	7.12E-07	4.62E-04	1.98E-04	1.22E-06	7.12E-07	4.63E-04	1.99E-04
As	4.84E-04	2.07E-04	1.28E-06	7.46E-07	1.61 E+00	6.91E-01	4.26E-03	2.49E-03	1.62 E+00	6.94E-01
Ba	4.70E-03	2.01E-03	1.24E-05	7.25E-06	2.35E-02	1.01E-02	8.86E-04	5.18E-04	2.44E-02	1.06E-02
Be	4.10E-04	1.76E-04	1.08E-06	6.32E-07	2.05E-01	8.78E-02	7.72E-02	4.51E-02	2.82E-01	1.33E-01
B	6.78E-04	2.90E-04	1.79E-06	1.05E-06	3.39E-03	1.45E-03	8.95E-06	5.23E-06	3.40E-03	1.46E-03
Cd	7.52E-04	3.22E-04	1.99E-06	1.16E-06	7.52E-01	3.22E-01	3.97E-02	2.32E-02	7.92E-01	3.46E-01
Co	5.80E-05	2.49E-05	1.53E-07	8.95E-08	1.93E-01	8.28E-02	5.10E-04	2.98E-04	1.94E-01	8.31E-02
Cr	9.56E-05	4.10E-05	2.52E-07	1.47E-07	3.19E-02	1.37E-02	3.36E-03	1.97E-03	3.52E-02	1.56E-02
Cu	1.41E-04	6.06E-05	3.73E-07	2.18E-07	3.53E-03	1.51E-03	9.33E-06	5.45E-06	3.54E-03	1.52E-03
Fe	2.49E-02	1.07E-02	6.56E-05	3.84E-05	3.55E-02	1.52E-02	9.38E-05	5.48E-05	3.56E-02	1.53E-02
Li	4.24E-04	1.82E-04	1.12E-06	6.55E-07	2.12E-01	9.09E-02	5.60E-04	3.27E-04	2.13E-01	9.13E-02
Mn	1.08E-02	4.62E-03	2.85E-05	1.66E-05	7.71E-02	3.30E-02	2.03E-04	1.19E-04	7.73E-02	3.31E-02
Ni	2.16E-04	9.25E-05	5.70E-07	3.33E-07	1.08E-02	4.62E-03	7.12E-04	4.16E-04	1.15E-02	5.04E-03
Sb	3.79E-06	1.62E-06	1.00E-08	5.84E-09	9.47E-03	4.06E-03	1.67E-04	9.74E-05	9.64E-03	4.16E-03
Se	9.30E-06	3.99E-06	2.46E-08	1.44E-08	1.86E-03	7.97E-04	4.91E-06	2.87E-06	1.87E-03	8.00E-04
V	4.60E-05	1.97E-05	1.22E-07	7.10E-08	9.21E-03	3.95E-03	9.35E-04	5.46E-04	1.01E-02	4.49E-03
Zn	1.45E-02	6.22E-03	3.83E-05	2.24E-05	4.83E-02	2.07E-02	1.28E-04	7.46E-05	4.85E-02	2.08E-02
F-	1.02E-02	4.38E-03	2.70E-05	1.58E-05	2.56E-01	1.10E-01	6.75E-04	3.94E-04	2.56E-01	1.10E-01
NO_3^-	1.36E-01	5.82E-02	3.58E-04	3.84E-05	8.49E-02	3.64E-02	2.24E-04	2.40E-05	8.51E-02	3.64E-02
Sum	**2.05E-01**	**8.77E-02**	**5.40E-04**	**1.45E-04**	**3.57E + 00**	**1.53E + 00**	**1.30E-01**	**7.57E-02**	**3.70E + 00**	**1.61E + 00**

Carcinogenic Risk

Species	CDI (mg.kg^{-1}. day^{-1})		DAD (mg.kg^{-1}. day^{-1})		CR_{ing}		CR_d		CR	
	Children	Adult	Children	Adult	Children	Adult	Children	Adult	Children	Adult
As	4.84E-04	2.07E-04	1.28E-06	7.46E-07	7.26E-04	3.11E-04	1.92E-06	1.12E-06	7.28E-04	3.12E-04
Cr	9.56E-05	4.10E-05	2.52E-07	1.47E-07	4.78E-05	2.05E-05	5.05E-06	2.95E-06	5.28E-05	2.34E-05
Sum	**5.79E-04**	**2.48E-04**	**1.53E-06**	**8.94E-07**	**7.73E-04**	**3.31E-04**	**6.96E-06**	**4.07E-06**	**7.80E-04**	**3.36E-04**

4.6.1. Non-carcinogenic risk assessment

To compute the extent of health hazard resulted due to the exposure to trace and potentially toxic heavy metals/metalloids (n = 19), hazard quotient (HQ) and hazard index (HI) were evaluated. Reference Dose (RfD) values were available only for Al, As, Ba, Be, B, Cd, Co, Cr, Cu, Fe, Li, Mn, Ni, Sb, Se, V, Zn, F^-, and NO_3^-. Therefore, the non-carcinogenic risk was evaluated only for these elements. The computed overall non-carcinogenic ingestion risk (HQ_{ing}) values for children was (3.57 E+00) while for adults (1.53 E+00). The lowest and the highest non-carcinogenic risk associated with exposure via ingestion was estimated for Al and As. It is noteworthy that HQ_{ing} for all the elements was <1.00 E+00, except for As in children. The HQ_{ing} values of As for children was (1.61 E+00), which indicates that children are more susceptible to the non-carcinogenic risk posed by drinking As contaminated water. Higher ingestion of As may have a negative impact on the growth of children and may trigger cardiovascular diseases (WHO, 2011). The total non-carcinogenic dermal risk (HQ_d) value for adults and children was 1.30E-01 and 7.57E-02, respectively, within the safe limit of $HQ_d = 1.00$ E+00 for all the elements. It indicates non-carcinogenic dermal risk in adults as well as in children.

Non-carcinogenic total risk estimated by HI_{total} value evaluated for both the exposure routes both in children and adults was found 3.70 E+00 and 1.61 E+00, respectively, above the threshold limit of 1.00 E+00. The HI value of all other elements was within the limit except for

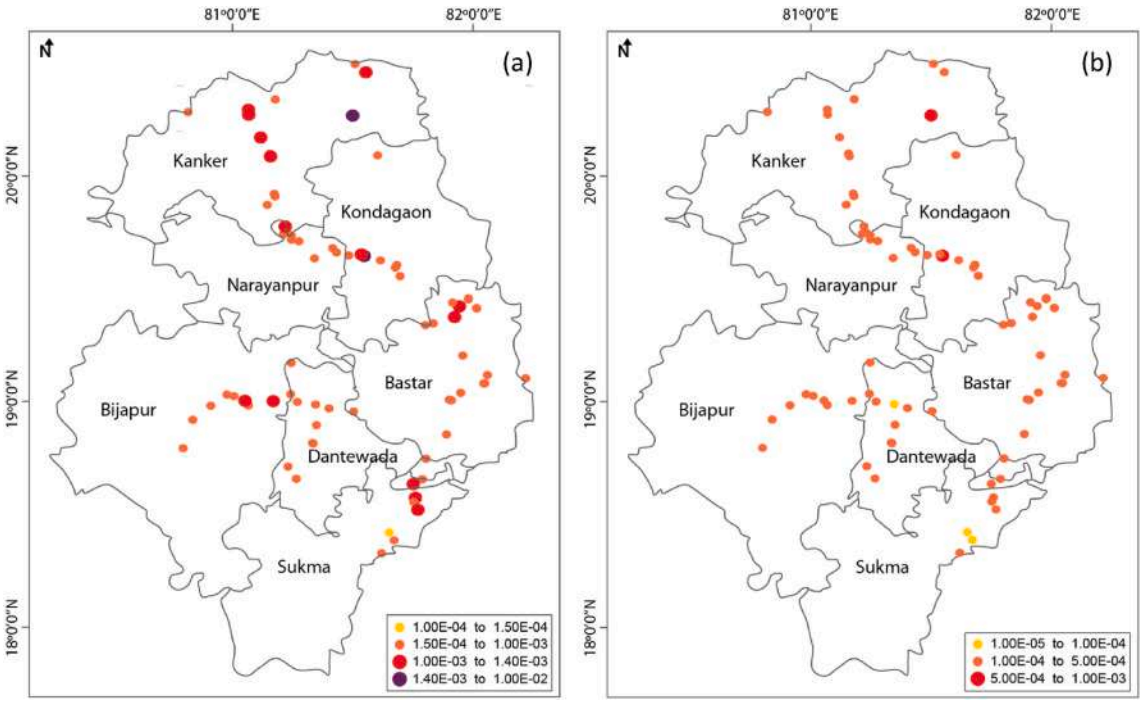

Fig. 8. Total Risk distribution for (a) children; and (b) adults.

As (1.62 E+00) in children. The results show that the non-carcinogenic risk is posed only by the As in the groundwater of the study area and children are more susceptible to risk than adults.

4.6.2. Carcinogenic risk assessment

The potential carcinogenic risk was estimated for only As and Cr as the slope factor was available only for these two elements. The overall carcinogenic risk calculated via the ingestion route (CR_{ing}) was 7.73E-04 in children and 3.31E-04 in adults, both above the maximum threshold limit (1.00E-04). The results estimated for groundwater of the study area have shown that among the two elements, As has a higher CR the ingestion risk is 7.76E-04 and 3.11E-04 for children and adults, respectively. It suggests that lifelong consumption of As-rich water may raise the cancer risk in the inhabitants. The total carcinogenic dermal risk (CR_d) in children and adults was below the safe limit (1.00E-04). The total carcinogenic risk (CR) from As and Cr in children and adult groups were found to be 7.80E-04 and 3.36E-04, respectively.

While As resulted in CR value of 7.28E-04 in children and 3.12E-04 in adults. The results suggested that the carcinogenic risk is more vulnerable to children than to adults. CR distribution by samples on the study area is presented in Fig. 8. The CR distribution shows that the geogenic sources (mineral leaching) may be the major contributor of arsenic in the groundwater of the study region. Volcanic rock weathering leads to the leaching of arsenic onto ferric hydroxide and gets deposited with the sediment which later on interaction with groundwater aquifers result in As contamination of groundwater (Pandey et al., 2006).

5. Conclusion

This study reports the spatiotemporal variability, source apportionment, and health risk assessment of trace and toxic elements, including heavy metals, ions, and metalloids in the groundwater of the tribal belt of the Bastar region. The concentration of Al, As, Fe, Mn, and Ni were significantly higher than the permissible limit in the groundwater of the study area in both PRM and POM. Source apportionment result of PCA and PMF shows that Natural, geogenic, and agricultural sources contributed to the groundwater chemical contaminants in the study area.

The exposure risk model has shown that all elements were under a safe limit except for As, which has shown higher carcinogenic and non-carcinogenic risk values. Result predicts that prolonged exposure to arsenic through contaminated water may cause carcinogenic or non-carcinogenic risks among the inhabitants of the study area. It is noteworthy that children were more susceptible to the carcinogenic and non-carcinogenic risk as compared to adults. Hence, a conclusion can be drawn that the overall groundwater of the field area is appropriate for both drinking except for some locations where concentrations of some trace elements, especially As are higher and require proper groundwater treatment. Very few works have been done in the Bastar region on groundwater quality. Thus, this study would provide detailed knowledge so that policymakers would take proper steps to improve the water quality of the Bastar region. Further awareness among the people regarding the harmful health impacts resulting from toxic elements in groundwater is desired.

Declaration of competing interest

The authors declare the following financial interests/personal relationships which may be considered as potential competing interests: Shamsh Pervez reports financial support was provided by Science and Engineering Research Board. Princy Dugga reports financial support was provided by University Grants Commission.

Acknowledgment

The presented piece of work was primarily supported by the Science and Engineering Research Board (SERB), India (EMR/2015/000928) and partially supported by the DST FIST program (SR/FST/CSI-259/2014 (c)) and UGC-SAP-DRS-II program (F-540/7/DRS-II/2016 (SAP-I)). Princy Dugga (PD) is grateful to UGC and Pt. Ravishankar Shukla University for providing Joint UGC-CSIR Fellowship [F.No.16-6 (Dec.2017)/2018(NET/CSIR)] along with laboratory and library facilities, respectively. Authors Shamsh Pervez (SP) and (PD) are also grateful to Thermo Fischer Scientific, Mumbai (India) for providing instrumentation facilities.

Appendix A. Supplementary data

Supplementary data to this article can be found online at https://doi.org/10.1016/j.gsd.2021.100628.

References

Ahada, C.P.S., Suthar, S., 2018. Assessing groundwater hydrochemistry of Malwa Punjab, India. Arab. J. Geosci. 11 https://doi.org/10.1007/s12517-017-3355-8.

Behera, B., Das, M., Rana, G.S., 2012. Studies on ground water pollution due to iron content and water quality in and around, Jagdalpur, Bastar district, Chattisgarh, India. J. Chem. Pharmaceut. Res. 4, 3803–3807.

Belkhiri, L., Narany, T.S., 2015. Using multivariate statistical analysis, geostatistical techniques and structural equation modeling to identify spatial variability of groundwater quality. Water Resour. Manag. 29, 2073–2089.

Bhutiani, R., Kulkarni, D.B., Khanna, D.R., Gautam, A., 2016. Water quality, pollution source apportionment and health risk assessment of heavy metals in groundwater of an industrial area in North India. Expo. Heal 8, 3–18. https://doi.org/10.1007/s12403-015-0178-2.

BIS, 2012. Indian standard drinking water specification (second revision). Bur. Indian Stand. IS 10500, 1–11.

Boateng, T.K., Opoku, F., Acquaah, S.O., Akoto, O., 2016. Groundwater quality assessment using statistical approach and water quality index in Ejisu-Juaben Municipality, Ghana. Environ. Earth Sci. 75, 1–14. https://doi.org/10.1007/s12665-015-5105-0.

Bouderbala, A., Gharbi, B.Y., 2017. Hydrogeochemical characterization and groundwater quality assessment in the intensive agricultural zone of the Upper Cheliff plain, Algeria. Environ. Earth Sci. 76, 1–17. https://doi.org/10.1007/s12665-017-7067-x.

Brindha, K., Paul, R., Walter, J., Tan, M.L., Singh, M.K., 2020. Trace metals contamination in groundwater and implications on human health: comprehensive assessment using hydrogeochemical and geostatistical methods. Environ. Geochem. Health 42, 3819–3839. https://doi.org/10.1007/s10653-020-00637-9.

Chen, R., Teng, Y., Chen, H., Hu, B., Yue, W., 2019. Groundwater pollution and risk assessment based on source apportionment in a typical cold agricultural region in Northeastern China. Sci. Total Environ. 696, 133972. https://doi.org/10.1016/j.scitotenv.2019.133972.

Clark, R., Lawrence, A., Foster, S., 1996. Groundwater: A Threatened Resource. United Nations Environ. Program.

Comero, S., Capitani, L., Gawlik, B.M., 1999. Positive Matrix Factorisation (PMF) Environmental Monitoring Data Using PMF. Environmetrics. https://doi.org/10.2788/2497.

Defarge, N., Spiroux de Vendômois, J., Séralini, G.E., 2018. Toxicity of formulants and heavy metals in glyphosate-based herbicides and other pesticides. Toxicol. Rep. 5, 156–163. https://doi.org/10.1016/j.toxrep.2017.12.025.

https://dolr.gov.in/sites/default/files/Old_SPSP_of_CG%20opt.pdf.

Dora, M.L., 2014. PGE mineralization in Bastar Craton, central India: prospects and constraints. Indian J. Geosci 68.

Drever, J.I., 1997. The Geochemistry of Natural Waters: Surface and Groundwater Environments, third ed. Prentice Hall, Upper Saddle River, NJ).

Dugga, P., Pervez, S., Tripathi, M., Siddiqui, M.N., 2020. Spatiotemporal variability and source apportionment of the ionic components of groundwater of a mineral-rich tribal belt in Bastar, India. Groundw. Sustain. Dev. 10 https://doi.org/10.1016/j.gsd.2020.100356.

Duggal, V., Rani, A., 2018. Carcinogenic and Non-carcinogenic Risk Assessment of Metals in Groundwater via Ingestion and Dermal Absorption Pathways for Children and Adults in Malwa Region of Punjab, vol. 92, pp. 187–194. https://doi.org/10.1007/s12594-018-0980-0.

Edition, F., 2011. Guidelines for drinking-water quality. WHO Chron. 38, 104–108.

El Nemr, A., El-Said, G.F., Ragab, S., Khaled, A., El-Sikaily, A., 2016. The distribution, contamination and risk assessment of heavy metals in sediment and shellfish from the Red Sea coast, Egypt. Chemosphere 165, 369–380. https://doi.org/10.1016/j.chemosphere.2016.09.048.

Emenike, P.G.C., Tenebe, I., Ogarekpe, N., Omole, D., Nnaji, C., 2019. Probabilistic risk assessment and spatial distribution of potentially toxic elements in groundwater sources in Southwestern Nigeria. Sci. Rep. 9, 1–15. https://doi.org/10.1038/s41598-019-52325-z.

EPA, 1989. Risk Assessment Guidance for Superfund. Volume I Human Health Evaluation Manual (Part A) I, p. 289.

Gimeno-García, E., Andreu, V., Boluda, R., 1996. Heavy metals incidence in the application of inorganic fertilizers and pesticides to rice farming soils. Environ. Pollut. 92, 19–25. https://doi.org/10.1016/0269-7491(95)00090-9.

Guo, X., Zuo, R., Shan, D., Cao, Y., Wang, J., Teng, Y., Fu, Q., Zheng, B., 2017. Source apportionment of pollution in groundwater source area using factor analysis and positive matrix factorization methods. Hum. Ecol. Risk Assess. 23, 1417–1436. https://doi.org/10.1080/10807039.2017.1322894.

Gupta, A., Kunar, S., Shekhar, S., J, A.M.-I.I., 2016. undefined, 2012. Water and Food Security of the Central Indian Craton. Academia, Edu.

Haji Gholizadeh, M., Melesse, A.M., Reddi, L., 2016. Water quality assessment and apportionment of pollution sources using APCS-MLR and PMF receptor modeling techniques in three major rivers of South Florida. Sci. Total Environ. 566 (567), 1552–1567. https://doi.org/10.1016/j.scitotenv.2016.06.046.

Helena, B., Pardo, R., Vega, M., Barrado, E., Fernandez, J.M., Fernandez, L., 2000. Temporal evolution of groundwater composition in an alluvial aquifer (Pisuerga River, Spain) by principal component analysis. Water Res. 34, 807–816.

Hossain, M., Patra, P.K., 2020. Contamination zoning and health risk assessment of trace elements in groundwater through geostatistical modelling. Ecotoxicol. Environ. Saf. 189, 110038. https://doi.org/10.1016/j.ecoenv.2019.110038.

Hu, G., Mian, H.R., Dyck, R., Mohseni, M., Jasim, S., Hewage, K., Sadiq, R., 2020. Drinking water treatments for arsenic and manganese removal and health risk assessment in white rock, Canada. Expo. Heal 12, 793–807. https://doi.org/10.1007/s12403-019-00338-4.

Hudak, P.F., 2012. Nitrate and chloride concentrations in groundwater beneath a portion of the trinity group outcrop zone, Texas. Int. J. Environ. Res. 6, 663–668. https://doi.org/10.22059/ijer.2012.536.

IARC Working Group on the Evaluation of Carcinogenic Risks to Humans, 2012. Chemical agents and related occupations. IARC Monogr. Eval. Carcinog. Risks Hum. 100, 9–562.

Islam, A.R.M.T., Bodrud-Doza, M., Rahman, M.S., Amin, S.B., Chu, R., Al Mamun, H., 2019. Sources of Trace Elements Identification in Drinking Water of Rangpur District, Bangladesh and Their Potential Health Risk Following Multivariate Techniques and Monte-Carlo Simulation, Groundwater for Sustainable Development. Elsevier B.V. https://doi.org/10.1016/j.gsd.2019.100275.

Jassas, H., Merkel, B., 2015. Assessment of hydrochemical evolution of groundwater and its suitability for drinking and irrigation purposes in Al-Khazir Gomal Basin, Northern Iraq. Environ. Earth Sci. 74, 6647–6663. https://doi.org/10.1007/s12665-015-4664-4.

Kashyap, R., Verma, K.S., Uniyal, S.K., Bhardwaj, S.K., 2018. Geospatial distribution of metal(loid)s and human health risk assessment due to intake of contaminated groundwater around an industrial hub of northern India. Environ. Monit. Assess. 190 https://doi.org/10.1007/s10661-018-6525-6.

Krishna, A.K., Satyanarayanan, M., Govil, P.K., 2009. Assessment of heavy metal pollution in water using multivariate statistical techniques in an industrial area: a case study from Patancheru, Medak District, Andhra Pradesh, India. J. Hazard Mater. 167, 366–373. https://doi.org/10.1016/j.jhazmat.2008.12.131.

Li, P., Li, X., Meng, X., Li, M., Zhang, Y., 2016. Appraising groundwater quality and health risks from contamination in a semiarid region of Northwest China. Expo. Heal 8, 361–379. https://doi.org/10.1007/s12403-016-0205-y.

Liu, J., Gao, M., Jin, D., Wang, T., Yang, J., 2020. Assessment of groundwater quality and human health risk in the aeolian-sand area of Yulin City, Northwest China. Expo. Heal. 12, 671–680. https://doi.org/10.1007/s12403-019-00326-8.

Loh, Y.S.A., Akurugu, B.A., Manu, E., Aliou, A.S., 2020. Assessment of groundwater quality and the main controls on its hydrochemistry in some Voltaian and basement aquifers, northern Ghana. Groundw. Sustain. Dev. 10, 100296. https://doi.org/10.1016/j.gsd.2019.100296.

Lu, K.L., Liu, C.W., Jang, C.S., 2012. Using multivariate statistical methods to assess the groundwater quality in an arsenic-contaminated area of Southwestern Taiwan. Environ. Monit. Assess. 184, 6071–6085. https://doi.org/10.1007/s10661-011-2406-y.

Mahato, M.K., Singh, P.K., Tiwari, A.K., Singh, A.K., 2016. Risk assessment due to intake of metals in groundwater of east bokaro coalfield, Jharkhand, India. Expo. Heal. 8, 265–275. https://doi.org/10.1007/s12403-016-0201-2.

Mineral Resources Department 2014.http://chhattisgarhmines.gov.in/sites/default/files/treasure-trove-cg-minerals.pdf.

Mohammadi, A.A., Zarei, A., Majidi, S., Ghaderpoury, A., Hashempour, Y., Saghi, M.H., Alinejad, A., Yousefi, M., Hosseingholizadeh, N., Ghaderpoori, M., 2019. Carcinogenic and non-carcinogenic health risk assessment of heavy metals in drinking water of Khorramabad, Iran. MethodsX 6, 1642–1651. https://doi.org/10.1016/j.mex.2019.07.017.

Mondal, N.C., Singh, V.S., Puranik, S.C., Singh, V.P., 2010. Trace element concentration in groundwater of Pesarlanka Island, Krishna Delta, India. Environ. Monit. Assess. 163, 215–227. https://doi.org/10.1007/s10661-009-0828-6.

Norris, G., Duvall, R., Brown, S., Bai, S., 2014. Epa Positive Matrix Factorization (Pmf) 5.0 Fundamentals and User Guide Prepared for the Us Environmental Protection Agency Office of Research and Development. Inc., washington, dc.

Paatero, P., 1997. Least squares formulation of robust non-negative factor analysis. Chemometr. Intell. Lab. Syst. 37, 23–35.

Pandey, P.K., Sharma, R., Roy, M., Roy, S., Pandey, M., 2006. Arsenic contamination in the Kanker district of central-east India: geology and health effects. Environ. Geochem. Health 28, 409–420. https://doi.org/10.1007/s10653-005-9039-4.

Prasanth, S.V.S., Magesh, N.S., Jitheshlal, K.V., Chandrasekar, N., Gangadhar, K., 2012. Evaluation of groundwater quality and its suitability for drinking and agricultural use in the coastal stretch of Alappuzha District, Kerala, India. Appl. Water Sci. 2, 165–175.

Rahman, M.M., Naidu, R., Bhattacharya, P., 2009. Arsenic contamination in groundwater in the Southeast Asia region. Environ. Geochem. Health 31, 9–21. https://doi.org/10.1007/s10653-008-9233-2.

Ravindra, K., Mor, S., 2019. Distribution and health risk assessment of arsenic and selected heavy metals in Groundwater of Chandigarh, India. Environ. Pollut. 250, 820–830. https://doi.org/10.1016/j.envpol.2019.03.080.

Rubina, S., Kavita, T., 2013. International journal of Research in advent technology. Monitoring of fluoride contamination in southern region of Chhattisgarh , India : correlation with physico-chemical parameters international journal of Research in advent technology. Int. J. Res. Advent Technol. 1.

Sethy, S.N., Syed, T.H., Kumar, A., Sinha, D., 2016. Hydrogeochemical characterization and quality assessment of groundwater in parts of Southern Gangetic Plain. Environ. earth Sci. 75, 232.

Singh, G., Kamal, R.K., 2017. Heavy metal contamination and its indexing approach for groundwater of Goa mining region, India. Appl. Water Sci. 7, 1479–1485. https://doi.org/10.1007/s13201-016-0430-3.

Sinha, M.K., 2011. Ethnobotany in Relation to Health and Livelihood Security in District Bastar of Chhattisgarh State. Raipur.

US-EPA, 2014. EPA Positive M Atrix Factorization (PM F) 5 . 0 Fundamentals and 136.

US Environmental Protection Agency, 2011. Exposure Factors Handbook: 2011 Edition. U.S. Environ. Prot. Agency EPA/600/R.

USEPA, 2004. Risk Assessment Guidance for Superfund (RAGS). Volume I. Human Health Evaluation Manual (HHEM). Part E. Supplemental Guidance for Dermal Risk Assessment.

Varghese, J., Jaya, D.S., 2014. Metal pollution of groundwater in the vicinity of Valiathura sewage farm in Kerala, South India. Bull. Environ. Contam. Toxicol. 93, 694–698.

Wang, C.H., Hsiao, C.K., Chen, C.L., Hsu, L.I., Chiou, H.Y., Chen, S.Y., Hsueh, Y.M., Wu, M.M., Chen, C.J., 2007. A review of the epidemiologic literature on the role of environmental arsenic exposure and cardiovascular diseases. Toxicol. Appl. Pharmacol. 222, 315–326. https://doi.org/10.1016/j.taap.2006.12.022.

WHO, 2019. Drinking-water. https://www.who.int/news-room/fact-sheets/detail/drinking-water.

Yavar Ashayeri, N., Keshavarzi, B., 2019. Geochemical characteristics, partitioning, quantitative source apportionment, and ecological and health risk of heavy metals in sediments and water: a case study in Shadegan Wetland, Iran. Mar. Pollut. Bull. 149, 110495. https://doi.org/10.1016/j.marpolbul.2019.110495.

Environmental Research xxx (xxxx) xxx

Contents lists available at ScienceDirect

Environmental Research

journal homepage: www.elsevier.com/locate/envres

Using functionalized asphaltenes as effective adsorbents for the removal of chromium and lead metal ions from aqueous solution

Mohammad Nahid Siddiqui [a,*], Shamsh Pervez [b,**], Indrapal Karbhal [b], Princy Dugga [b], Saravanan Rajendran [c], Yasmeen Fatima Pervez [d]

[a] Department of Chemistry and IRC for Membranes and Water Security, King Fahd University of Petroleum & Minerals, Dhahran, 31261, Saudi Arabia
[b] School of Studies in Chemistry, Pt. Ravishankar Shukla University, Raipur, 492010, Chhattisgarh, India
[c] Laboratorio de Investigaciones Ambientales Zonas Áridas, Departamento de Ingeniería Mecánica, Facultad de Ingeniería, Universidad de Tarapacá, Avda. General Velásquez, 1775, Arica, Chile
[d] Department of Chemistry, Government Elvaya College, DOndi-Lohara, Balod, CG, India

ARTICLE INFO

Keywords:
Asphaltene
Functionalization
Cr(VI)
Pb(II)
Adsorption
Wastewater treatment

ABSTRACT

For the first time, functionalized asphaltene has been designed, synthesized, and used for the removal of heavy metals from the water. Asphaltene was separated from the crude oil with the addition of n-alkanes. Asphaltene having a complex chemical structure including multilayered and clustered aromatic fused rings bearing aliphatic chains. Asphaltene also contains heteroatoms like N, S, and O atoms along with Ni and V as prominent trace metals. On functionalization of asphaltene with nitric acid, the aliphatic chains and some of the naphthenic rings broke down and developed –COOH, –C═O, C–O, and other oxygen functional groups which are playing key roles as surface-active agents in the removal of the heavy metals via chemisorption. The study was conducted using different parameters such as dose, time, pH, and concentration. The adsorption efficiency for this material at pH 4 is excellent for the removal of chromium and lead. The Langmuir, Freundlich and Temkin adsorption isotherm models as well as Lagergren pseudo second-order kinetic model were investigated. The positive enthalpies ΔHs confirm that the adsorption process is endothermic and the negative free energies ΔGs confirm the spontaneity of the process. The good efficiency of the adsorption implies the efficacy in the removal of the heavy metal ions, as well as the good efficiency in desorption, which implies the excellent recovery of the adsorbent. The effective reusability of this adsorbent makes it applicable for industrial water treatment from contaminants.

1. Introduction

The consumption of crude oil increased dramatically in the last decades. About 70% of the heavy crude oil residue is drilled out and a very small amount is being used without significant process (Speight, 1990).

One of the fractions that are considered as the most troublemaker is the asphaltenes in the refinery and cracking processing of the petroleum, that's due to the precipitation of the asphaltenes can reduce the flow of the oil and also can lead to blockage problems in several types of equipment (Cimino et al., 1995). Moreover, these compounds can form sludges and can deactivate the hydro-desulfurization and hydro-cracking catalysts which lead to a reduction in conversion efficiency for the two processes (Bartholomew, 1994; Miyauchi and de Wind, 1994).

The structure of these compounds was very difficult to study due to their chemical complexity & composition, it was reported that this material is composed of poly-aromatic groups in the center connected with alicyclic and aliphatic groups along with some heteroatoms and some metal ions (Hasan et al., 1988; Shirokoff et al., 1997).

The contamination of water by heavy metal ions is a very serious issue, the source of these metals are different industries such as mining, battery, and other chemical industries. Small concentrations of these heavy metal ions can cause dangerous diseases such as anaemia, cancer, renal and kidney failure, mental retardation, and other serious diseases (Nordberg et al., 2014).

These metal ions are non-biodegradable that's why they need to be removed from the water. There are many methods available for the removal of these materials such as hydroxide or sulfide precipitation, ion

* Corresponding author.
** Corresponding author.
E-mail addresses: mnahid@kfupm.edu.sa (M.N. Siddiqui), shamshpervez@gmail.com (S. Pervez).

https://doi.org/10.1016/j.envres.2021.112361
Received 5 September 2021; Received in revised form 31 October 2021; Accepted 3 November 2021
Available online 9 November 2021
0013-9351/

exchange, flocculation, membrane separation, and adsorption. Among these methods, adsorption is one of the most promising and effective methods due to its eco-friendly, simple, cost-effectiveness, and applicability for the industry.

Many sorbents are used for the removal of these heavy metals such as activated carbon (Rao et al., 2007), fly ash (Ayala et al., 1998), peat (Ho and McKay, 1999), recycled alum sludge (Chu, 1999), peanut hulls (Brown et al., 2000), resins (Diniz et al., 2002), kaolinite (Arias et al., 2002), zeolite (Biškup and Subotić, 2005), biomaterials, carbon nanomaterial (Ekmekyapar et al., 2006; Li et al., 2004), and multi-walled carbon nanomaterial (Rao et al., 2007) Graphene Oxide (Sahoo and Hota, 2019). But there are several drawbacks for metal oxides due to their poor stability and corrosion. On the other hand, carbon-based materials such as graphene oxide (GO), carbon nanotubes (CNTs), and different forms of carbon have been widely used due to their high surface area, stability, and reusability. Moreover, recently the functionalization of carbon-based materials has attracted great attention due to their strong affinity towards metal ions (Shaikh et al., 2021; Siddiqui, 2017; Siddiqui et al., 2020, 2021; Suliman et al., 2020). Functionalization of carbon-based material can generate high surface active sites such as –OH, –COOH, –C═O, -C-O, $–NH_2$, and -S- etc resulting in enhanced hydrophilicity and wettability as well as they play key roles for strong interaction with metal ions by complexation, hard-hard or borderline hard and soft interaction. Although, GO and CNTs have been widely used as an adsorbent but due to their limitations and cost-effectiveness, it is needed to develop low cost, reusable and environmentally friendly materials.

Looking to the current scenario, in this work the asphaltenes have been isolated and functionalized as adsorbents for the removal of water pollutants such as some types of heavy metals ions (Cr and Pb). Hexavalent chromium and lead are known to be mutagenic and carcinogenic in nature (IARC 2012). WHO water quality standards recommend permissible limits of hexavalent Cr (0.05 $mg.L^{-1}$) and Pb (0.01 $mg.L^{-1}$) for potable water (WHO, 2017). Many industrial effluents including textile industries, metal finishing, leather tanneries and lead acid batteries are known for higher contents of Cr(VI) and Pb(II) ions and contaminate the adjoining natural water streams and soils (Mahato et al., 2016; Singh et al., 2017). Looking in to the advantages of the functionalized asphaltene, different functional group such as –OH, COOH, $–NH_2$, -S- etc act as chelation centres to bind with metal ions and remove the Cr(VI) and Pb(II) from water via hard-hard or borderline hard and soft interaction (Ravikumar et al., 2016). In cases of most of the environmental samples, Cr(VI) and Pb(II) are found in ionic forms and asphaltene has different functional groups which can bind either with coordinated bond due to presence of lone pair of electron on O, N and C or ion exchange mechanism takes place at certain pH (Xiao and Lin, 2020).

There are several advantages to use functionalized asphaltene such as reusability, low cost, durability, and the presence of surface-active functional groups such as –COOH, –OH, –C═O, -C-O, $–NH_2$, and -S- etc show more promising behaviour to adsorb metal ions. Heavy metal ions could interact with the hydrophilic functional group through H-bonding or complexation and electrostatic interaction and can adsorb more metal ions than non-functionalized (Coughlin and Ezra, 1968; McKay et al., 1985; Yang and Xing, 2010).As functionalized asphaltene is metal-free and has high surface-active agents influencing the adsorption performance and can open the new window to develop sustainable material from the waste.

2. Experimental

2.1. Asphaltenes separation

About 7.0 g of Arabian heavy residue was transferred to a beaker and heated with a very small amount of n-heptane. The solution was mixed properly and transferred to 2 L container, then to this solution 700 ml of n-heptane was added. The solution was placed in a mechanical shaker with a water bath. To increase the residue solubility in the heptane, it was heated at 90 °C for 2 h with continuous stirring. Then the solution was covered using aluminium foil and was stand for cooling overnight. The gradual cooling helps to produce efficient precipitation of asphaltenes. After that, the solution was filtered with 0.8 μm pore size filter paper. The residue part was extracted by soxhlet using toluene as extracting solvent, and the extract was filtered with the same microfilter paper. After the evaporation of the extract, the asphaltenes were collected in a beaker. Then it was washed many times with a small amount of n-heptane. Finally, the solid asphaltene was dried at 105 °C for 2 h.

2.1.1. Functionalization of asphaltenes

About 10 g of the asphaltenes were dispersed in nitric acid (70%) and the solution was sonicated for 60 min. The mixture was refluxed for 6 h. Then the mixture was cooled down. The functionalized asphaltenes were washed with water many times until the deionized water became clear, then the asphaltenes were dried for 24 h in an oven at 100 °C and were pulverized in a ball mill.

2.2. Sample characterization

The functionalized asphaltenes were characterized using scanning electron microscopy (SEM) and Fourier transform infrared spectroscopy (FTIR). FESEM/FIB/GIS (Tescan Lyra-3) was used for the morphological studies of the material operated at 20.0 kV. Nicolet 6700 FT-IR spectrometer was used in the range 400–4000 cm^{-1} for the FT-IR spectral measurements of the material. The Brunauer–Emmett–Teller (BET) analysis was performed using a micromeritics (Tristar II PLUS) instrument under the continuous adsorption conditions to determine the surface area.

2.3. Adsorption experiments

The adsorption properties of the adsorbent for Cr and Pb ions were determined by spectrophotometric method; the procedure for heavy metal ions adsorption was as follows: A mixture of adsorbent (200 mg) in 25 ml of 50 mg/L heavy metals ions solution was stirred using a temperature-controlled shaker-bath at various pH for overnight. pH was adjusted using both 0.1M and 1.0M nitric acid and 0.1M and 1M sodium hydroxide solutions; at pH 4 the adsorption was relatively higher than neutral pH. The adsorbent was filtered and the filtrate is then analyzed by an AAS spectrophotometer to find out the remaining heavy metals ion concentration.

The capacity of adsorption (q_{ion}) was calculated by Eq. (1):

$$q_{ions} = \frac{(C_i - C_e)\,V}{W}\ mmol \Big/ g \tag{1}$$

Where C_i and C_e are the initial and equilibrium concentrations of heavy metals ion respectively, W is the weight of the adsorbent in g and V is the volume of the solution in a milliliter (Sahoo et al., 2019).

Adsorption kinetic studies were carried out by stirring 25 ml of 50 mg/L solution in a preferred pH buffer with the adsorbent (200 mg) at different temperatures and determining the heavy metals ion concentrations by taking a small amount of filtered aliquots at various time intervals. Adsorption isotherms were constructed by determining the adsorption capacities of the adsorbent at different heavy metals ion Concentration ranging from 10 mg/L to 100 mg/L at ambient temperature. Experiments were carried out at different temperatures, thermodynamic parameters such as a change in enthalpy ΔH, change in free energy ΔG, and change in entropy ΔS were calculated.

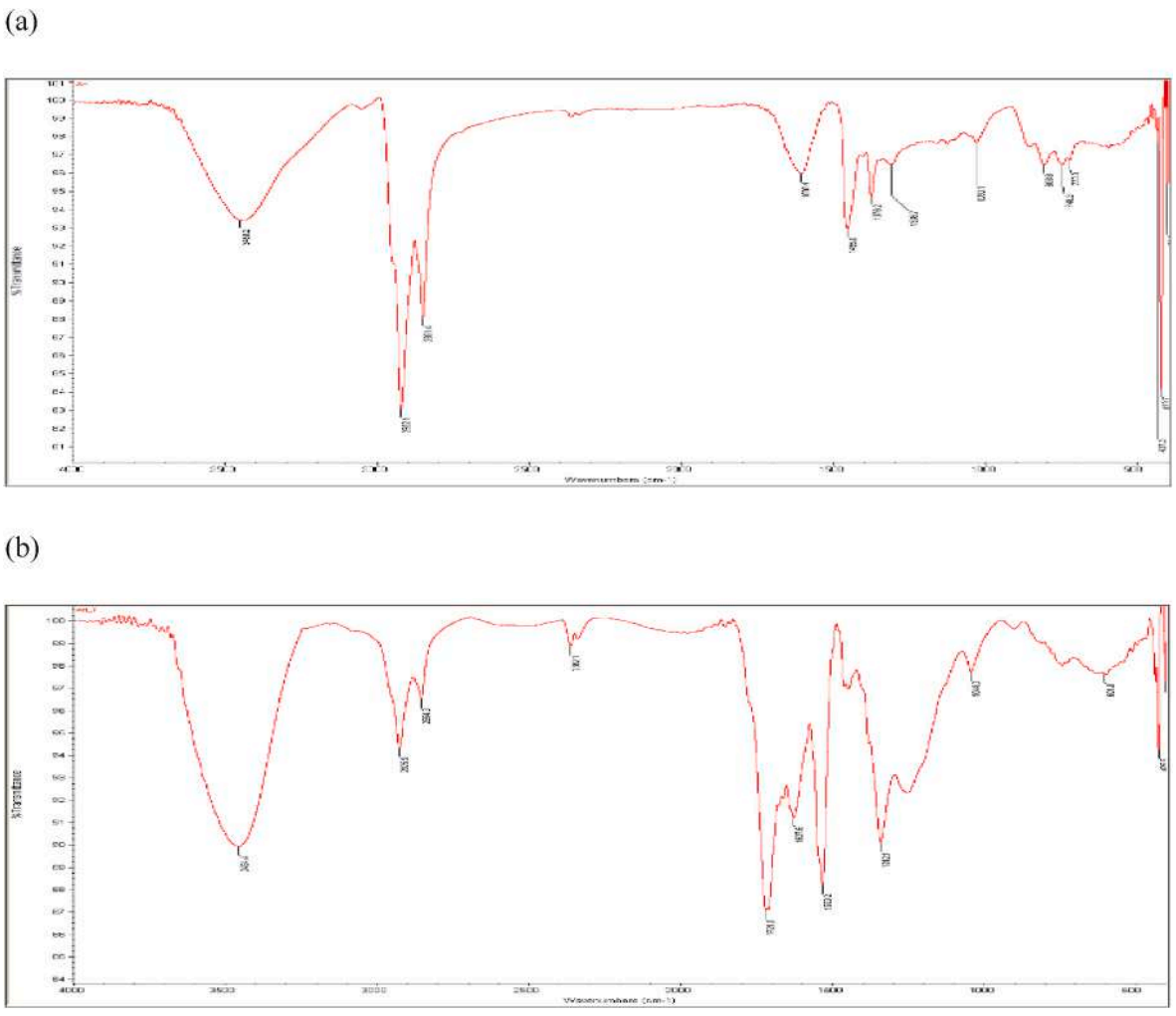

Fig. 1. (a) IR spectra of virgin asphaltenes (b) IR spectra of asphaltenes after functionalization.

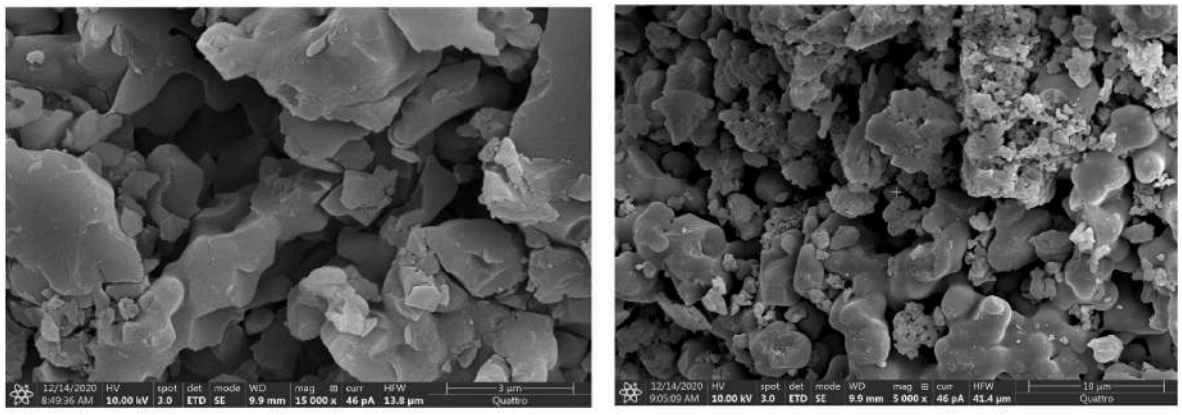

Fig. 2. (a) SEM of AH virgin asphaltenes (b) SEM of AH functionalized asphaltenes.

3. Results and discussion

3.1. Functionalized asphaltenes characterization

The functionalized asphaltenes were characterized using different techniques: SEM, FT-IR, Elemental analysis, and EDX.

Fig. 1 represents the IR spectra of AH asphaltene and functionalized asphaltene. The presence of a broad peak at 3450 cm^{-1} is due to the –OH stretching frequency in both samples. After functionalization, the peak appeared at 1720 cm^{-1}, which confirms the presence of the carbonyl (C═O) group compared to the non-functionalized. Moreover, there are other peaks such as at 2925 cm^{-1} and 2854 cm^{-1} are due to the –NH

Table 1
Elemental analysis (%).

Sample	C	H	N	S	O (by difference)
AH	81.28	7.44	1.19	7.17	2.92
AH-F	57.08	4.13	5.31	5.65	27.83

stretching vibration of the amine group. 1627 cm^{-1} C═C stretching of the aromatic ring, 1533 cm^{-1} is due to NH_2 bending, 1455 cm^{-1} is due to C–OH, 1376 cm^{-1} and 1342 cm^{-1} are due to pyridinic ring stretching, 1044 cm^{-1} C–O and stretching vibration and bending vibration of secondary amine, 748 cm^{-1} is due to C–S stretching frequency (Du et al., 2020; Pooja et al., 2017; Sahoo and Hota, 2019) All the data confirm the presence of functional groups in asphaltene which significantly play a key role in the formation of the chelate ring or complex with the metals.

Fig. 2 (a) shows the SEM image of AH virgin asphaltenes and Fig. 2 (b) shows the functionalized asphaltenes. SEM images clearly show the morphological difference between both images.

After functionalization of asphaltene, it became spongy because of the gaining of the extra-functional groups like –OH and –COOH etc.

The type of porosity and the surface area of the virgin asphaltene and funtionalized asphaltene were obtained by the nitrogen adsorption isotherm (BET). The surface area of the virgin asphaltene was found to be 5.4144 m^2/g. However, the functionalized asphaltene has a significantly lower a surface area of 3.8268 m^2/g. This is a substantial drop in the surface area of functionalized asphaltene is due to the development of oxygen moieties on the surface of virgin asphaltene after functionalization. Similarly, adsorption average pore width was found to be 64.4673 Å for virgin asphaltene and 52.8895 Å for functionalized asphaltene. The higher values of surface area and average pore width in asphaltene are due to the development of several oxygen containing functional and chemical groups on functionalized asphaltene.

Table 1 shows the elemental analysis of asphaltenes and functionalized asphaltenes, this clearly shows the gaining of extra oxygen after functionalization, which has increased from 2.92% to 27.83%. This indicates the very good functionalization of the asphaltenes, and SEM image also reveals the functionalization of asphaltene. Variation in the concentrations (%) of major constituent elements (C, H, N, S) of functionalized asphaltene (carbon C-81.28 to 57.08, H-7.44 to 4.13, N- 1.19 to 5.31 and S- 7.17 to 5.65%) indicates the gaining of extra elements after functionalization These functional groups act as chelating agents and play a key role to bind the metal ions via complexation.

3.2. *Adsorption properties of the adsorbent*

The adsorbent showed high ion exchange capacity (IEC), and excellent adsorption ability for heavy metal ions due to the presence of different kinds of functional groups available such as –OH, COOH, –C═O, -C-O, $–NH_2$, and -S- etc which are responsible for ion-exchange and complex formation. Because of these functional groups, functionalized asphaltenes show promising adsorbent properties.

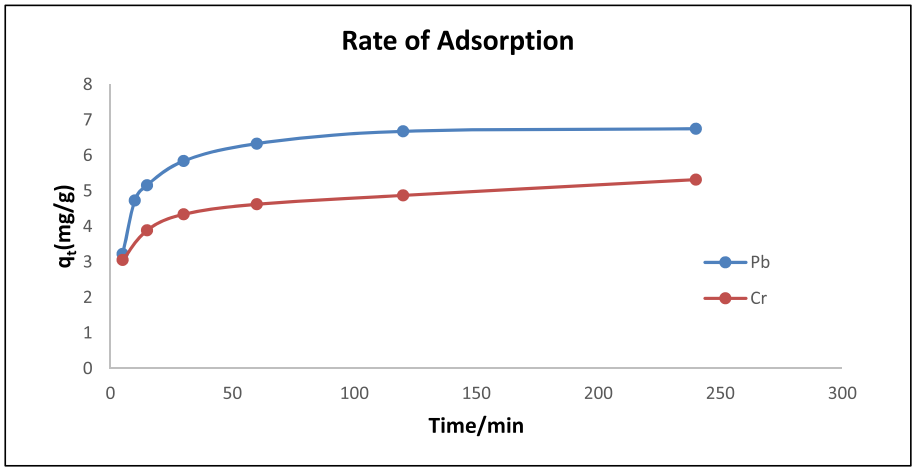

Fig. 3. Adsorption curves with the time of 25 ppm for Cr & Pb solution at their optimum pH.

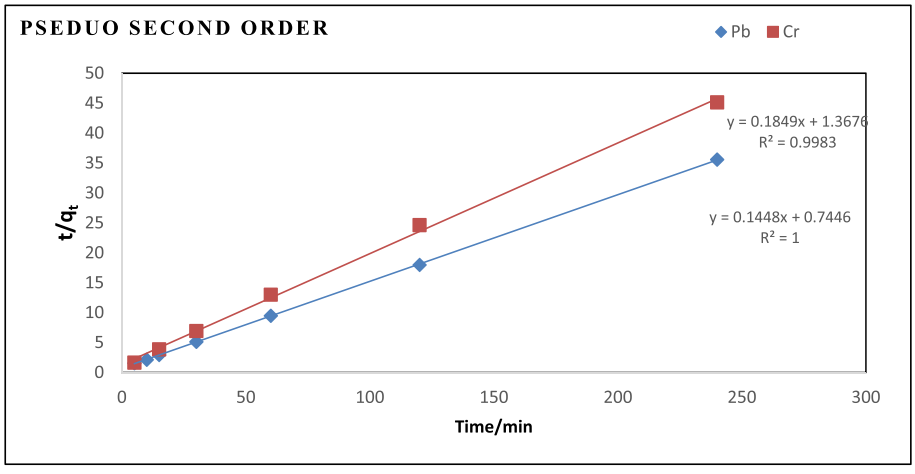

Fig. 4. Adsorption pseudo second order model for Cr and Pb at 295 K.

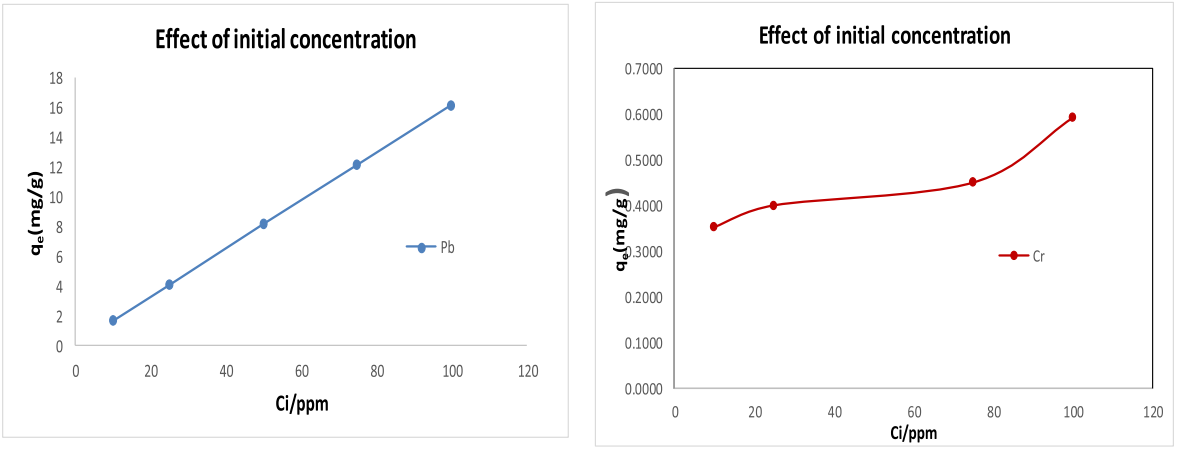

Fig. 5. The initial Concentration effect on the removal of heavy metal ions for Pb and Cr for 24 h at 25 0C.

3.3. Adsorption kinetics

A plot of adsorption capacity versus time determines the adsorption rate in the below Fig. 3. It has been found that the adsorption equilibrium for Cr and Pb ions by adsorbent reached about 1.0 h. Lagergren's adsorption kinetic model has been reported as an optimum method to study the properties of adsorption. The kinetic orders were expressed by the equations below (first and second-order models respectively).

$$\log (q_e - q_t) = \log q_e - \frac{k_1 t}{2.303} \quad (2)$$

$$\frac{t}{q_t} = \frac{1}{k_2 q_e^2} + \frac{t}{q_e} \quad (3)$$

Where k_1 is the first-order constant and k_2 is the second-order rate constant; q_t and q_e are the capacities of the adsorption for the adsorbent at time t and equilibrium. Although Cr and Pb both gave regression values (R^2) above 0.9 for the pseudo-first-order Lagergren kinetic model. In Fig. 4 linear plot between t/qt and time indicates that Cr and Pb were best fitted for the second-order model and hence more appropriate to explain the adsorption kinetics of both the elements (Fan et al., 2020).

3.4. Initial concentration effect on the removal of Cr and Pb

The adsorption capacity of adsorbent with change in initial concentrations of Cr and Pb metal ions is depicted in Fig. 5. The effect of concentrations of Cr and Pb were observed at the range of 10–100 ppm and all other parameters were kept constant. The adsorption capacity of both Cr and Pb metal ions has shown a significant increase with increasing initial metal ion concentrations. This may probably be due to the driving force provided by the higher initial concentration to overcome mass transfer barriers between all the molecules of solid and liquid phases which enables the attraction of metal ions from solution onto the surface of functionalized asphaltenes (Gupta et al., 2012).

The Langmuir isotherm is based on the assumptions that on the structurally homogeneous adsorbent, all adsorption sites are energetically equivalent and identical as well as the intermolecular force decreases rapidly with distance. So it follows the mechanism of adsorption of a monolayer on the adsorbent surface. The Langmuir Constants and adsorption capacities can easily be calculated by linearized Langmuir isotherm equation (5) as follows

$$\frac{C_e}{q_e} = \frac{C_e}{Q_m} - \frac{1}{Q_m b} \quad (4)$$

Where q_e is millimoles of metal adsorbed per gram of the adsorbent; C_e is the metal residual Concentration in solution at equilibrium, Q_m is the maximum specific uptake corresponding to the site saturation and b is the ratio of adsorption and desorption rates, the Langmuir constant (Cabeza et al., 2002). Fig. 6 represents the plot of C_e/q_e versus C_e. On the other hand, the Freundlich isotherm model describes heterogeneous adsorption systems with uniform energy (Fig. 7); the model was expressed by the below equation:

$$Q_e = k_f C_e^{1/n} \quad (5)$$

$$\log q_e = \log k_f + \frac{1}{n} \log C_e \quad (6)$$

Where q_e the concentration at the equilibrium of the heavy metal ions on the adsorbent and C_e on the sample solution; the constants k_f and n, can be calculated from the slope and intercept.

The Temkin isotherm equation suggests that owing to adsorbent-

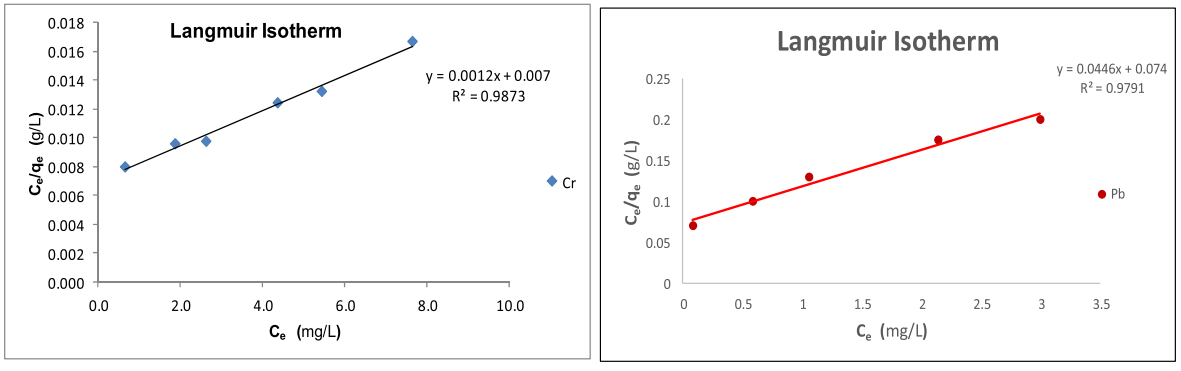

Fig. 6. Adsorption Langmuir isotherm of Cr and Pb on adsorbent.

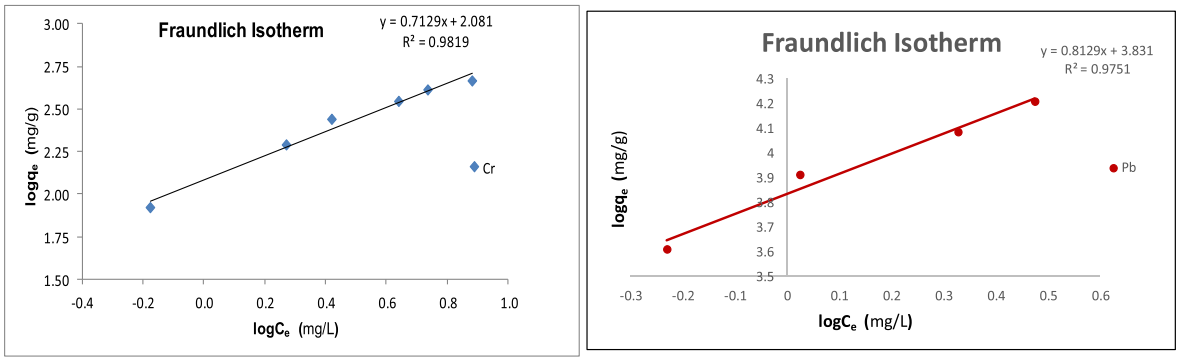

Fig. 7. Adsorption Freundlich isotherm of Cr and Pb on adsorbent.

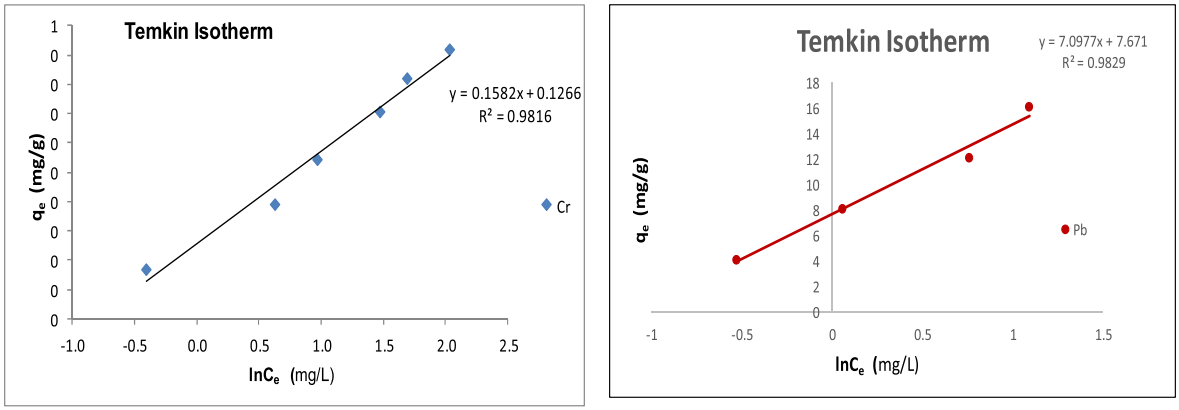

Fig. 8. Adsorption Temkin isotherm of Cr and Pb on the adsorbent.

Table 2
Langmuir Freundlich and Temkin isotherm model Constants for Cr and Pb removal.

a)Langmuir isotherm model				
Entry No	Heavy metals ion	Q_m (mmol g^{-1})	b (dm^3 $mmol^{-1}$)	R^2
1	Cr	833.3	0.171	0.987
2	Pb	22.42	0.599	0.980
b)Freundlich isotherm model				
Entry No	Heavy metal ions	n	k_f	R^2
1	Cr	1.402	0.008	0.982
2	Pb	1.230	0.0001	0.975
c)Temkin-isotherm model				
Entry No	Heavy metal ions	B	A	R^2
1	Cr	0.158	2.230	0.982
2	Pb	7.100	2.945	0.983

adsorbate interactions, the heat of adsorption of molecules in layer decreases linearly with Coverage, and the adsorption is characterized by a uniform distribution of the binding energies. The Temkin isotherm can be expressed by the following equation:

$$q_{e} = \frac{RT}{b} \ln(AC_e) \quad (7)$$

and can be linearized as:

$$q_e = B \ln A + B \ln C_e \quad (8)$$

Where *B* Corresponds to the adsorption potential of the adsorbent (KJ/mol), *A* is the Temkin isotherm Constant (L/g). A plot of qe versus lnCe (Fig. 8) is used to calculate the Temkin isotherm Constants A and B.

Table 3
The RL values based on the Langmuir isotherm model.

C_i (mg dm^{-3})	R_L value	
	Cr	Pb
10	0.370	0.143
25	0.190	0.063
50	0.105	0.032
75	0.072	0.022
100	0.055	0.016

Table 2 shows the Langmuir Freundlich and Temkin isotherm model Constants for Cr and Pb removal.

From the figures above we can say that the adsorption of the heavy metal ions on asphaltenes surface could be homogeneous or monolayer because the adsorption obeyed the three above isotherms.

The affinity of the adsorption of the heavy metal ions on the adsorbent surface can be described by the separation factor (R_L) in the Langmuir isotherm is given in eq (9):

$$R_L = \frac{1}{(1 + bC_0)} \quad (9)$$

Where C_o is the initial heavy metals ion concentration and *b* is the Langmuir equilibrium constant. When the value of (R_L) falls between 0 and 1 it indicates the favorability of the adsorption on the adsorbent surface, as its clear in the below Table 3 the value falls in the range, and that means good adsorption favorability for the heavy metal ions on the adsorbent surface.

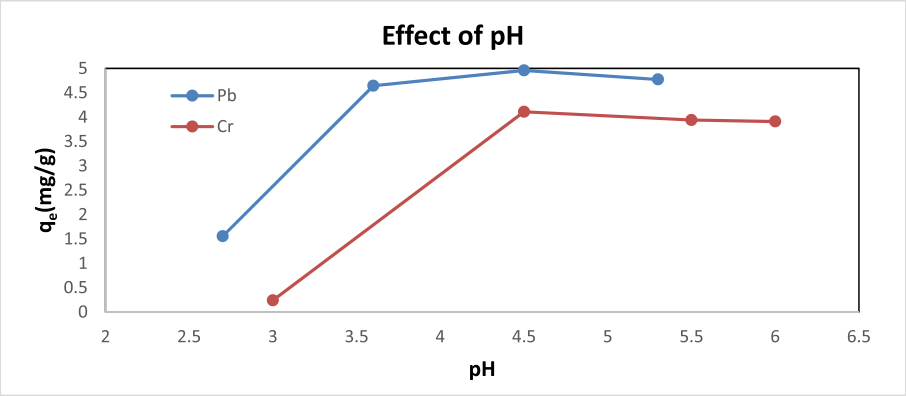

Fig. 9. pH dependence of heavy metal ions uptake by the adsorbent.

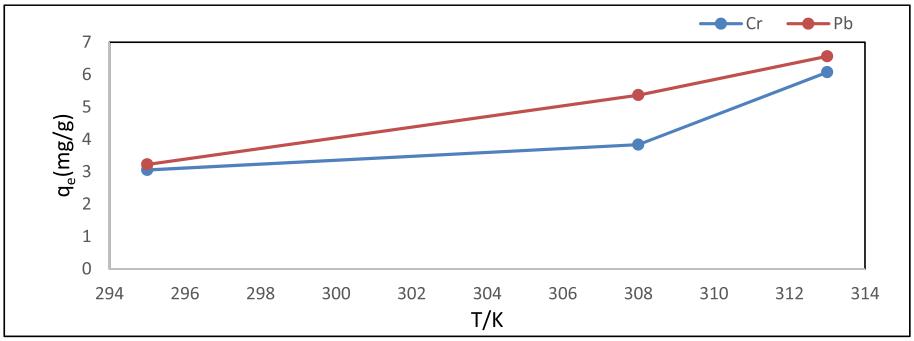

Fig. 10. Effect of temperature on the adsorption capacity of the adsorbent.

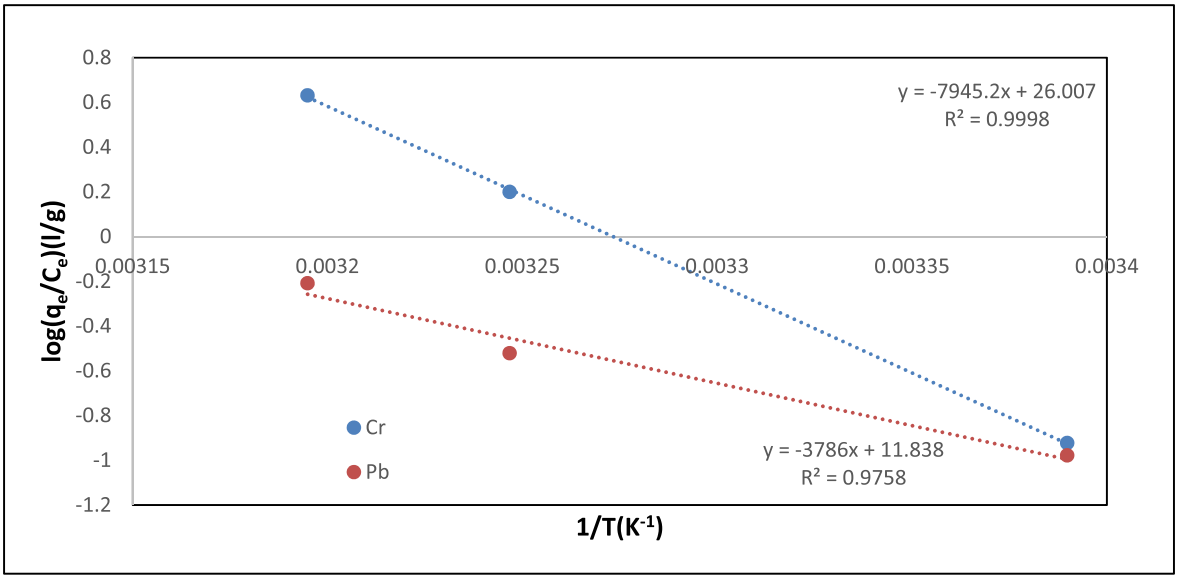

Fig. 11. Vant-Hoff's plot for adsorption of Pb and Cr on adsorbent.

3.5. pH and temperature effect on the removal

pH is an important parameter that determines the effectiveness of the adsorption process as with the varying pH of the solution, the degree of ionization and surface properties of adsorbent also varies. The experiment demonstrating the effect of pH on the adsorption capacity of Pb and Cr metal ions was carried out at pH ranging between 2.5 – 5 and 3–6 respectively by using acetate buffer. The optimum pH was found to be 4.5 for Cr and Pb. This could be explained that at lower pH, due to protonation functional groups that are present at the surface are most likely linked with H^+ ions, which makes them inaccessible for metal ions. At moderate pH, functional groups get deprotonated due to which the probability of attachment of metal ions increases, and hence adsorption capacity also increases. At higher pH i.e. above pH 4.5 complexes of soluble hydroxide form which tend to decrease the adsorption capacity of Cr and Pb ions. Fig. 9 indicates pH dependence of heavy metal ions uptake by the adsorbent.

The thermodynamic parameters were obtained from the adsorption

Table 4
Thermodynamic Data for Cr and Pb adsorption.

Heavy metals ion	Temp	ΔG	ΔH	ΔS	R^2
		KJ.mole^{-1}	KJ.mole^{-1}	J.K^{-1}mole^{-1}	
Cr	295	−298.87	−152.07	497.64	0.9998
Pb	295	−139.09	−724.64	225.85	0.9758

The comparative Table S1 and Table S2 have been given in the supporting information for the adsorption efficiency of Cr and Pb respectively and showing very good removal efficiency of functionalized asphaltenes than other adsorbents.

Table 5
The adsorbent regeneration using 0.1M H_2SO_4 and HCl on Chromium and Lead Adsorbent.

(a) Treatment of 0.1M H_2SO_4 on Chromium & Lead Adsorbent			
S.No	Sample time	Cr (mg/L)	Pb (mg/L)
1	10min	0.00	3.41
2	30min	0.00	3.21
3	60min	0.00	3.57
4	120min	0.00	4.19
5	24 Hr	0.00	3.98
(a) Treatment of HCl 0.1 M on Chromium & Lead Adsorbent			
S.No	Sample time	Cr (mg/L)	Pb (mg/L)
1	10min	0.00	213.00
2	30min	0.00	214.00
3	60min	0.00	210.00
4	120min	0.00	211.00
5	24 Hr	0.00	219.00

Table 6
The reusability of the adsorbent for a) Cr and b)Pb.

S.No	Sample time	Cr (mg/L)
1.00	15min	19.74
2.00	30min	17.58
3.00	60min	14.04
4.00	120min	8.80
5.00	24 Hr	8.00
S.No	Sample time	Pb (mg/L)
1.00	15min	49.90
2.00	30min	46.17
3.00	60min	45.19
4.00	120min	43.58
5.00	24 Hr	42.52

experiment, and the results were explained in the figure below. As clear in Fig. 10, the removal efficiency increases with the temperature, which means the adsorption is endothermic.

A plot of log (qe/Ce) against 1/T (Fig. 11) using the Vant-Hoff equation the thermodynamic parameters were obtained, and are tabulated in Table 4 (Coşkun et al., 2006; Ramesh et al., 2007). The negative free energies ΔGs confirm the spontaneity of the process.

$$log\left(\frac{q_e}{C_e}\right) = -\frac{\Delta H}{2.303RT} + \frac{\Delta S}{2.303\ R} \quad (10)$$

The negativity of ΔG increases with the temperature that shows that the adsorption is more favorable at higher temperatures. Favorable adsorption at higher temperatures is attributed to the greater swelling of the adsorbent and increased diffusion of heavy metal ions into the adsorbent. The positive enthalpies ΔHs confirm that the adsorption process is endothermic. In addition, it can be found in Table 6 that the ΔS values are positive, suggesting that the randomness increased during adsorption of metal ions because of the release of water molecules from the large hydration shells of the metal ions.

4. Adsorbent regeneration and reuse

The regeneration and the reusability of the adsorbent were investigated for the two contaminants (Table 5(a)(b) and 6(a)(b)), two solutions were used for the regenerate 0.4g of the adsorbent was placed in 30 ml of 0.1M sulfuric acid solution and 0.1M hydrochloric acid and the desorption time was from 10 min to 24 h, as we can see in the table below the Pb ions were almost removed from the adsorbent in hydrochloric solution but it didn't desorb from the adsorbent in sulfuric acid solution, the Cr ions showed good desorption efficiency in both solutions.

The reusability of the adsorbent also was investigated by taking the regenerated adsorbent from the first part washed it with water and dried for overnight then it was placed in a 200 ppm solution of chromium and lead ions, as clear in the below tables the adsorbent was reusable, and the adsorbent showed higher adsorption capacity toward the lead ions.

5. Conclusion

A novel adsorbent from the functionalization of asphaltenes was prepared to form low-cost material with very good yield. The adsorbent was found to have a good removal efficiency for Cr and Pb ions due to the development of functional groups such as –C═O, –COOH, -C-O, and others. These functional groups are responsible for the ion exchange and complexation with the metals. The adsorption process obeyed Langmuir, Freundlich and Temkin isotherm models and, also fitted Lagergren pseudo second-order kinetic model. The positive enthalpies ΔHs confirm that the adsorption process is endothermic, the negative free energies ΔGs confirm the spontaneity of the process. The good efficiency of the adsorption implies the efficacy in the removal of the heavy metal ions, as well as the good efficiency in desorption, which implies the excellent recovery of the adsorbent. The effective reusability of this adsorbent makes it applicable for industrial water treatment from contaminants. As functionalized asphaltene is metal-free as well as has high surface-active agents influencing the adsorption performance of the materials and this process can open a new avenue to develop sustainable material from the waste.

Author contributions

Mohammad Nahid Siddiqui: Conceptualization, Funding acquisition, Writing – original draft preparation, Supervision. Shamsh Pervez: Conceptualization, Writing – original draft preparation, Supervision. Indrapal Karbhal: Writing – review & editing. Princy Dugga: Writing – review & editing, Saravanan Rajendran: Writing – review & editing. Yasmeen Fatima Pervez: Writing – review & editing.

Declaration of competing interest

The authors declare that they have no known competing financial interests or personal relationships that could have appeared to influence the work reported in this paper.

Acknowledgments

The author would like to acknowledge the support provided by the Deanship of Scientific Research (DSR) at King Fahd University of Petroleum & Minerals (KFUPM), Dhahran, Saudi Arabia, for funding this work through project number SB141007.

Appendix A. Supplementary data

Supplementary data to this article can be found online at https://doi.org/10.1016/j.envres.2021.112361.

References

Arias, M., Barral, M.T., Mejuto, J.C., 2002. Enhancement of copper and cadmium adsorption on kaolin by the presence of humic acids. Chemosphere 48, 1081–1088. https://doi.org/10.1016/S0045-6535(02)00169-8.

Ayala, J., Blanco, F., García, P., Rodriguez, P., Sancho, J., 1998. Asturian fly ash as a heavy metals removal material. Fuel 77, 1147–1154. https://doi.org/10.1016/S0016-2361(98)00027-1.

Bartholomew, C.H., 1994. In: Oballa, M.C., Shih, S.S. (Eds.), Catalytic Hydroprocessing of Petroleum and Distillates. Marcel Decker, New York, p. 42.

Bišķup, B., Subotić, B., 2005. Removal of heavy metal ions from solutions using zeolites. III. Influence of sodium ion concentration in the liquid phase on the kinetics of exchange processes between cadmium ions from solution and sodium ions from zeolite A. Separ. Sci. Technol. 39, 925–940. https://doi.org/10.1081/ss-120028454.

Brown, P., Atly Jefcoat, I., Parrish, D., Gill, S., Graham, E., 2000. Evaluation of the adsorptive capacity of peanut hull pellets for heavy metals in solution. Adv. Environ. Res. 4, 19–29. https://doi.org/10.1016/S1093-0191(00)00004-6.

Cabeza, A., Ouyang, X., Sharma, C.V.K., Aranda, M.A.G., Bruque, S., Clearfield, A., 2002. Complexes formed between nitrilotris(methylenephosphonic acid) and M2+ transition metals: isostructural organic-inorganic hybrids. Inorg. Chem. 41, 2325–2333. https://doi.org/10.1021/ic0110373.

Chu, W., 1999. Lead metal removal by recycled alum sludge. Water Res. 33, 3019–3025. https://doi.org/10.1016/S0043-1354(99)00010-X.

Cimino, R., Correra, S., Del Bianco, A., Lockhart, T.P., 1995. Asphaltenes: Fundamentals and applications. Plenum Press, New York, pp. 97–130.

Coşkun, R., Soykan, C., Saçak, M., 2006. Removal of some heavy metal ions from aqueous solution by adsorption using poly(ethylene terephthalate)-g-itaconic acid/acrylamide fiber. React. Funct. Polym. 66, 599–608. https://doi.org/10.1016/j.reactfunctpolym.2005.10.012.

Coughlin, R.W., Ezra, F.S., 1968. Role of surface acidity in the adsorption of organic pollutants on the surface of carbon. Environ. Sci. Technol. 2, 291–297. https://doi.org/10.1021/es60016a002.

Diniz, C.V., Doyle, F.M., Ciminelli, V.S.T., 2002. Effect of pH on the adsorption of selected heavy metal ions from concentrated chloride solutions by the chelating resin Dowex M-4195. Separ. Sci. Technol. 37, 3169–3185. https://doi.org/10.1081/SS-120006155.

Du, L., Gao, P., Meng, Y., Liu, Y., Le, S., Yu, C., et al., 2020. Highly efficient removal of Cr (VI) from aqueous solutions by polypyrrole/monodisperse latex spheres. ACS Omega 5, 6651–6660. https://doi.org/10.1021/acsomega.9b04438.

Ekmekyapar, F., Aslan, A., Bayhan, Y.K., Cakici, A., 2006. Biosorption of copper(II) by nonliving lichen biomass of Cladonia rangiformis hoffm. J. Hazard Mater. 137, 293–298. https://doi.org/10.1016/j.jhazmat.2006.02.003.

Fan, Y., Wang, H., Deng, L., Wang, Y., Kang, D., Li, C., Chen, H., 2020. Enhanced adsorption of Pb(II) by nitrogen and phosphorus co-doped biochar derived from Camellia oleifera shells. Environ. Res. 191, 110030. https://doi.org/10.1016/j.envres.2020.110030.

Gupta, V.K., Ganjali, M.R., Nayak, A., Bhushan, B., Agarwal, S., 2012. Enhanced heavy metals removal and recovery by mesoporous adsorbent prepared from waste rubber tire. Chem. Eng. J. 197, 330–342. https://doi.org/10.1016/j.cej.2012.04.104.

Ho, Y.S., McKay, G., 1999. The sorption of lead(II) ions on peat. Water Res. 33, 578–584. https://doi.org/10.1016/S0043-1354(98)00207-3.

IARC Working Group on the Evaluation of Carcinogenic Risks to Humans, 2012. Chemical agents and related occupations. IARC Monogr. Eval. Carcinog. Risks Hum. 100, 9–562.

Li, Q., Wu, S., Liu, G., Liao, X., Deng, X., Sun, D., Hu, Y., Huang, Y., 2004. Simultaneous biosorption of cadmium (II) and lead (II) ions by pretreated biomass of Phanerochaete chrysosporium. Separ. Purif. Technol. 34, 135–142. https://doi.org/10.1016/S1383-5866(03)00187-4.

Mahato, M.K., Singh, P.K., Tiwari, A.K., Singh, A.K., 2016. Risk assessment due to intake of metals in groundwater of east bokaro coalfield, Jharkhand, India. Expo. Heal. 8, 265–275. https://doi.org/10.1007/s12403-016-0201-2.

McKay, G., Otterburn, M.S., Aga, A.J., 1985. Fuller's earth and fired clay as absorbents for dyestuffs external mass transport processes during adsorption. Water Air Soil Pollut. 24, 307–322.

Miyauchi, Y., de Wind, M., 1994. Hydroprocessing. In: Proceedings of the Akzo Nobel Catalysts Symposium, Amsterdam, The Netherlands, pp. 123–140.

Nordberg, G.F., Fowler, B.A., Nordberg, M., Friberg, L., 2014. Handbook on the Toxicology of Metals. Academic press, New York.

Pooja, D., Saini, S., Thakur, A., Kumar, B., Tyagi, S., Nayak, M.K., 2017. A "Turn-On" thiol functionalized fluorescent carbon quantum dot based chemosensory system for arsenite detection. J. Hazard Mater. 328, 117–126. https://doi.org/10.1016/j.jhazmat.2017.01.015.

Ramesh, A., Hasegawa, H., Maki, T., Ueda, K., 2007. Adsorption of inorganic and organic arsenic from aqueous solutions by polymeric Al/Fe modified montmorillonite. Separ. Purif. Technol. 56, 90–100. https://doi.org/10.1016/j.seppur.2007.01.025.

Rao, G.P., Lu, C., Su, F., 2007. Sorption of divalent metal ions from aqueous solution by carbon nanotubes: a review. Separ. Purif. Technol. 58, 224–231. https://doi.org/10.1016/j.seppur.2006.12.006.

Ravikumar, K.V.G., Kumar, D., Kumar, G., Mrudula, P., Natarajan, C., Mukherjee, A., 2016. Enhanced Cr(VI) removal by nanozerovalent iron-immobilized alginate beads in the presence of a biofilm in a continuous-flow reactor. Ind. Eng. Chem. Res. 55, 5973–5982. https://doi.org/10.1021/acs.iecr.6b01006.

Sahoo, S.K., Hota, G., 2019. Amine-functionalized GO decorated with ZnO-ZnFe2O4 nanomaterials for remediation of Cr(VI) from water. ACS Appl. Nano Mater. 2, 983–996. https://doi.org/10.1021/acsanm.8b02286.

Shaikh, A.R., Chawla, M., Hassan, A.A., Abdulazeez, I., Salawu, O.A., Siddiqui, M.N., Shamsh Pervez, S., Cavallo, L., 2021. Adsorption of industrial dyes on functionalized and nonfunctionalized asphaltene: A combined molecular dynamics and quantum mechanics study. J. Mol. Liquids 337, 116433. https://doi.org/10.1016/j.molliq.2021.116433.

Shirokoff, J.W., Siddiqui, M.N., Ali, M.F., 1997. Characterization of the structure of Saudi crude asphaltenes by X-ray diffraction. Energy and Fuels 11, 561–564. https://doi.org/10.1021/ef960025c.

Siddiqui, M.N., 2017. Developing an effective adsorbent from asphaltene for the efficient removal of dyes in aqueous solution. Desalin. Water Treat. 67, 371–380. https://doi.org/10.5004/dwt.2017.20450.

Siddiqui, M.N., Ali, I., Asim, M., Chanbasha, B., 2020. Quick removal of nickel metal ions in water using asphalt-based porous carbon. J. Mol. Liquids 308, 113078. https://doi.org/10.1016/j.molliq.2020.113078.

Siddiqui, M.N., Basheer, C., Al-Arfaj, A.A., Kon'kova, T., Ali, I., 2021. Super-fast removal of cobalt metal ions in water using inexpensive mesoporous carbon obtained from industrial waste material. Environ. Technol. Innovat. 21, 101257 https://doi.org/10.1016/j.eti.2020.101257.

Singh, H., Pandey, R., Singh, S.K., Shukla, D.N., 2017. Assessment of heavy metal contamination in the sediment of the River Ghaghara, a major tributary of the River Ganga in Northern India. Appl. Water Sci. 7, 4133–4149. https://doi.org/10.1007/s13201-017-0572-y.

Speight, J.G., 1990. Fuel Science and Technology Handbook. Marcel Dekkar, New York.

Suliman, M.H., Siddiqui, M.N., Chanbasha, B., 2020. Surface functionalization of mesoporous carbon for the enhanced removal of strontium and cesium radionuclides. Coatings 10 (10), 923. https://doi.org/10.3390/coatings10100923.

WHO (World Health Organization), 2017. Guidelines for Drinking-Water Quality: Fourth Edition Incorporating the First Addendum. WHO, Geneva.

Xiao, C., Lin, J., 2020. Efficient removal of Cr(VI) ions by a novel magnetic 4-vinyl pyridine grafted Ni3Si2O5(OH)4multiwalled nanotube. ACS Omega 5, 23099–23110. https://doi.org/10.1021/acsomega.0c02874.

Yang, K., Xing, B., 2010. Adsorption of organic compounds by carbon nanomaterials in aqueous phase: polanyi theory and its application. Chem. Rev. 110, 5989–6008. https://doi.org/10.1021/cr100059s.